SYNTHESIS, CHARACTERIZATION, AND STABILIZATION OF MXENE TWO-DIMENSIONAL NANOMATERIALS

A Dissertation

by

XIAOFEI ZHAO

Submitted to the Graduate and Professional School of
Texas A&M University
in partial fulfillment of the requirements for the degree of

DOCTOR OF PHILOSOPHY

Chair of Committee,	Micah J. Green
Committee Members,	Miladin Radovic
	Jodie L. Lutkenhaus
	Mustafa Akbulut
Head of Department,	Arul Jayaraman

December 2021

Major Subject: Chemical Engineering

ABSTRACT

MXenes are two-dimensional (2D) transition metal carbides and nitrides; they are derived from their MAX phase precursors by top-down selective acid etching. These fascinating 2D nanomaterials have a combination of functional properties suitable for a variety of applications such as batteries, supercapacitors, electromagnetic shielding, nanocomposites, and sensors. However, fabrication and usage of devices and functional coatings based on MXenes remains challenging because MXenes are prone to oxidize and degrade rapidly in aqueous and humid environments. MXenes are known reacting with water molecules resulting in the structural and chemical degradation. Differences in the oxidation rates of MXene nanosheets have been evaluated and reported in various media (air, liquid, and solid) via multiple types of measurements to assess their performance and shelf stability.

In this work, the degree of MXene oxidation is measured by the chemical composition, crystallographic structure, and electrical property changes. The oxidation rate of MXene nanosheets was observed dependent on various factors such as temperature, humidity, pH, and dispersion concentration. The oxidation rate is also determined by the chemical stoichiometry, surface functionality, and quality of MXenes and influenced by the ions and molecules present in the dispersion.

More importantly, several novel methods have been demonstrated to mitigate or eliminate the oxidation of $Ti_3C_2T_x$ and Ti_2CT_x MXene nanosheets and films. First, we discovered that “MXene antioxidants”, such as sodium L-ascorbate, ascorbic acid, citric acid, tartaric acid, and oxalic acid, can effectively extend the chemical stability of MXene nanosheets in aqueous dispersions. The success of this method is evident in the stable morphology, unchanged chemical structure, and colloidal stability of MXene nanosheets. The minimal electrical property changes also reveal that the resistance to oxidation persists in the dehydrated MXenes as well after antioxidant pretreatment. This study also focuses on the structural-activity relationship of MXene antioxidants which helps to identify the protection mechanism and to choose more effective antioxidants for MXenes. In addition to the introduction of antioxidants, we demonstrated that thermally annealing free-standing MXene films under inert argon gas can induce surface and structural modifications, which can remarkably enhance the chemical stability of the films and improve their electronic properties. These methods have potential to be also used in protecting other types of MXenes besides $Ti_3C_2T_x$ and Ti_2CT_x. Findings in this dissertation can help to solve one of the most pressing challenges in the field of MXene engineering.

DEDICATION

To my parents (Zhao, Jianjun; Ma, Yun), my wife and son (Shen, Dongning; Lucas), and in memory of my grandparents (Ma, Aiqun; Zhao, Xiuying). For their selfless, unconditional love and support.

ACKNOWLEDGEMENTS

I am grateful to my PhD research advisor, Dr. Micah Green, for your constant guidance and support along my journey as a graduate student at Texas A&M. Your invaluable expertise, foresights in research projects, and insightful knowledge are pivotal to my growth as a young researcher and chemical engineer. I truly appreciate your patience and help in all our discussions on research projects and in developing my academic communication/writing skills. Thank you so much for your consistent support on developing my professionalism and career!

Special thanks to Dr. Miladin Radovic, Dr. Jodie L. Lutkenhaus, and Dr. Mustafa Akbulut for your time to serve on my PhD committee. I benefit so much from your guidance, feedbacks, and all the discussions with you on research projects. I want to acknowledge Zeyi, Ian, Kasturi, Shuhao, Dustin, Evan, and all other collaborators and members in Radovic, Lutkenhaus, and Akbulut research groups. Thank you for your collaborative efforts, offering me instrument trainings, and fruitful discussions.

I am grateful to former members Dr. Smit Shah, Dr. Touseef Habib, Dr. Wanmei Sun, Dr. Nutan Patil, and Dr. Muhammad Anas for helping me and making me feel welcomed in the group. Thank you to my fellow colleagues Aniruddh, Huaixuan, Jackson, Bryan, Julie, Kailash, and all other members in Green group for your contribution in my projects.

Finally, I am thankful for my Lord giving me courage, comfort, and teaching me the truth. Your word is a lamp for my feet, a light on my path. Endless thanks to all my family members and friends for your love and support.

CONTRIBUTORS AND FUNDING SOURCES

Contributors

This work was supervised by a dissertation committee consisting of Dr. Micah J. Green (PhD advisor), Dr. Jodie L. Lutkenhaus, Dr. Mustafa Akbulut of the Artie McFerrin Department of Chemical Engineering, and Dr. Miladin Radovic of the Department of Materials Science and Engineering.

All the MAX phase samples used in this dissertation were synthesized by members in Dr. Miladin Radovic lab in Texas A&M University. The molecular simulation data and results were provided by Dr. Aniruddh Vashisth. All other work conducted for the dissertation was completed by the student independently.

Funding Sources

Graduate study was supported by the Artie McFerrin Department of Chemical Engineering with their graduate student assistantship. This work was funded by the US National Science Foundation under award number 1760859.

TABLE OF CONTENTS

Page

LIST OF FIGURES

LIST OF TABLES

1. INTRODUCTION

1.1. Introduction of MXenes 2D nanomaterials

Two-dimensional (2D) nanomaterials draw much attention in nanoengineering and fabrication since the discovery of graphene, because of their uniqueness of high aspect ratio, tunable surface properties, and versatility to be assembled into various structures. As a new member of 2D nanomaterials, the first MXene, $Ti_3C_2T_x$, was discovered in 2011 by Naguib *et al.* [1, 2] In general, the term "MXene" refers to a family of two-dimensional (2D) transition metal carbides, nitrides and carbonitrides; in recent years, there has been an avalanche of research studies and material applications focused on MXenes because of their excellent chemical, physical, mechanical, and electrical properties.[2-4] Prior studies have highlighted MXenes' hydrophilicity, excellent electrical and thermal conductivities, ease of aqueous processability, and in-plane stiffness. [5, 6] Most of those properties can be traced back to their metallic-like 2D structure and functional groups attached during the etching and exfoliation processes.[2, 7-10] In addition, the versatile chemistry of the MXene family and various functional properties make these materials holding promise for a wide range of applications in energy storage,[3, 11-15] sensors,[16, 17] electromagnetic interference shielding,[18, 19] functional coatings,[20-23] plasmonics,[24] water filtration,[25, 26] and electrocatalysts[18, 27-34].

1.2. Composition of MXenes

MXenes are generally described with the chemical formula of $M_{n+1}X_nT_x$, where M represents an early transition metal element such as Ti, V, Nb, Hf, Ta, Cr, Mo, or Zr, X is carbon or nitrogen, T refers to one or multiple surface terminal groups formed during the synthesis which include -OH, -O-, -F, and -Cl; in most cases, *n* ranges from 1 to 3,[4] and *x* reflects the number of terminal groups.[32, 35] MXenes are typically synthesized from a parent MAX phase (ternary ceramics) bearing a atomically layered crystal structure[36], in which $M_{n+1}X_n$ layers are interleaved by a layer of the A element (from group 13 or 14), such as aluminum (Al), tin (Sn) or silicon (Si). Multilayered MXenes can be derived by selective etching and removal of the A layer from the parent MAX phase[37, 38]. Furthermore, multilayered MXenes may be intercalated and exfoliated to yield single or few-layer MXene nanosheets.

There are more than 30 types of experimentally derived MXenes reported so far, with many more predicted to be thermodynamically stable by simulation but yet to be synthesized.[39] Depending on the MAX stoichiometries, MXenes generally have chemical formulas of M_2XT_x, $M_3X_2T_x$, or $M_4X_3T_x$.[8] For example, $Ti_3C_2T_x$ is the most studied and first-ever reported MXene.[2] MXenes can also be categorized into mono-transition metal MXenes, solid solution MXenes, and ordered double-transition metal MXenes depending on the composition and arrangement of M element in MAX phase shown in **Figure 1-1**.[3]

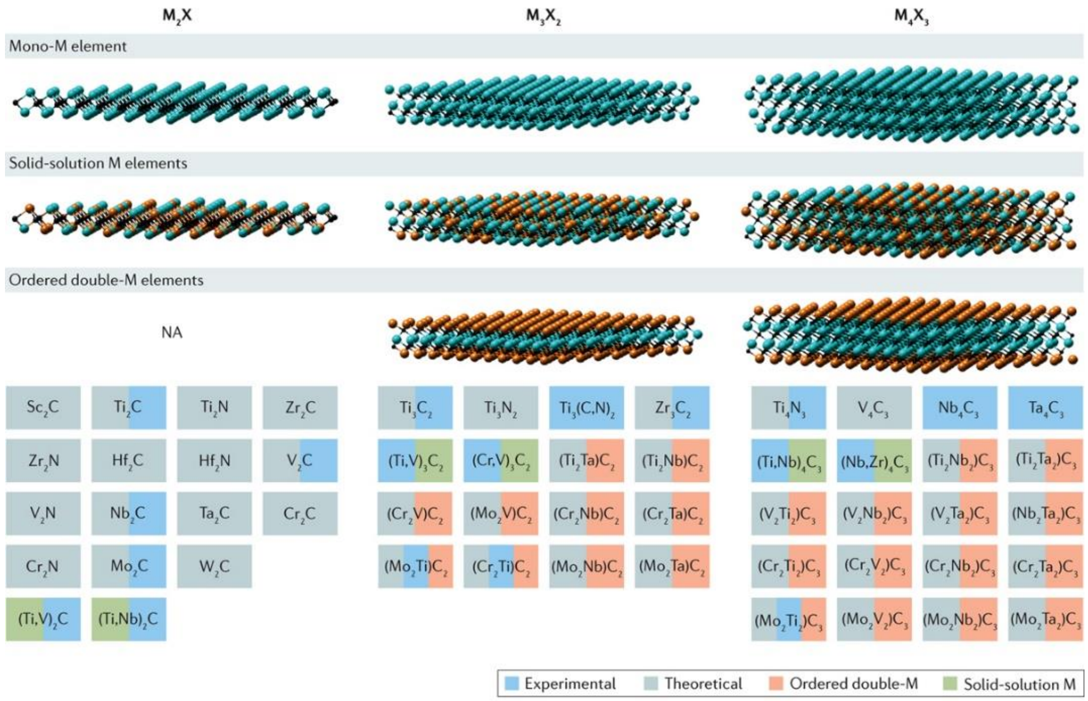

Figure 1-1 Potential MXene compositions. Reprinted with permission from reference[3], Copyright 2017 Springer Nature.

1.3. Synthesis and processing methods to derive MXene nanosheets

The majority of the reported MXenes are solution-processed and derived by selective acid etching in aqueous environments. MXene nanosheets cannot be made by physical exfoliation directly from their layered parent MAX phase. Unlike graphene oxide and boron nitrides, which can be typically exfoliated by overcoming the relatively weak out-of-plane bonding that holds 2D sheets together, such as van der Waals bonding and hydrogen bonding, MXenes have to be chemically etched first to break the primary bonds (metallic M-A bonds) in the MAX phase before exfoliation. In MAX phase precursors, metallic bonding between M and A layers keeps the $M_{n+1}X_n$ sublayers together.[40] M-X bonds are much stronger than M-A bonds, which makes them exhibiting differences in wet etch selectivity. This allows the A element layer to be removed while retaining the strength of M-X bonds. To yield single or few-layer MXene nanosheets, two major steps are required: the first one is to break the metallic M-A bonds and remove the A element from MAX precursors; the second step is to exfoliate (or delaminate) the multilayered etched particles by overcoming the strength of secondary bonding between the $M_{n+1}X_n$ layers, such as van der Waals bonding and hydrogen bonding.

Current research show that the majority of MXenes are synthesized by a top-down method by etching MAX precursors in fluorine-containing etchant solutions. The commonly used etchants include concentrated solutions of hydrofluoric acid (HF, 47 wt.%), and HF-forming etchants, such as mixtures of LiF and HCl, and bifluoride salts.[41-43] In the case of Ti_3AlC_2, its reaction with HF can be written as

$$Ti_3AlC_2 + 3\ HF \rightarrow Ti_3C_2 + AlF_3 + 1.5\ H_2$$

which is a gas-forming exothermic reaction.[44] In this reaction, interleaved Al layer is removed by HF as soluble AlF_3, resulting in the formation of an accordion-like structure comprised of multiple layers of Ti_3C_2 (**Figure 1-2**).

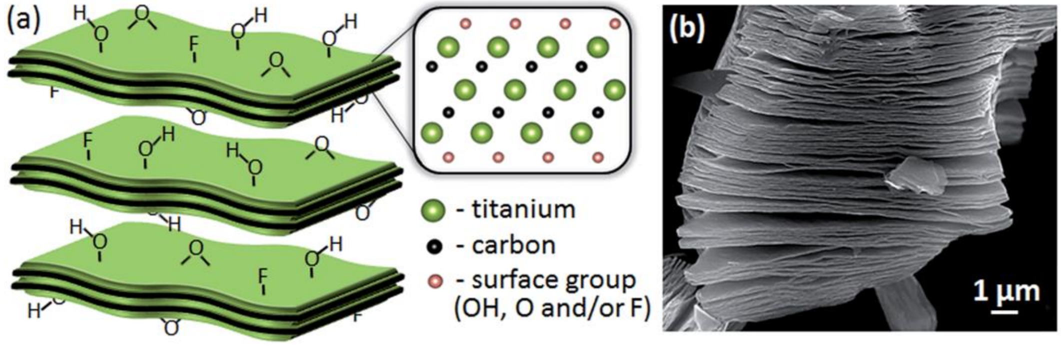

Figure 1-2 (a) Schematic of $Ti_3C_2T_x$ layered structure with a side view atomic model of a single sheet. (b) SEM image of a multi-layered $Ti_3C_2T_x$ particle. Reprinted with permission from reference[45], Copyright 2014 Royal Society of Chemistry.

In a newer approach, mixtures of LiF and HCl are used in the synthesis of single or few-layer nanosheets. The intercalation of Li^+ cations in the etched multilayered MXenes helps to weaken the van der Waals forces during the etching step which allows more complete etching and easier exfoliation in the following step. Even though the A layer is removed, the interlayer interactions between the $M_{n+1}X_n$ sheets (which are also called $M_{n+1}X_n$ sublayers) are still strong, which prevents the efficient nanosheet delamination. Hence, an additional intercalation step is usually required to further weaken the interactions between the adjacent $M_{n+1}X_n$ sheets and separate them from one another. This can be achieved by the diffusion of some large organic, inorganic molecules, or ionic species into spaces between adjacent sub-layers, such as dimethyl sulfoxide (DMSO), tetramethylammonium hydroxide (TMAOH), tetrabutylammonium hydroxide (TBAOH), urea. Along with co-intercalation of water molecules, the energy barrier required for MXene delamination may be much reduced. A swelling or volume expansion is also observed after the intercalation of multi-layered MXene clay.[8] Following the intercalation, the multilayered structures can be delaminated by probe or bulk sonication.[3, 46]

The composition of etchants, etching conditions, and post-etching processing steps will have significant effects on the selection of synthesis routes, yield, morphology, size distribution, defect level, chemical and physical properties of the derived MXene nanosheets.[47-50] For example, inadequate etching time, low etching temperature, and etchant concentration may result in low yield of MXenes. In contrast, increasing the concentration of HF etchant and TBAOH intercalation agent result in the formation of higher numbers of defect and nanopores on nanosheets.[49] Based on the clay method, Naguib *et al.* and Alhabeb *et al.* discovered that increasing the HCl concentration and weight ratio of LiF and MAX can result in exfoliation as the clay sample being washed to close neutral after etching.[8, 51] This allows to delaminate multi-layered MXene clay particles merely with gentle hand shaking and mild agitation, without application of high-power sonication. This method is referred as minimally intensive layer delamination process (MILD method). Nanosheets produced by MILD method exhibits larger size with distinctive and straight edges than sheets produced by clay method with sonication involved (**Figure 1-3**)[52]. Sonication can break off nanosheets during exfoliation which results in smaller size distribution (**Figure 1-4**). The composition of etchants can also affect the terminal groups on nanosheets. Hope *et al.* have carried out the quantitative nuclear magnetic resonance (NMR) experiments and discovered that the composition of the surface functional groups of the derived $Ti_3C_2T_x$ produced by LiF-HCl clay method showed lower -OH, -F contents, but higher =O content, compared to MXenes derived by HF etching (**Figure 1-5**).[53]

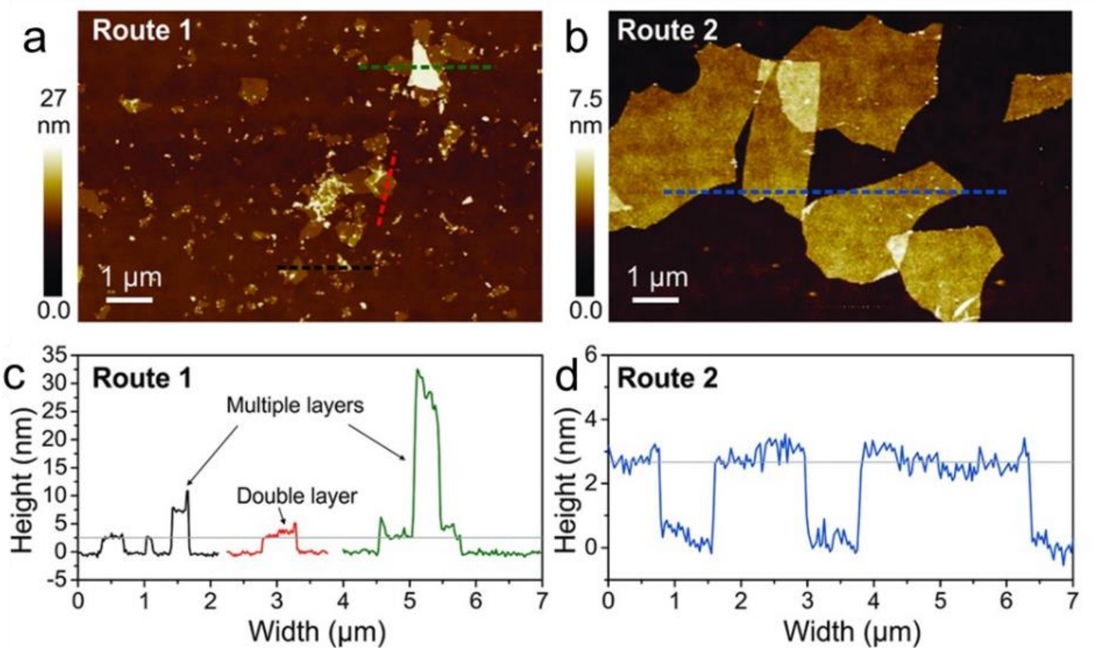

Figure 1-3 Atomic force microscopy (AFM) images of the $Ti_3C_2T_x$ flakes produced by Route 1 (clay method) and Route 2 (MILD method). Reprinted with permission from reference[52], Copyright 2016 WILEY-VCH Verlag GmbH & Co.

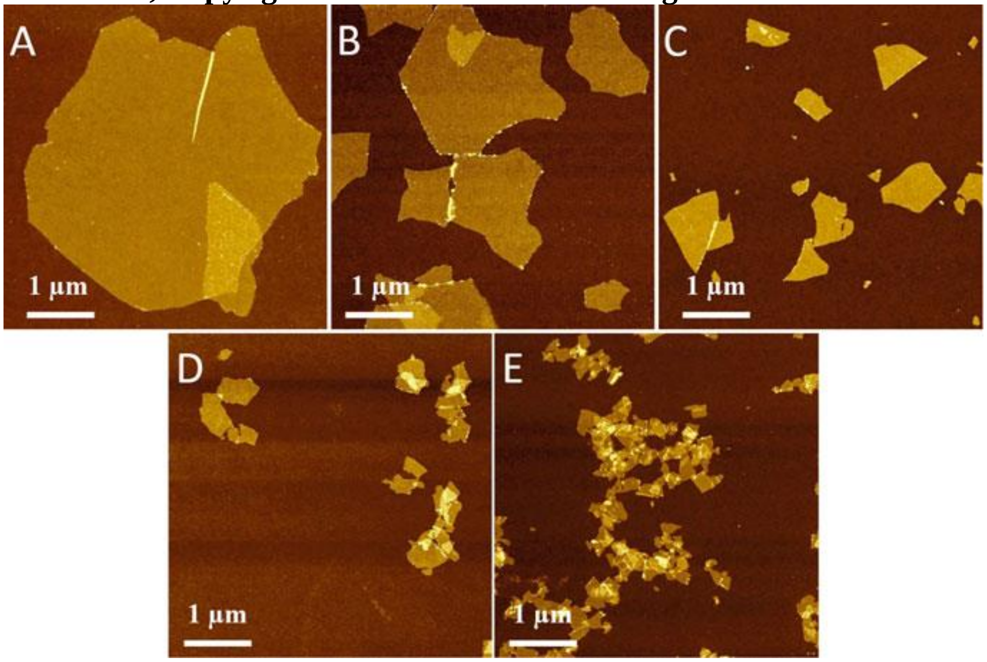

Figure 1-4 AFM images of $Ti_3C_2T_x$ sheets (a) without sonication and sonicated for (b) 1 minute (c) 5 minutes (d) 15 minutes (e) 30 minutes. Reprinted with permission from reference[54]. Copyright 2019 Springer International Publishing.

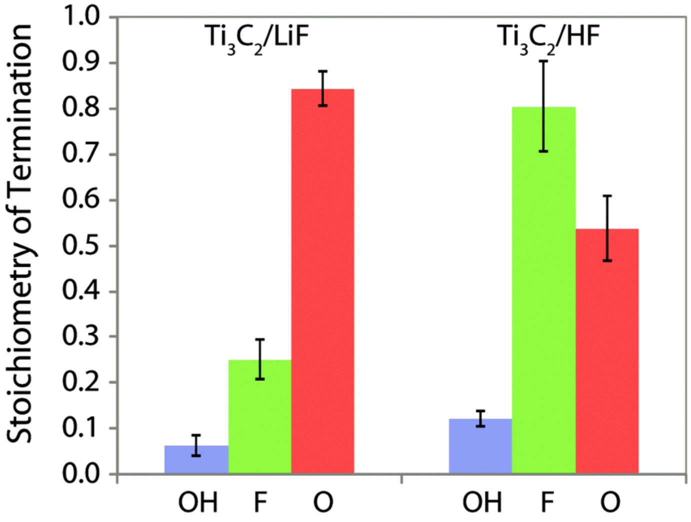

Figure 1-5 Composition of the $Ti_3C_2T_x$ surface functional groups produced by etching of the Ti_3AlC_2 in HF and LiF-HCl solutions, per Ti_3C_2 formula unit, i.e., $Ti_3C_2(OH)_xF_yO_z$. Reprinted with permission from reference[53], Copyright 2016 Royal Society of Chemistry.

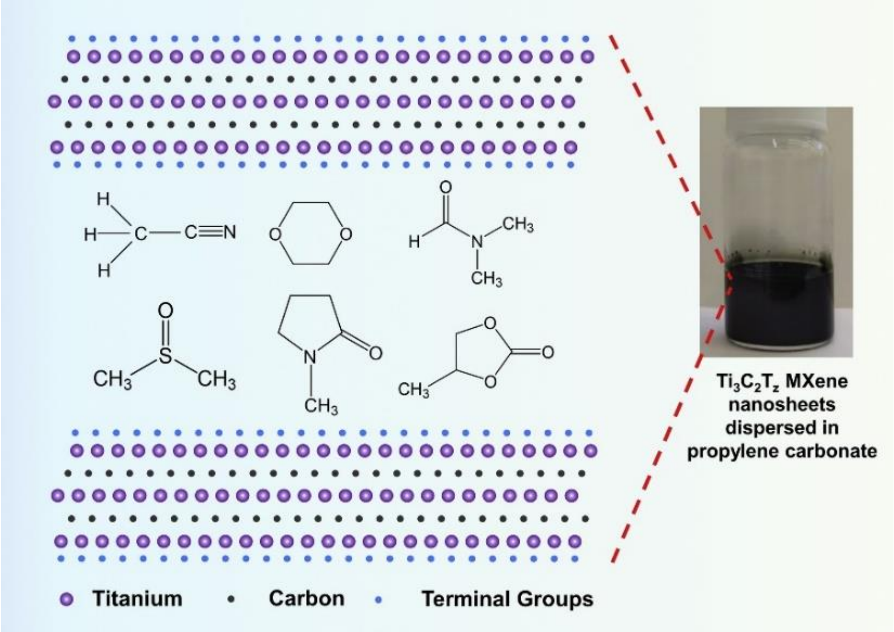

Figure 1-6 Schematic of $Ti_3C_2T_z$ nanosheets delaminated and dispersed stably in several organic solvents, including propylene carbonate (shown in the photo, reproduced from Natu *et al.*), dioxane, acetonitrile, N,N-dimethylformamide, dimethyl sulfoxide, and N-methyl-2-pyrrolidone. Reprinted with permission from references[42, 43], Copyright 2020 Elsevier Ltd.

Novel non-aqueous etching methods to synthesize MXenes have been attempted by researchers to avoid the inherent danger of using HF-containing solution and also explore the possibility to derive new types of MXenes, which cannot be synthesized by selective acid etching, and new possible surface terminations. Natu *et al.* reported that etching and dispersion of $Ti_3C_2T_z$ MXenes can be achieved in several polar organic solvents by using ammonium bifluoride as the etchant (**Figure 1-6**).[42, 43] The formed nanosheets were found readily dispersed as stable colloids in those same organic solvents. In addition, molten salt methods were developed to create multi-layered MXenes by etching MAX phase in the melt of -Cl and -F containing salts.[55-57] $Ti_3C_2T_z$ clay made by a molten salt approach was typically found to be halogen-terminated. Recently, Kamysbayev *et al.* demonstrated that MXene clay made by molten salt etching can also be delaminated into $Ti_3C_2T_n$ nanosheets (T = Cl, S, NH), which can form stable colloidal dispersions in N-methyl formamide (NMF).[58] However, so far, no water-dispersible nanosheets have been reported with using the molten salt etching method.

1.4. Colloidal properties of MXenes

$Ti_3C_2T_x$ nanosheets produced by selective acid etching have a variety of terminal groups including hydroxy (-OH), oxygen (-O), fluoride (-F), and chloride (-Cl).[8, 10, 59] These polar terminal groups result in strong hydrophilicity and electronegativity, which allow them to be dispersed in water and form a colloidal suspension. The colloidal stability of MXene nanosheets may be affected by factors such as the types of surface terminal groups, dispersion pH,[17, 60] ionic strength,[60] concentration, extent of oxidation[61] etc.

$Ti_3C_2T_x$ MXene nanosheets synthesized by selective acid etching method show a ζ potential value from -30 mV to -40 mV. Natu *et al.*, Naguib *et al.*, and Ying *et al.* reported that the ζ potential and averaged hydrodynamic size of MXene nanosheets measured by the dynamic light scattering (DLS) technique show strong dependency on dispersion pH values.[51, 60, 62]

At neutral pH, MXene surface is overall negatively-charged due to the deprotonation of terminal groups, such as -OH, resulting in the electrostatic repulsion between nanosheets. At acidic pH, abundant protons (H^+) in the dispersion restrict the deprotonation of the attached surface functional groups, rendering the ζ-potential less negative. The electrostatic repulsion among the nanosheets decreases in this case. Hence, lower the dispersion pH below 4 was observed causing the aggregation of MXene nanosheets (**Figure 1-7a** and **1-7b**). Ying *et al.* measured that $Ti_3C_2T_x$ has the isoelectric points (similar to point of zero charge (PZC)) at around pH of 2.36 (**Figure 1-7c**).[62] The surface of the nanosheets will become positively charged when the pH of dispersion drops below the isoelectric point due to the presence of positively-charged protonated terminal groups. Naguib *et al.* reported that V_2CT_x and Ti_3CNT_x MXenes have different isoelectric points and ζ potentials but displaying the similar trend with pH changes (**Figure 1-7d**). At basic pH, ζ potential of $Ti_3C_2T_x$ was observed remaining relatively constant up to a pH pf 12. Sedimentation observed at extreme high pH may be presumably caused by the absorption of cations supplied by the base, resulting in a reduction in the double-layer thickness.[60]

The colloidal stability of $Ti_3C_2T_x$ is also a function of ionic strength. Similar to other water-dispersible 2D nanomaterials, the colloidal behavior of 2D MXene nanosheets is in agreements and can be estimated based on Derjaguin-Landau-Verwey-Overbeek (DLVO) theory, considering a combined effect from the van der Waals attraction and electrostatic repulsion forces.[21, 60, 61] An electric double layer is believed to be present around the nanosheet surface in electrolytes. Increasing the solute concentration or ionic strength reduces the electric double layer thickness, causing the reduction of repulsion force, thus leading to the flocculation of nanosheets.

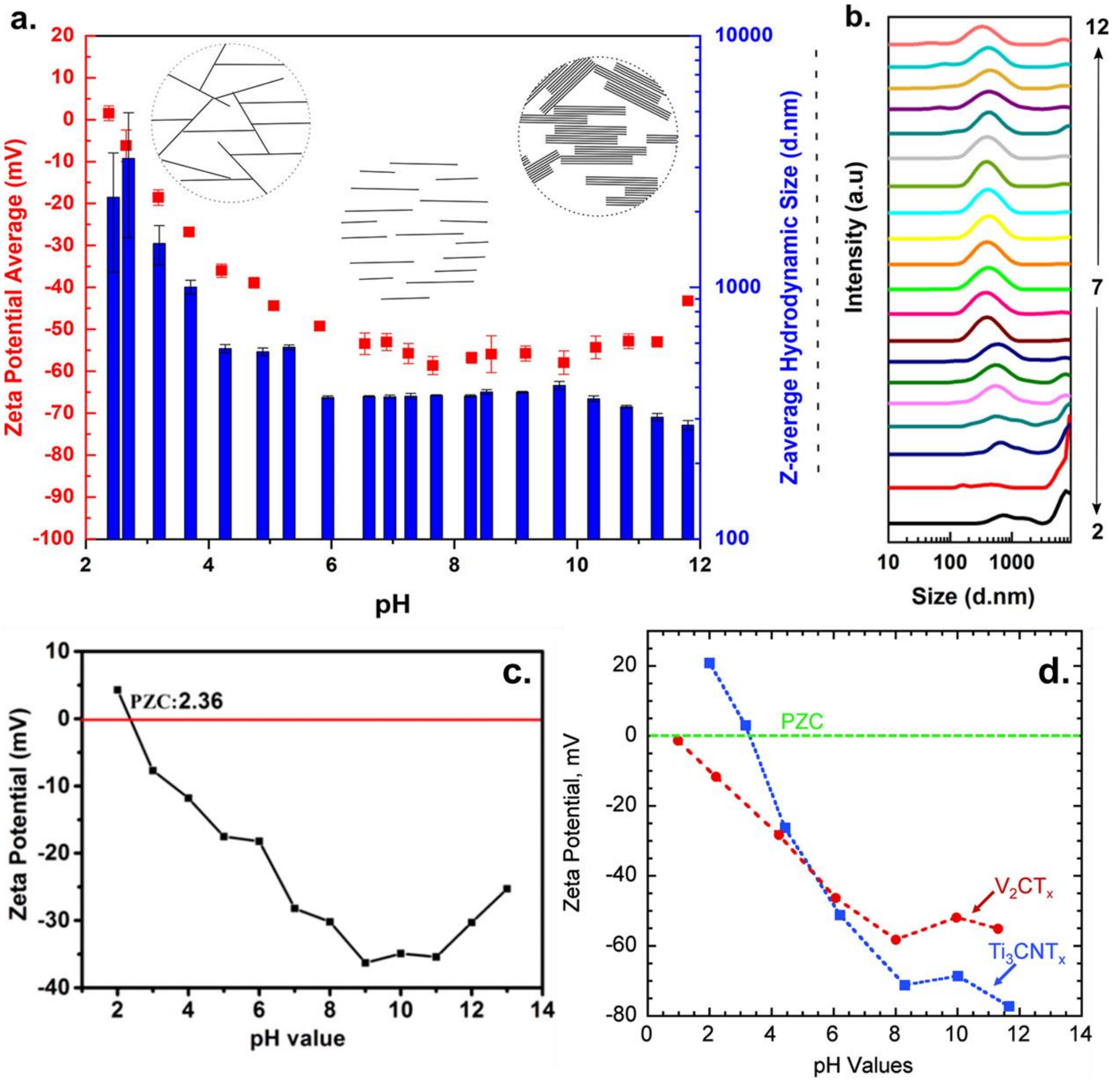

Figure 1-7 (a) Zeta potential (left y-axis) and average hydrodynamic size (right y-axis) vs pH. Insets show probable aggregate structures formed at low pH (left) and high pH (right), whereas complete deflocculation is represented by the middle inset. (b) Dynamic light scattered intensity vs size distribution between 10 and 9000 nm at various pH values. Reprinted with permission from reference [60], Copyright 2018 American Chemical Society. (c) Zeta potential of 0.1 mg/mL $Ti_3C_2T_x$ suspension depends on pH. Reprinted with permission from reference[62], Copyright 2015 American Chemical Society. (d) Zeta potential dependence on pH for Ti_3CNT_x and V_2CT_x multi-layer powders with a concentration of 1 mg/mL. The horizontal green dashed line indicates the position of zero zeta potential, which intersects with the zeta potential plot at the point of zero charge (PZC). Reprinted with permission from reference[51], Copyright 2002 Royal Society of Chemistry.

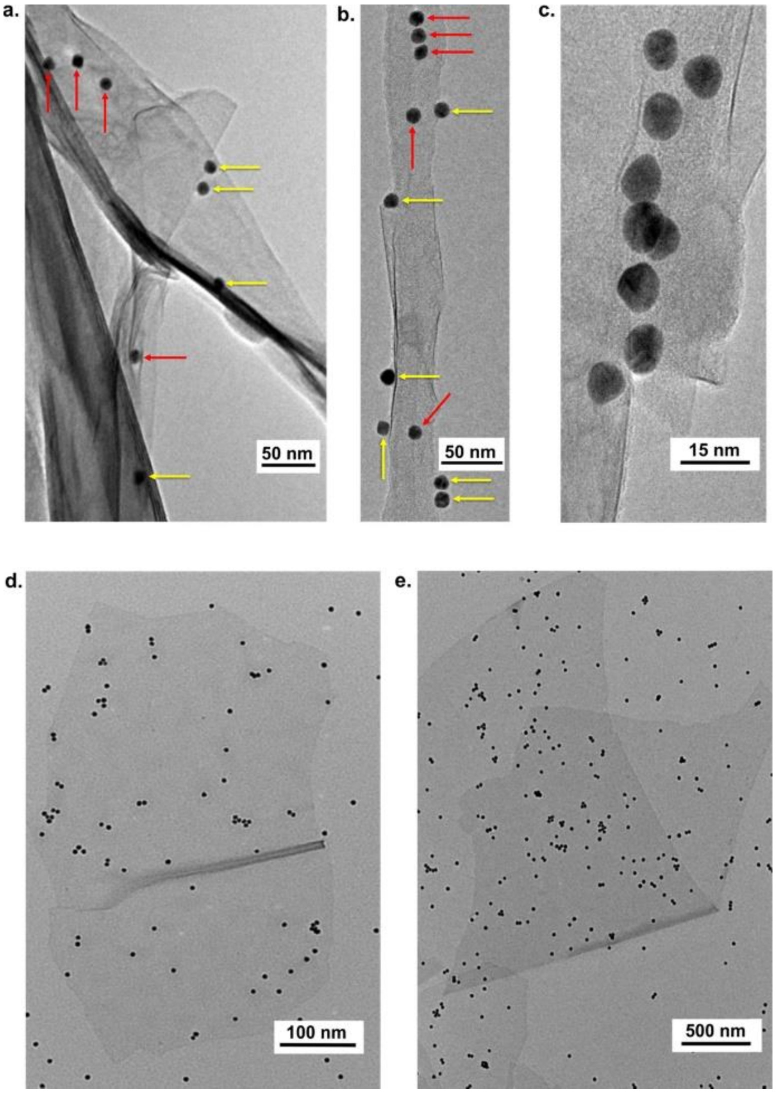

Figure 1-8 Typical TEM images of $Ti_3C_2T_x$ flakes decorated by Au nanoparticles. In panels (a)–(c), the gold NPs were negatively charged; in panels (d) and (e), they were positive. Reprinted with permission from reference[60], Copyright 2018 American Chemical Society.

Surface of MXene nanosheets is commonly believed to carry oxygen-containing groups, such as -OH, whose deprotonation renders the presence of negative charges on MXene surface. Natu *et al.* shows an interesting finding that the edges of $Ti_3C_2T_x$ nanosheets are more positively charge at neutral pH than the basal plane. They observed under a transmission electron microscope (TEM) that the introduced negatively charged Au nanoparticles were more prone to be absorbed along the nanosheet edges, however, the positively charged Au nanoparticles prefers basal plane (**Figure 1-8**). Natu *et al.* claims that some of the Ti bonds at the edges remain unsatisfied during etching and exfoliation, and thus causes the edge to become positively charged.

1.5. Oxidation stability of MXenes

Even though MXenes have been praised for their fascinating physical and electrical properties, one particular problem has plagued both the science and applications of these materials: Most-known MXenes are prone to oxidation, resulting in structural degradation and the loss of functional properties. This oxidation has been observed by transmission electron microscopy and even by direct observation of color changes of nanosheet dispersions from a black/dark green color (for $Ti_3C_2T_x$) to a cloudy white/brownish color showing in **Figure 1-9**.[63]

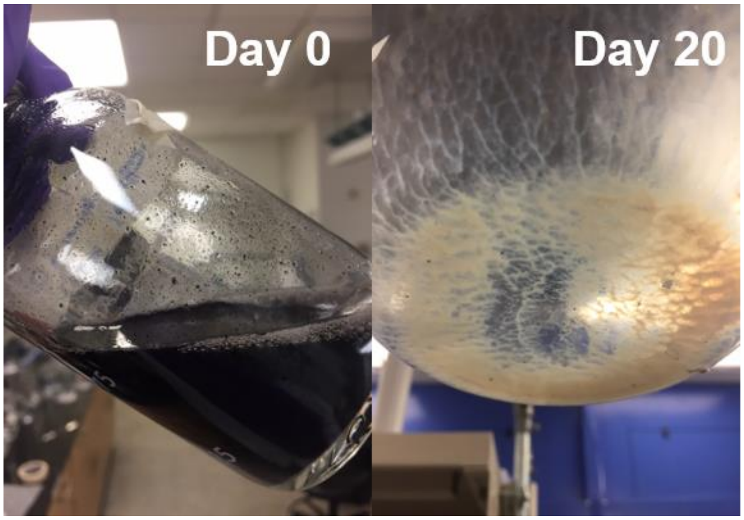

Figure 1-9 Oxidation of dispersed $Ti_3C_2T_x$ nanosheet in water after 20-day storage.

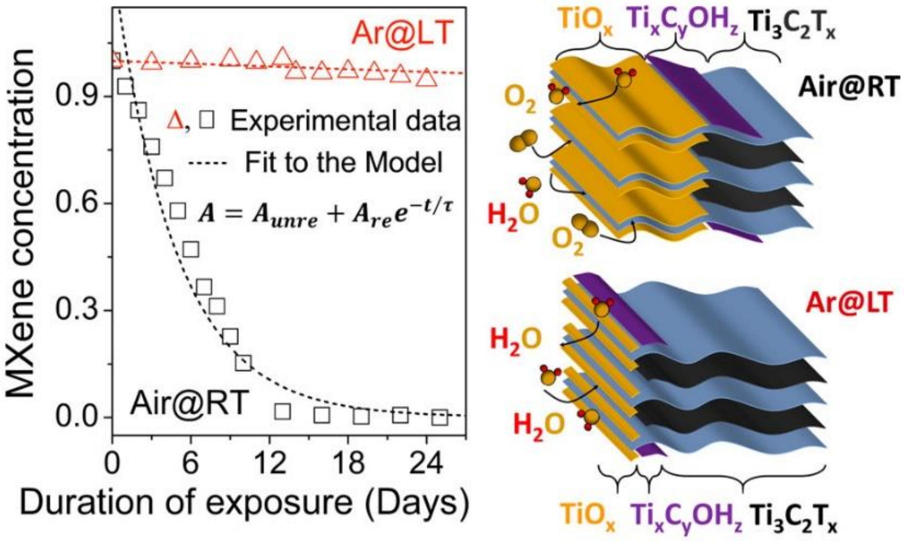

Figure 1-10 Stability of colloidal delaminated $Ti_3C_2T_x$ different environments. Oxidation rate was found much slower in argon-filled vial under low temperature (5 °C). Reprinted with permission from reference[64], Copyright 2017 American Chemical Society.

Prior studies have reported and explored the issue of oxidation of delaminated MXene nanosheets. Mashtalir *et al.* firstly observed that $Ti_3C_2T_x$ can oxidize and various Ti oxides forms after 1-week in methylene blue aqueous solution.[45] The oxidation was believed to occur due to O_2 adsorption on under-coordinated Ti atoms on nanosheets. Zhang *et al.* investigated the oxidation stability of $Ti_3C_2T_x$ in air- and argon-filled vials respectively at room and low temperatures (**Figure 1-10**).[64] The slower oxidation in argon-filled vial was reported due to the eliminated the dissolved oxygen molecules, which was considered as the main oxidant of the MXene flakes. After 15 days of storage in open vials, $Ti_3C_2T_x$ solution degraded completely, leading to the formation of anatase (TiO_2). However, in these studies, delaminated $Ti_3C_2T_x$ single flakes were also found reacting with water in the absence of air. But the reaction with water had not been considered as the primary cause for the oxidation.

Huang *et al.* and Habib *et al.* investigated and compared the oxidation behaviors of MXenes dispersed in water and organic solvents at conditions with and without oxygen present, respectively.[46, 65] Rapid oxidation was observed for MXenes dispersed in argon-filled/bubbled water. However, no sign of oxidation and degradation was observed for $Ti_3C_2T_x$ dispersed in iso-propanol saturated with pure oxygen (**Figure 1-11**). They concluded that the reaction between MXene and water plays the primary role leading to the degradation of MXene.

Oxidation stability of MXene nanosheets can be affected by a variety of factors. Habib *et al.* investigated the $Ti_3C_2T_x$ oxidation and electrical performance changes at various medium and discovered that oxidation of $Ti_3C_2T_x$ is fastest in liquid media, such as water, organic solvents, and slowest in solid media such as polymer matrices (**Figure 1-12**).[46] MXene nanosheets oxidize in much slower rates in organic solvents compared to aqueous solvents.[46, 66] In addition, the acceleration of MXene oxidation has been demonstrated under the exposure to UV light and plasmonic laser.[46, 67, 68] Besides the factors like dispersion medium and UV exposure, storage conditions are also found greatly controlling the kinetics of MXene oxidation. Chae *et al.* claimed that $Ti_3C_2T_x$ dispersion maintains chemically stable for more than 39 weeks when the storage temperature is sufficiently low (-80 °C).[69]

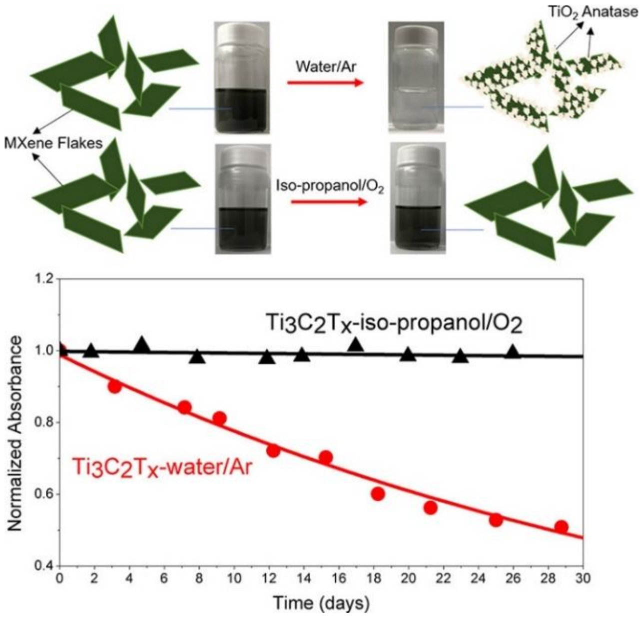

Figure 1-11 Stability of $Ti_3C_2T_x$ colloidal solutions in water (Ar-filled) and iso-propanol (pure O_2-filled) over time. Reprinted with permission from reference[65], Copyright 2019 American Chemical Society.

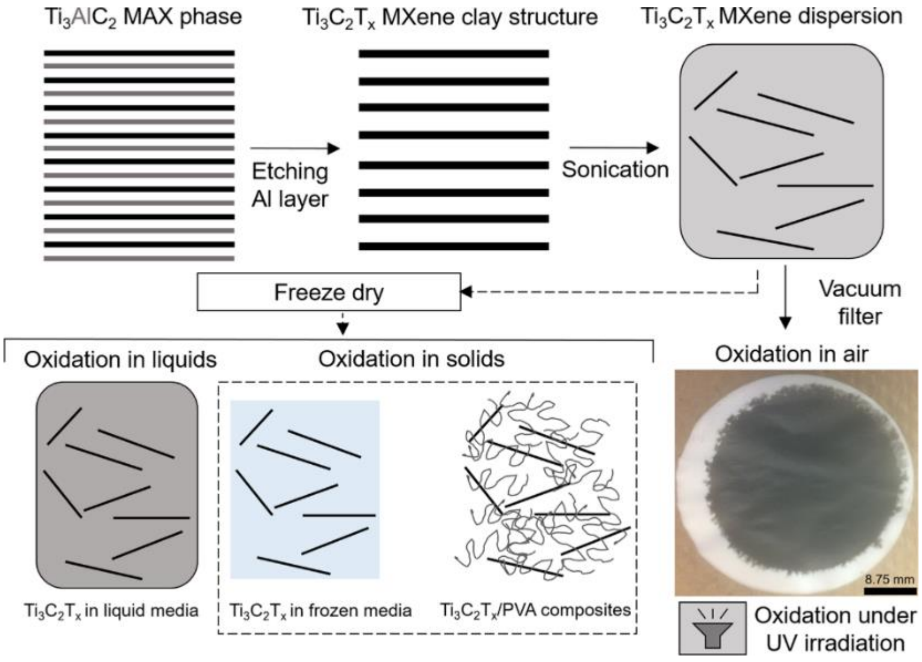

Figure 1-12 After the synthesis of $Ti_3C_2T_x$ MXene nanosheets from parent MAX phases, their oxidation stability was evaluated after being dispersed in various media. Reprinted with permission from reference[46], Copyright 2019 Springer Nature.

Nanosheet size distribution and defect density of MXenes also play important roles in determining the oxidation rate. Prior studies by Liptov *et al.* and Chertopalov *et al.* have suggested that the oxidation of MXene starts at the nanosheet edges.[52, 67] We have also observed the same as shown in **Figure 1-13**. The as-formed metal oxide nanocrystals can then develop throughout the MXene flake by nucleation and growth.[3, 64] Hence, smaller nanosheets oxidize faster than large nanosheets due to the low aspect ratio with more edges exposed. Xia *et al.* proposed that MXenes with less defects are more environmentally stable.[70] Ti vacancies on MXene nanosheets were identified as the preferential sites for carbon oxidation. The edges of layers and peaks or valleys of wrinkles were identified as the preferred sites for Ti oxidation.[70]

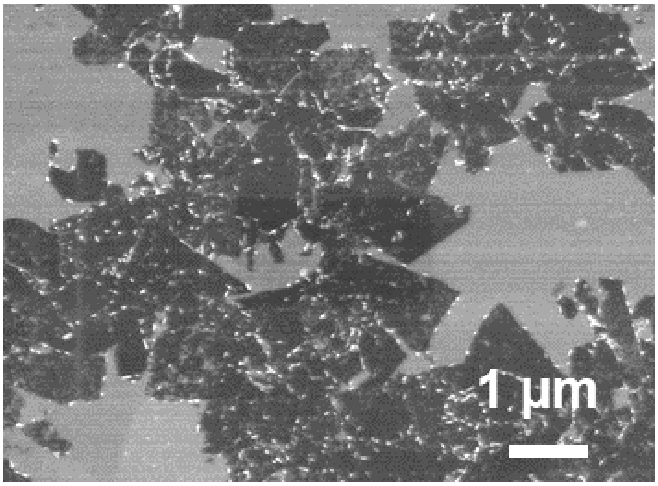

Figure 1-13 Oxidation and formation of TiO_2 nanocrystals start at the $Ti_3C_2T_x$ nanosheet edges.

MXenes with multilayered/stacked structures, i.e. MXene clay particles, are less prone to rapid oxidation than single or few-layer nanosheets due to the lower surface-to-volume ratio; even so, Mashtalir *et al.* and Habib *et al.* observed oxidation of multilayered clay particles over the course of several days to weeks indicated by the appearance of titanium dioxide nanocrystals on surface and edges of clay particles, and the dramatical decrease of electrical conductivity for films made from multilayered MXenes. [45, 46] Single to few-layer MXene nanosheets typically exhibit much higher aspect ratio, colloidal stability, and processability, but much lower oxidation stability, compared to multilayered MXene clay.

The chemistry of MXene oxidation has not been fully understood. Oxidation of $Ti_3C_2T_x$ MXene is believed spontaneous causing the formation of solid products including TiO_2 nanocrystals and amorphous carbon.[46] Huang *et al.* analyzed the gaseous products arise from oxidation of Ti_2CT_x and $Ti_3C_2T_x$. The investigators confirmed the formation of methane (CH_4) using gas chromatography without observing any formation of CO, CO_2. The release of intercalated acidic species, such as HF and HCl, was proposed to occur after oxidation due to the observed dispersion pH drop.[71]

The oxidation of MXenes causes the spontaneous formation of transition metal oxides, which can be studied quantitively by the increased chemical state of the transition mental M element. X-ray photoemission spectroscopy (XPS) is a powerful tool to determine the atomic percentage of surface M element in their oxide state, which can be similarly considered as the degree of sample oxidation. As the oxidation proceeds, the Ti(IV) peaks become more pronounced.[35, 46, 72, 73] In addition, MXene-assembled buckypaper was found showing a gradual reduction of electrical conductivity while oxidation happened. Hence, four-point probe measurements of the electrical conductivity of MXene-assembled films can also be used in determining the extent of oxidation (**Figure**

1-14). X-ray diffraction, UV-Vis, and electron microscopy have also been used in determining the oxidation of MXenes and the formation of transition metal oxides.[70, 74, 75]

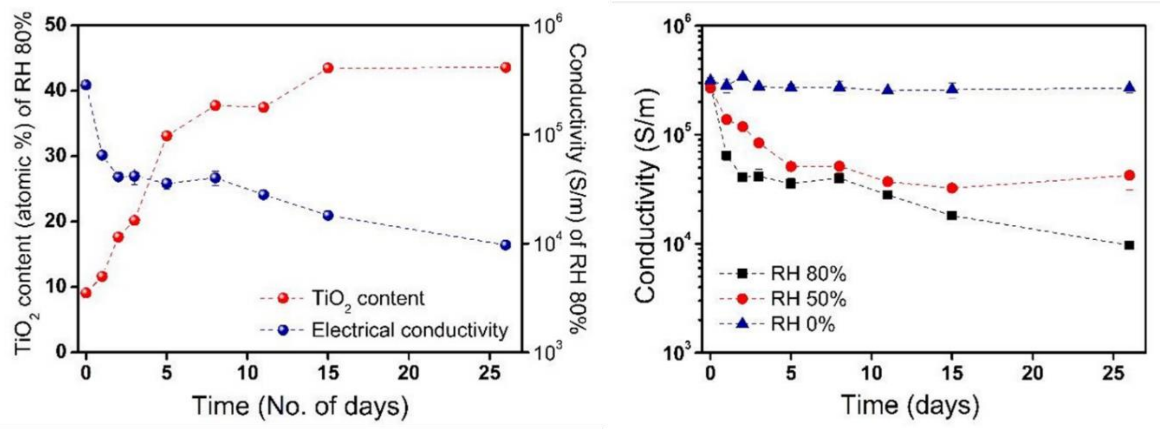

Figure 1-14 Conductivity and TiO_2 content as a function of time for samples stored in humidity-controlled environments. Reprinted with permission from reference[46], Copyright 2019 Springer Nature.

1.6. Mitigation of MXene oxidation

The rapid degradation of MXene 2D nanomaterials has prompted investigations into the mechanism of MXene oxidation, and more importantly, the methods to prolong their shelf and usage life. Multiple research groups recently observed that the oxidation kinetics varies widely depending on the surrounding media and storage conditions.[46, 69] Specifically, the oxidation rates were substantially higher in aqueous phases compared to in organic solvents, air, and solid media. Hence, early efforts on improving the oxidation stability of MXenes focused on the optimization of storage medium and conditions.

Maleski *et al.* and Habib *et al.* suggested that dispersions in organic solvents could mitigate or prevent oxidation and extend the shelf life of $Ti_3C_2T_x$ in solution[46, 65, 66]. It was believed that the solvation shell of the organic solvent molecules can restrict the reactions of the nanosheets with water and/or oxygen.[66, 76] Since the oxidation rate of $Ti_3C_2T_x$ nanosheets depends on both temperature and available oxidant concentration, efforts have been centering on the restriction of oxygen exposure and storing MXene dispersion at low temperatures. Reports by Anasori *et al.* and Zhang *et al.* implied that MXenes might be stored in oxygen-free degassed water or in dry air to avoid oxidation and that light exposure should be avoided.[3] In addition, storage in frozen dispersion was also reported to slow down the oxidation rates of $Ti_3C_2T_x$ nanosheets.[64, 77] Other techniques to slow down oxidation include freeze-drying MXene suspension and storage of the MXene product in a powder form under vacuum[46].

Surface modification is another approach to mitigate MXene oxidation. Wu *et al.* proposed a carbon nanoplating technique to modify Ti_3C_2 MXene surface for inhibiting oxygen diffusion[78]. Ji *et al.* demonstrated that functionalization of MXene surface with (3-Aminopropyl) triethoxysilane by a facile silylation reaction can stabilize the MXene against structural degradation[79]. Lee *et al.* claimed that reducing $Ti_3C_2T_x$ surface by H_2 annealing at elevated temperature can reduce the surface of partially oxidized MXene films[80].

The synthesis of the parent MAX phase was also demonstrated to show an influence on the oxidation stability of derived MXene nanosheets. Shuck *et al.* reported that $Ti_3C_2T_x$ MXenes derived from MAX phase made from graphite as the carbon source are more stable than that from lampblack and titanium carbide (TiC)[81] (**Figure 1-15**). The differences in stability caused by carbon source were attributed to size effects, defect density, and the presence of Ti_2AlC impurities. Mathis *et al.* showed that including excess aluminum during the Ti_3AlC_2 MAX phase synthesis results in the increased resistance to oxidation for derived MXenes, because of the enhanced crystallinity and stoichiometry[82].

Despite these efforts, effective techniques to eliminate or restrict the oxidation of MXene nanosheets remain elusive, particularly in the dispersed aqueous state. This dissertation focuses on improving the oxidation stability by innovative ways and investigating the mechanism of MXene oxidation.

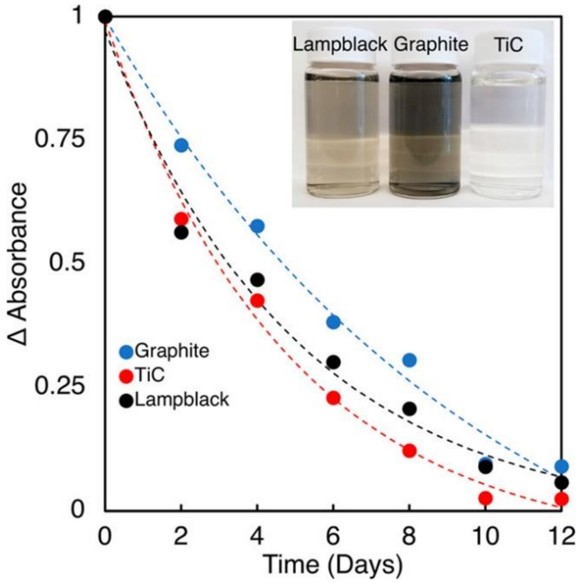

Figure 1-15 Solution stability of the 0.15 mg/mL MXene colloidal solutions dispersed in deionized water calculated by the change in solution absorbance. The digital image (inset) displays the differences in concentration of lampblack-, graphite-, and TiC-produced $Ti_3C_2T_x$ samples (left to right) after 12 days. Reprinted with permission from reference[81], Copyright 2019 American Chemical Society.

2. ANTIOXIDANTS UNLOCK SHELF-STABLE $TI_3C_2T_X$ (MXENE) NANOSHEET DISPERSIONS[*]

2.1. Summary

MXenes such as $Ti_3C_2T_x$ are fascinating two-dimensional nanomaterials with an attractive combination of functional properties suitable for applications such as batteries, supercapacitors, and sensors. Although MXene nanosheets have attracted significant scientific and industrial attention, however, these materials are highly susceptible to oxidation, which leads to their chemical degradation and loss of functional properties in a matter of days. Hence, fabrication of devices and functional coatings based on MXenes remains challenging.

We demonstrate an effective approach to arrest the oxidation of colloidal $Ti_3C_2T_x$ MXene nanosheets by introducing antioxidants such as sodium L-ascorbate. The success of the method is evident as the $Ti_3C_2T_x$ nanosheets maintain composition, morphology, electrical conductivity, and colloidal stability. This study reveals that the resistance to oxidation persists in the dehydrated MXenes as well. We propose that the sodium L-ascorbate protects the edges of the nanosheets, restricting water molecules from otherwise reactive sites; this is supported by molecular dynamics simulations that show association of the ascorbate anion with the nanosheet edge. We also show that other antioxidants may

---

[*] Reprinted with permission from "Antioxidants Unlock Shelf-Stable $Ti_3C_2T_x$ (MXene) Nanosheet Dispersions" by Xiaofei Zhao; Aniruddh Vashisth; Evan Prehn; Wanmei Sun; Smit A. Shah; Touseef Habib; Yexiao Chen; Zeyi Tan; Jodie L. Lutkenhaus; Miladin Radovic; Micah J. Green. 2019, *Matter*, 1, 513-526, Copyright 2019 Elsevier Inc.

be similarly effective. A graphic abstract of this finding is shown in **Figure 2-1**. These findings have the potential to be generalized to protect other types of MXenes and solve the most pressing challenge in the field of MXene engineering.

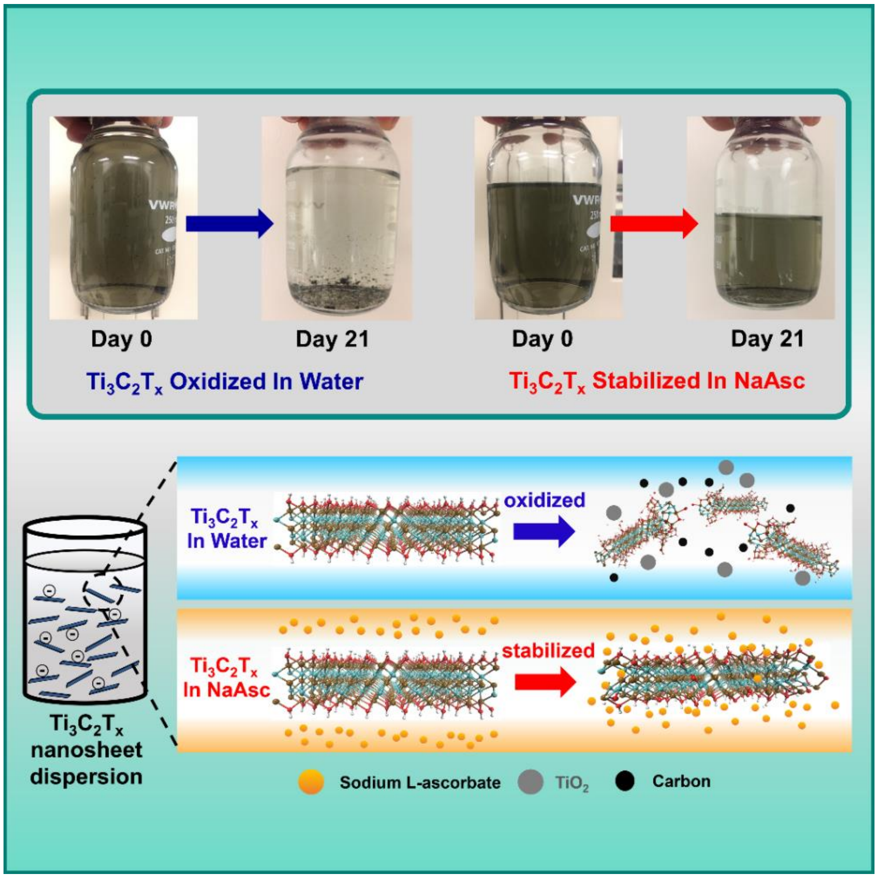

Figure 2-1 Graphic abstract figure shows that sodium L-ascorbate (vitamin C) can be used as MXene antioxidant to improve the chemical and colloidal stabilities of $Ti_3C_2T_x$ MXene nanosheets. Reprinted with permission from reference[75], Copyright 2019 Elsevier Ltd.

2.2. Introduction

MXenes are a family of two-dimensional (2D) transition metal carbides, carbonitrides, and nitrides; in recent, there has been an avalanche of research studies and material applications focused on MXenes because of their fascinating combination of physical and electrochemical properties [2]; prior studies have highlighted MXenes' hydrophilicity, excellent electrical- and thermal- conductivities, ease of processability, and in-plane stiffness [5, 6]. These materials hold promise for a wide range of applications in batteries, supercapacitors, electronic sensors, electromagnetic interference shielding, and electrocatalysts [18, 27-32]. Even though MXenes have been praised for their physical and electrochemical properties, one particular problem has plagued both the science and applications of these materials: Most known MXenes are prone to oxidation, resulting in the loss of both their nanosheet structure and functional properties.

MXenes are generally described as 2D materials with the chemical formula of $M_{n+1}X_nT_x$, where M represents an early transition metal element such as titanium (Ti), vanadium (V) or niobium (Nb), X is carbon and/or nitrogen, T refers to one or multiple terminal groups, *n* ranges from 1 to 3, and *x* reflects the number of terminal groups [32, 35]. MXenes are typically synthesized from a parent MAX phase bearing a atomically layered crystal structure [36], in which $M_{n+1}X_n$ layers are interleaved by a layer of the A element (from group 13 or 14), such as aluminum (Al), tin (Sn) or silicon (Si). Layered MXene "clay" can be derived by selective etching and removal of the A layer from the parent MAX phase [37, 38]. Furthermore, this clay may be intercalated, delaminated, and exfoliated to yield individual MXene nanosheets.

This study focuses on $Ti_3C_2T_x$ nanosheets, one of the most-studied members in the MXene family. These are typically derived by the wet acid etching of parent Ti_3AlC_2 to produce $Ti_3C_2T_x$ nanosheets where the terminal groups include hydroxy (-OH), oxygen (-O), fluoride (-F) and chloride (-Cl), depending on the acid in question [8, 10, 59]. These polar terminal groups result in strong hydrophilicity and electronegativity, which allow them to be dispersed in water and form a suspension. In addition, the types and distribution of terminal groups can have a strong impact on the properties, stability and functionality of MXenes [59].

Unfortunately, $Ti_3C_2T_x$ tends to oxidize and degrade rapidly over the course of days when exposed to air and/or water, leading to the disassembly of the layered, two-dimensional structure and formation of titanium oxide (TiO_2) and carbon (C) [45, 52, 64]. This degradation has been observed by transmission electron microscopy and even by direct observation of color changes of nanosheet dispersions from a black/dark green color to a cloudy white/brownish color [63]. Several prior studies have explored the issue of MXene oxidation. Our group recently observed that the oxidation rate varies widely depending on the surrounding media; specifically, the oxidation rates were substantially higher in aqueous phases compared to organic solvents, air, and solid media [46]. Maleski *et al.* also reported evidence showing that organic solvents can mitigate or slow MXene degradation compared to water [66]. Reactive molecular dynamics simulations suggest that the $Ti_3C_2T_x$ oxidation rate depends on both temperature and available oxidant concentration [83]. Prior studies have also indicated that the oxidation starts at the MXene edges and defects. The as-formed metal oxide nanocrystals can then develop throughout the MXene flake by nucleation and growth [3, 64]. It is noteworthy that MXenes with multilayered/stacked structures are less prone to oxidation than individual nanosheets due to the stacked structure's lower surface-to-volume ratio; even so, Mashtalir *et al*. and Habib *et al*. observed oxidation of multilayer stacks over the course of several days indicated by the rapid appearance of titanium dioxide and the dramatical decrease in electrical conductivity [45, 46]. In the individual nanosheet form, MXenes typically show better electrical performance, colloidal stability and processability but lower oxidation stability compared to multilayered MXene clay [46, 84]. Zhang *et al.* studied the degradation of delaminated $Ti_3C_2T_x$ colloidal solutions stored in open vials and concluded that $Ti_3C_2T_x$ MXenes can severely oxidize and degrade after 15 days [64]. Thus, strategies to preserve MXene nanosheets and avoid oxidation are critical, for both MXene nanosheets in dispersions and stacked MXenes in clays or bucky paper films.

Only a handful of studies have suggested strategies for mitigating $Ti_3C_2T_x$ oxidation, mostly centering on the restriction of oxygen exposure at low temperature. Anasori *et al.* mentioned that MXenes are more stable in oxygen-free degassed water or in dry air and that light exposure can accelerate the oxidation [3]. Zhang *et al.* proposed the storage of degassed $Ti_3C_2T_x$ aqueous dispersions in hermetic argon-filled containers at 5 °C [64]. However, they reported that oxidation still occurs at those conditions, but at slower rate. It is noteworthy that oxygen solubility is quite low (around 8 mg/L at 25 °C), so it is difficult to attribute oxidation solely to dissolved oxygen and water itself is likely play a major role in oxidation [46, 64, 65]; we explore this possibility in further detail below. Other techniques to slow or prevent oxidation include freezing and freeze-drying MXenes under vacuum [46]. Wu *et al.* proposed a carbon nanoplating technique to modify Ti_3C_2 MXene surface for inhibiting oxygen diffusion [78]. Despite these efforts, effective techniques to eliminate or restrict the oxidation of MXene nanosheets remain elusive, particularly in the dispersed aqueous state.

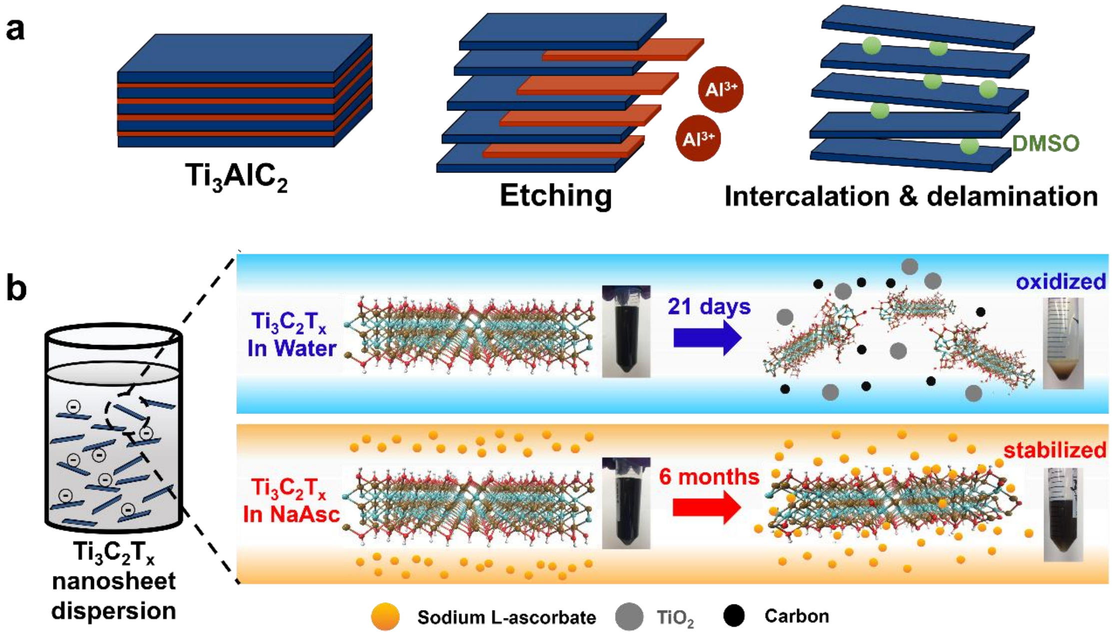

Figure 2-2 Schematics of shelf-stable $Ti_3C_2T_x$ nanosheet dispersion enabled by the antioxidant sodium L-ascorbate (NaAsc). (a) Schematic representation of $Ti_3C_2T_x$ nanosheet synthesis: Aluminum (Al) layer is removed from the parent Ti_3AlC_2 by acid etching, and the resulting multilayer MXene clay was intercalated by DMSO and delaminated by sonication. (b) Shelf-stable $Ti_3C_2T_x$ nanosheets stabilized by sodium L-ascorbate: The $Ti_3C_2T_x$ MXene nanosheets were stored both in deionized water and sodium L-ascorbate (NaAsc) solution. Without antioxidant, the $Ti_3C_2T_x$ oxidizes and degrades to form TiO_2 and carbon. Sodium L-ascorbate shields the nanosheet from being severely oxidized. The $Ti_3C_2T_x$ retained its as-prepared appearance after 6 months; however, the appearance of colloidal $Ti_3C_2T_x$ nanosheets stored in water was completely changed. Reprinted with permission from reference[75], Copyright 2019 Elsevier Ltd.

Here, we hypothesize that an antioxidant added to the aqueous MXene dispersion will preserve $Ti_3C_2T_x$ nanosheets by restricting oxidation and thus extending shelf life (shown schematically in **Figure 2-2**). To this end, we use sodium L-ascorbate, which is widely available and has been used in food and pharmaceutical industries as a preservative or antioxidant. We show that the chemical composition, 2D layered structure, and colloidal stability of $Ti_3C_2T_x$ nanosheets are retained even after 21 days when stored in sodium L-ascorbate stabilized dispersions, in stark contrast to those stored for the same duration as the $Ti_3C_2T_x$/water dispersions. Reactive molecular dynamics (ReaxFF) simulations are also used to probe the mechanism of these interactions between $Ti_3C_2T_x$ nanosheets and sodium L-ascorbate that led to the stabilization of $Ti_3C_2T_x$ nanosheets.

2.3. Materials and methods

2.3.1. Sample preparation

Synthesis of Ti_3AlC_2 MAX phase

Ti_3AlC_2 MAX phase was synthesized from Ti (with an average particle size of 44 μm and 99.5% purity), Al (with an average particle size of 44 μm and 99.5% purity), and TiC (with an average particle size of 2–3 μm and 99.5% purity) powders, which were weighed and mixed at the ratio of Ti/Al/C = 3.0:1.2:1.8. All chemicals were used as received from Alfa Aesar (MA, USA). To ensure the homogeneity of the blends, we mixed Ti, Al, and TiC powders in a laboratory ball mill filled with zirconia beads rotating at the speed of 300 rpm for 24 h. The bulk high-purity Ti_3AlC_2 samples were synthesized by sintering the powder mixture in a pressurized chamber of a pulsed electric current system at pressure of 50 MPa and temperature of 1,510 °C for 15 min. After sintering, the bulk Ti_3AlC_2 samples were drill milled. The drill-milled MAX phase was sieved to obtain the powder with particle size less than 45 μm.

Synthesis of $Ti_3C_2T_x$ MXene clay

$Ti_3C_2T_x$ MXene clay was obtained by etching the Al layer from the MAX phase following a wet etching method described by Ghidiu *et.al.* [38] First, 50 mL of 6 M hydrochloric acid (HCl) solution was prepared by diluting the concentrated HCl (37% [w/w], ACS reagent, Sigma-Aldrich) with deionized water. The 50 mL of 6 M HCL solution and 3.3 g of lithium fluoride (LiF) (with the purity of 98%+, Alfa Aesar) were mixed using a magnetic stir bar in a polytetrafluoroethylene (PTFE) bottle until all LiF was dissolved. The solution of HCl and LiF was heated to 40°C. Five grams of as-prepared MAX powder was slowly added into the solution over 15 min to prevent overheating (due to large exotherm of the etching reaction). The mixture was continuously agitated and reacted for 45 h. The suspension was then centrifuged, and the supernatant (which contained the unreacted HF and water-soluble salt ions) was removed. Deionized water was used to wash the MXene clay in the sediments. The dispersion was then vigorously shaken and centrifuged to remove the water effluent. This step was repeated several times until the pH of the water effluent reached a minimum value of 6.

Synthesis of $Ti_3C_2T_x$ MXene nanosheet dispersion

As-prepared $Ti_3C_2T_x$ MXene clay was intercalated with dimethyl sulfoxide (DMSO) (>99.5%, Sigma-Aldrich) and then bath sonicated to exfoliate into nanosheets.[33] One milliliter of DMSO was added to disperse every 60 mg of $Ti_3C_2T_x$ MXene clay. The MXene clay was intercalated at room temperature for 20 h with continuous magnetic stirring. After the intercalation, DMSO was removed by 3-4 cycles of solvent exchange with deionized water. The aqueous MXene clay dispersion was bath sonicated for 1 h to delaminate the multilayered MXene structures. The delaminated dispersion was centrifuged at 3,500 rpm for 1 h to crash out and separate the unexfoliated MXenes and other heavier components. The supernatant collected was the $Ti_3C_2T_x$ nanosheet dispersion. The deionized water used in the steps described above had been purged with argon gas for at least 1 h to remove the dissolved oxygen to the maximum extent. A concentration of 6.06 mg/mL for the delaminated $Ti_3C_2T_x$ nanosheet dispersion was determined by dividing the weight of freeze-dried nanosheets by the volume of MXene dispersion used for freeze-drying. 30 mL of the $Ti_3C_2T_x$ nanosheet dispersion was frozen in liquid nitrogen and freeze-dried for at least 3 days to remove the moisture. The dried nanosheets were weighed by an electronic balance with an accuracy of 0.1 mg. The lateral size of the delaminated nanosheets is around 0.5-5 μm, verified by transmission electron microscopy. [22]

Dilution of MXene nanosheet dispersion

For every 0.1 mL of as-prepared $Ti_3C_2T_x$ nanosheet dispersion, premixed NaAsc stock solution was added to make a 100-mL dispersion with a NaAsc concentration of 1 mg/mL. Deionized water diluted nanosheet dispersions were prepared in the same way for reference purposes. The concentration of NaAsc in the diluted dispersion was maintained at 1 mg/mL for maintaining the MXene colloidal stability.

Vacuum filtration to make buckypapers

The macro-assemblies of layered $Ti_3C_2T_x$ nanosheets were made by vacuum filtration of MXene dispersion using Polyethersulfone Membrane (Pall Laboratory). The MXene nanosheets were pretreated by antioxidants such as sodium L-ascorbate, tannic acid, and ascorbic acid at desired concentrations. The filtered films were then vacuum dried after filtration at 40°C for 12 h.

2.3.2. Characterization methods

X-Ray diffraction (XRD)

XRD patterns of dried $Ti_3C_2T_x$ were obtained using Bruker D8 powder X-ray diffractometer fitted with LynxEye detector, in a Bragg Brentano geometry with CuKα (λ = 1.5418 Å) radiation source. The X-ray scan was performed with a step size of 0.02° and a scan rate of 1.5 s per step. The $Ti_3C_2T_x$ samples were freeze-dried before the XRD measurements. A zero-background sample holder was used in all the tests.

Dynamic light scattering (DLS)

The average hydrodynamic diameters of aqueous $Ti_3C_2T_x$ nanosheets were determined at ambient temperature by DLS at a scattering angle of 90° using a Zetasizer Nano ZS90 from Malvern Instruments (UK). The colloidal aqueous dispersion of $Ti_3C_2T_x$ nanosheets was diluted to a concentration of around 0.006 mg/mL before measurements to ensure consistency. Each test was repeated at least six times, and an average value was derived to ensure accuracy.

ζ-Potential measurement

ζ-Potential changes of $Ti_3C_2T_x$ nanosheets in water and NaAsc solution were probed at ambient temperature using the Zetasizer Nano ZS90 from Malvern Instruments and the appropriate capillary cell, DTS 1070, from Malvern Instruments. The colloid of $Ti_3C_2T_x$ nanosheets was diluted to a concentration around 0.006 mg/mL before measurements to ensure consistency. Each test was repeated at least six times and an averaged value was derived to ensure accuracy.

X-Ray photoelectron spectroscopy (XPS)

The surface chemistry of as-prepared and stored $Ti_3C_2T_x$ nanosheets was probed using an Omicron X-ray photoelectron spectrometer employing a Mg-sourced X-ray beam to irradiate the sample surface. The emitted photoelectrons from the sample surface were collected by a 180° hemispherical electron energy analyzer. A takeoff angle of 40° between sample surface and the path to the photoelectron collector was used in all measurements. During all scanning, charge neutralization by a dual-beam charge neutralizer was performed to irradiate the low-energy electrons to eliminate the binding energy (BE) shifts in the recorded spectra. Samples for XPS measurements were prepared by repeatedly drop-casting the $Ti_3C_2T_x$ dispersion onto hydrophilic silicon wafer, which was pretreated in an oxygen plasma cleaner. The samples were then dried under vacuum at 40°C for 12 h to prevent any outgassing. High-resolution spectra of Ti 2p, C 1s, O 1s, and F 1s were recorded at a pass energy (constant analyzer energy) of 30.0 eV with a step size of 0.05 eV.

Component peak fitting and quantification of the spectra were carried out using CasaXPS curve fitting software (version 2.3.16). Prior to peak fitting, a region was created for each entry. The background contributions were subtracted by applying a Shirley type background function. All spectra were charge calibrated based on the adventitious C 1s component (C-C) with a BE of 284.8 eV. Peak fitting was performed using symmetric Gaussian-Lorentzian curves (GL30). A few rigid constraints were imposed during peaking fitting to ensure reasonable and consistent results with the literature. First, for all $2p^{3/2}$ and $2p^{1/2}$ components in the titanium spectra, the peak area ratios were constrained to be fixed exactly at 2:1 ($2p^{3/2}$:$2p^{1/2}$) as given by quantum mechanics selection rules. In addition, the full width at half maximum (FWHM) of each component was restricted. The same component present in each sample was expected to exhibit only small variations in the FWHM. The BE and delta values for $2p^{3/2}$-$2p^{1/2}$ splitting for each component were constrained according to a series of literature and NIST XPS database reported values. [35, 41, 72, 85] The standard deviations for the fitted components were computed using the Monte Carlo error analysis built into the CasaXPS software. The standard deviations of the fittings were found to range between 0.1% and 5.0% for all stated components.

The Ti 2p region was deconvoluted into five pairs of the $2p^{3/2}$ and $2p^{1/2}$ spin-orbit split components, which were assigned to Ti-C, Ti(II), Ti(III), Ti(IV), and Ti-F, respectively. Note that for the MXene sample stored in water, since the atomic percentage of fluorine became very low, the Ti-F curves were neglected in the fitting. The C 1s spectrum was deconvoluted into six components, namely C-C, C-Ti-T_{x1}, C-Ti-T_{x2}, CH_x/CO, C-OH, and COO, respectively. The O 1s spectrum was deconvoluted into five components, namely TiO_2, C-Ti-O_x, C-Ti-$(OH)_x$, Al_2O_3, and H_2O. The F 1s spectrum was deconvoluted into two components: AlF_x and C-Ti-F_x.

Scanning electron microscopy (SEM)

The morphologies of $Ti_3C_2T_x$ nanosheets after storage were observed with an FEI Quanta 600 field-emission scanning electron microscope. For imaging, the vigorously mixed dispersions of stored $Ti_3C_2T_x$ nanosheets were drop-casted on hydrophilic silicon wafers pretreated with oxygen plasma and then vacuum dried. The acceleration voltage used in the imaging was 2 kV.

Conductivity measurement

The electrical conductivity was measured using four-point resistivity probe powered by Keithley Instruments models, one 2000, one 6221, and two 6514. MXene films used for the conductivity measurements were prepared by vacuum filtering the $Ti_3C_2T_x$ nanosheet dispersions as described above.

Simulation setup*

ReaxFF is a reactive force-field molecular dynamics simulation technique that uses the bond-order concept to compute the interaction between atoms at each time step. Compared with other non-reactive atomistic simulation techniques, ReaxFF provides a smooth transition between the non-bonded states and the bonded states. In general, the total energy of the system in ReaxFF is described by several contributions and can be summed up as follows:

$$E_{system} = E_{bond} + E_{over} + E_{under} + E_{val} + E_{tors} + E_{vdW} + E_{Coulomb} + E_{lp} + E_{H\text{-}bond} \quad (1)$$

The total energy of the system (E_{system}) consists of bond-order dependent or covalent interactions and non-bonded interactions. Bond-order-dependent terms include the bond energy (E_{bond}), over-coordination (E_{over}), under-coordination (E_{under}), and hydrogen bond ($E_{H\text{-}bond}$) interactions. Energy penalty terms include torsion angle energy (E_{tor}), valence angle energy (E_{val}), and lone pair energy (E_{lp}), whereas the non-bonded interactions are van der Waals (E_{vdW}) and Coulomb energy ($E_{Coulomb}$). At every time step,

---

[*] The simulation work and paragraph were completed and written by Dr. Aniruddh Vashisth.

bond order is calculated between all pairs of atoms from their interatomic distances and updated. Also, non-bonded interactions such as van der Waals and Coulomb terms are considered for all atom pairs. Force field parameters describing energy terms are typically optimized by quantum mechanics calculations. The force field used in the current investigation has been fitted for Ti and C based MXene structure and has shown good correlation with experiments [86].

Two systems were generated, first with 200 water molecules and a single $Ti_3C_2(OH)$structure and second system had 50 NaAsc molecules was added to it. The water and the NaAsc molecules were randomly distributed around the MXene structure. The density of both the system was kept at ~1 g/cc. NVT simulations were carried out 500 ˚C (773 K) with 0.25 fs time-steps for a total time of 25 ps using LAMMPS [87]. Simulations were carried at elevated temperatures as compared to the experiments to accelerate the kinetics of the reactions. Although parameters for Ti-F are defined in the current force field [86], F group were neglected as Na-F force field parameters were not well defined. Radial distribution function (*rdf*) calculations were carried out using Visual Molecular Dynamics (VMD) [88] for the last 10 ps of the oxidation simulations.

2.4. Results and discussion

2.4.1. Sodium L-ascorbate promotes MXene stability against oxidation and aggregation

Colloidal $Ti_3C_2T_x$ nanosheet dispersions were diluted with a pre-mixed aqueous solution of sodium L-ascorbate (NaAsc), which acts as an antioxidant and ensures a reducing environment, to obtain a concentration of 6.1 x 10^{-3} mg/mL MXene and 1 mg/mL NaAsc. The NaAsc-stabilized dispersions were stored for 21 days in closed bottles at ambient temperature. No degassing was practiced before or during the storage, such that the MXene colloidal solution was in contact with the bottle's headspace (air). Control dispersions were made by diluting $Ti_3C_2T_x$ MXene colloid with deionized (DI) water to the same final concentration and stored at identical conditions for 21 days.

X-ray diffraction (XRD) patterns of (i) dried $Ti_3C_2T_x$ nanosheets previously stored in 1 mg/mL sodium L-ascorbate solution after 21 days were compared to those of (ii) as-prepared $Ti_3C_2T_x$ nanosheets, (iii) $Ti_3C_2T_x$ nanosheets previously kept in deionized water, and (iv) the parent Ti_3AlC_2 MAX phase in **Figure 2-3**. After etching, intercalation and further delamination, the pronounced (002) peak shifts from an 2θ angle of 9.7° that is typical for the parent MAX phase to a lower 2θ value around 6.5°, which is typical for $Ti_3C_2T_x$ nanosheets [89]. The (002) peak tends to broaden gradually in the processing stages, which most likely suggests an increased d-spacing and decreased thickness of $Ti_3C_2T_x$ layers [89, 90]. After being stored in sodium L-ascorbate solution for 21 days, the colloidal $Ti_3C_2T_x$ nanosheets retained their pronounced (002) peak at a 2θ angle around 6.5°. However, the (002) peak disappeared completely from the XRD spectrum for $Ti_3C_2T_x$ stored in deionized water, indicating the total oxidation of crystalline MXene to an amorphous structure. Collectively, these XRD results suggest that the crystalline structure of $Ti_3C_2T_x$ nanosheets can be effectively retained by introducing an antioxidant.

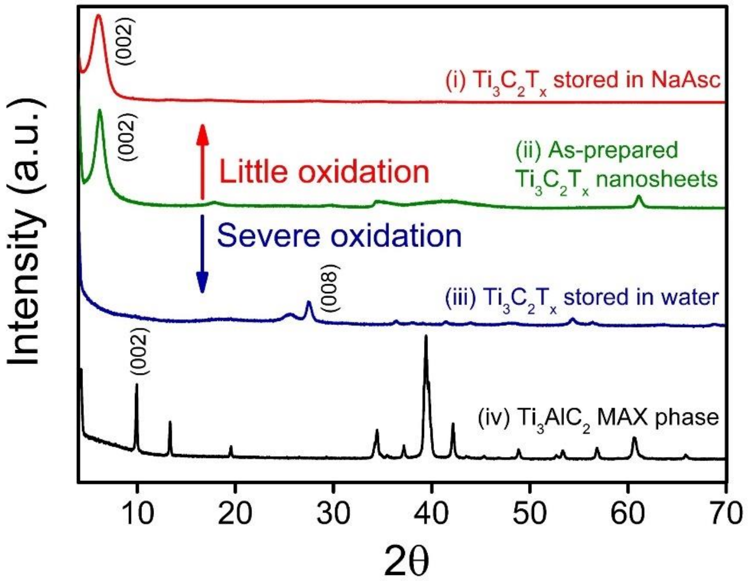

Figure 2-3 Crystalline structural properties of Ti_3AlC_2 and $Ti_3C_2T_x$ characterized using X-ray diffraction (XRD). XRD patterns for $Ti_3C_2T_x$ nanosheets stored for 21 days in deionized water (i) with and (iii) without sodium L-ascorbate, exhibiting little and severe oxidation, respectively, as compared to (ii) as-prepared $Ti_3C_2T_x$ nanosheets. All nanosheets were obtained after etching, intercalation, and delamination. (iv) XRD pattern for the Ti_3AlC_2 MAX phase. Samples used for XRD were prepared by vacuum filtration, followed by vacuum-drying at 40 °C for 12 hours. Reprinted with permission from reference[75], Copyright 2019 Elsevier Ltd.

To detect changes in colloidal stability caused by oxidation, the hydrodynamic size distributions (shown in **Figure 2-4a**) of $Ti_3C_2T_x$ dispersions were measured using dynamic light scattering (DLS). After six days, the average size of the material dispersed in water increased dramatically due to nanosheet agglomeration (corroborated by ζ potential measurements below). At around day 15, the average hydrodynamic diameter reached a maximum value of nearly 2200 nm. However, after 15 days, the hydrodynamic diameter declined; this is likely associated with further oxidation and degradation to TiO_2. In contrast, samples dispersed in the sodium L-ascorbate solution exhibited a much more constant size distribution over time. The average hydrodynamic diameter based on intensity was found to be invariant at around 500 nm, which suggests that introducing sodium L-ascorbate is an effective way to retain the lateral size of $Ti_3C_2T_x$ nanosheets, thus limiting oxidation and maintaining colloidal stability.

The colloidal stability of $Ti_3C_2T_x$ dispersions was further examined by characterizing ζ potential over time (**Figure 2-4b**). The surface of a $Ti_3C_2T_x$ nanosheet is negatively charged due to the terminal groups (i.e. -OH, -O, -Cl and -F). The change in ζ potential reflects a decrease in the amount of surface charge, which is caused by the oxidation of $Ti_3C_2T_x$ nanosheets. Nanosheets stored in sodium L-ascorbate solution generally maintained a stable ζ potential (below -35 mV) during the 21-day storage. In contrast, a significant weakening of ζ potential was observed for nanosheets stored in deionized water even during the first day, which indicates a rapid loss of colloidal stability.

The $Ti_3C_2T_x$ nanosheet dispersions stored in 1 mg/mL sodium L-ascorbate solution and water after 21 days are compared in **Figure 2-4c** and **2-4d**, respectively. In addition, aggregates were observed after only a few days in the water dispersion. When stored in deionized water without antioxidant, the $Ti_3C_2T_x$ MXene nanosheet dispersion shows a dramatic color change from day 0 to day 21: the dispersion became lighter on visual inspection as most $Ti_3C_2T_x$ nanosheets oxidized into TiO_2 and C. Visible precipitated clusters of $Ti_3C_2T_x$ MXene nanosheets were also observed during the storage. In contrast, the aqueous $Ti_3C_2T_x$ MXene nanosheet dispersion stored in sodium L-ascorbate exhibited little color change or aggregation.

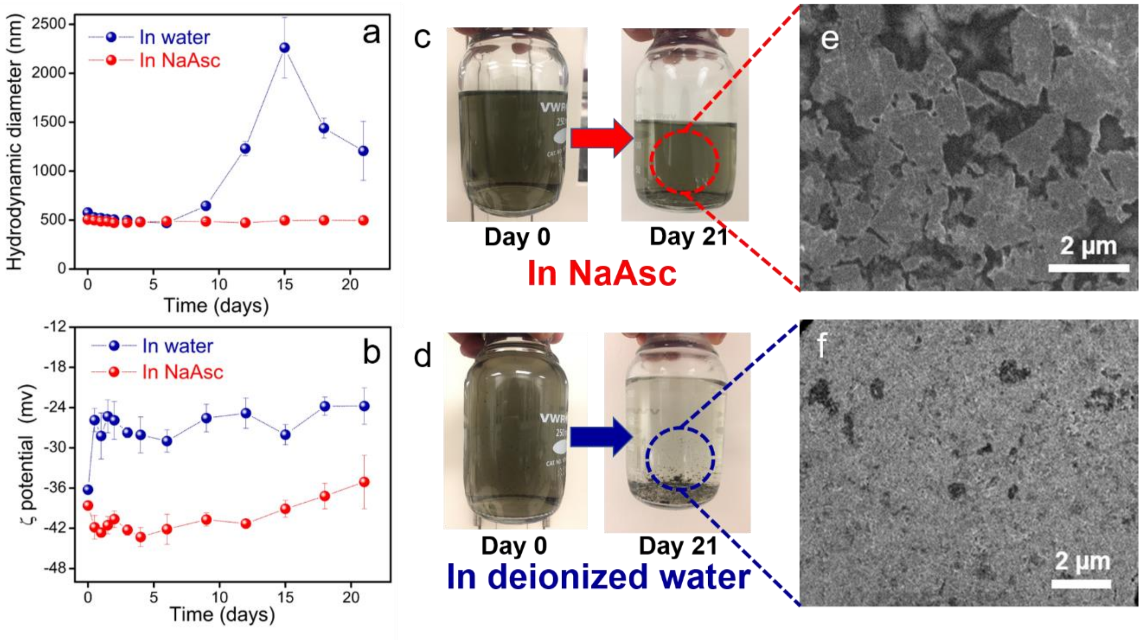

Figure 2-4 Colloidal stability and morphology of shelf-stable $Ti_3C_2T_x$ nanosheets. (a) The average hydrodynamic diameter of $Ti_3C_2T_x$ nanosheets measured as a function of time for dispersions in deionized water and 1 mg/mL sodium L-ascorbate solution. (b) Time evolution of ζ potential of $Ti_3C_2T_x$ dispersions in deionized water and 1 mg/mL sodium L-ascorbate solution (See also Figure 2-5). (c-d) Corresponding images of the dispersions at Day 0 and Day 21 are shown. (e) SEM image of $Ti_3C_2T_x$ nanosheets after being stored in 1 mg/mL sodium L-ascorbate solution for 21 days indicates that the nanosheets retain their morphology. (f) SEM image of drop-cast $Ti_3C_2T_x$ nanosheets after being stored in deionized water for 21 days shows an amorphous and dense structure. Reprinted with permission from reference[75], Copyright 2019 Elsevier Ltd.

The effectiveness of sodium L-ascorbate in protecting the MXene structure was analyzed by characterizing the final morphologies of the stored $Ti_3C_2T_x$ nanosheets using scanning electron microscopy (SEM). **Figure 2-4e** reveals that the morphology of the nanosheets was successfully retained for the materials preserved in sodium L-ascorbate solution after 21 days. However, the $Ti_3C_2T_x$ previously stored in water exhibited an amorphous TiO_2 structure, displayed in **Figure 2-4f**. The typical nanosheet morphology could not be observed in this sample; instead, a clay-like paste is seen.

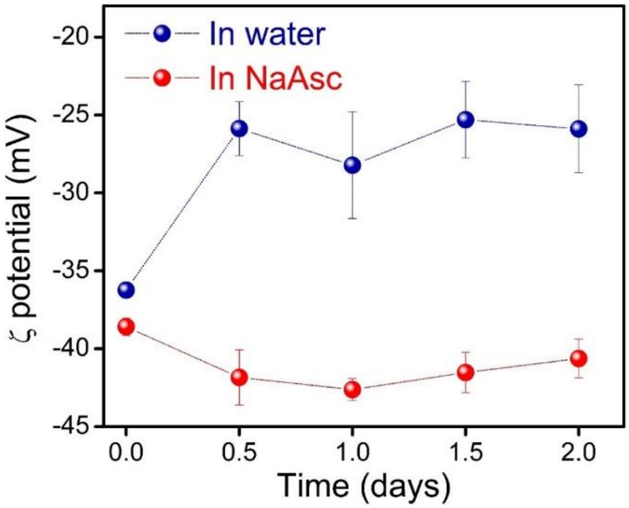

Figure 2-5 Zeta (ζ) potential changes of $Ti_3C_2T_x$ nanosheets dispersed in deionized water and 1 mg/mL sodium L-ascorbate solution (NaAsc) in the first 2 days of storage. A dramatic increase of ζ potential of $Ti_3C_2T_x$ MXene nanosheets/water dispersion is observed in the first 12 hours; in contrast, NaAsc stabilizes the colloidal dispersion and shows a relatively stable ζ potential. Reprinted with permission from reference[75], Copyright 2019 Elsevier Ltd.

The chemical composition of $Ti_3C_2T_x$ nanosheets was characterized using X-ray photoelectron spectroscopy (XPS). The presences of titanium (Ti), carbon (C), oxygen (O) and fluorine (F) in as-prepared and stored $Ti_3C_2T_x$ were confirmed in the survey spectra (**Figure 2-6**). High-resolution spectra of Ti 2p, C 1s, O 1s, and F 1s are displayed in **Figure 2-7a**. Ti 2p spectra were deconvoluted into Ti^+(Ti-C and Ti-F), Ti^{2+}, Ti^{3+} and Ti^{4+} (TiO_2) (**Figure 2-8**). For both the as-prepared $Ti_3C_2T_x$ and the $Ti_3C_2T_x$ stored in sodium L-ascorbate solution, the TiO_2 (Ti^{4+}) comprises relatively low atomic fractions in the Ti 2p region (around 6.1 at. % and 13.1 at. %, respectively). However, for the sample stored in water for 21 days, the TiO_2 (Ti^{4+}) comprises a much higher atomic fraction, around 64.6

at. % of the photoemission in Ti 2p region. This can be confirmed by the high-intensity peak around 459 eV which is evidence of the severe oxidation of $Ti_3C_2T_x$ MXene.

The XPS peaks of the Ti 2p region give important insights into the effect of sodium L-ascorbate on the oxidation states of titanium within the $Ti_3C_2T_x$ nanosheets. The relative atomic compositions of Ti $^{4+}$, Ti $^{3+}$, Ti $^{2+}$ and Ti^{+} species in aged aqueous $Ti_3C_2T_x$ dispersion (with and without antioxidant) are compared in **Figure 2-7b**. As expected, in the case of aging in water, we observe an increase in the relative composition of Ti species with higher oxidation states (*i.e.,* Ti $^{2+}$ and Ti $^{3+}$ are oxidized to Ti $^{4+}$, and Ti $^{+}$ is oxidized to Ti $^{2+}$ and Ti $^{3+}$). However, in the presence of sodium L-ascorbate, the chemical state transition from Ti $^{+}$ to Ti $^{2+}$/ Ti $^{3+}$ was inhibited; the increase of Ti $^{4+}$ with time was slow.

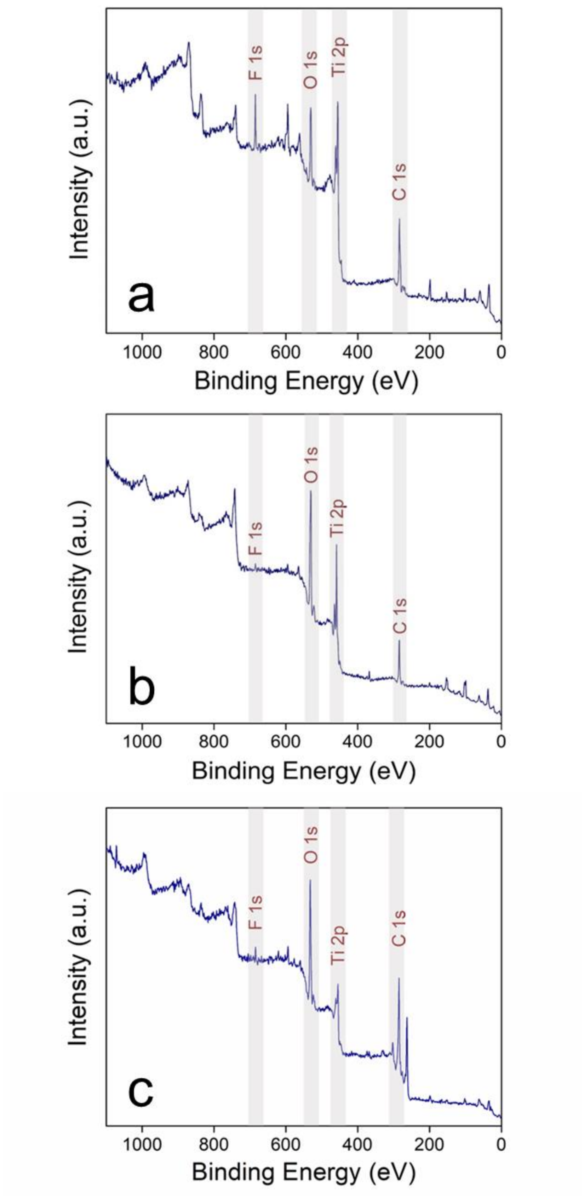

Figure 2-6 (a) XPS survey spectrum of as-prepared $Ti_3C_2T_x$ nanosheets dried after delamination labelled with characteristic peaks of Ti 2p, C 1s, O 1s, and F 1s. (b) XPS survey spectrum of the $Ti_3C_2T_x$ MXene nanosheets drop-cast and dried after being stored in deionized water for 21 days, labelled with characteristic peaks of Ti 2p, C 1s, O 1s, and F 1s. The F 1s peak is no longer prominent in this survey spectrum due to oxidation and degradation of the MXene structure. (c) XPS survey spectrum of the $Ti_3C_2T_x$ nanosheets dried after being stored in sodium L-ascorbate solution (1 mg/mL) for 21 days, labelled with characteristic peaks of Ti 2p, C 1s, O 1s, F 1s and Na 1s (from sodium L-ascorbate). Reprinted with permission from reference[75], Copyright 2019 Elsevier Ltd.

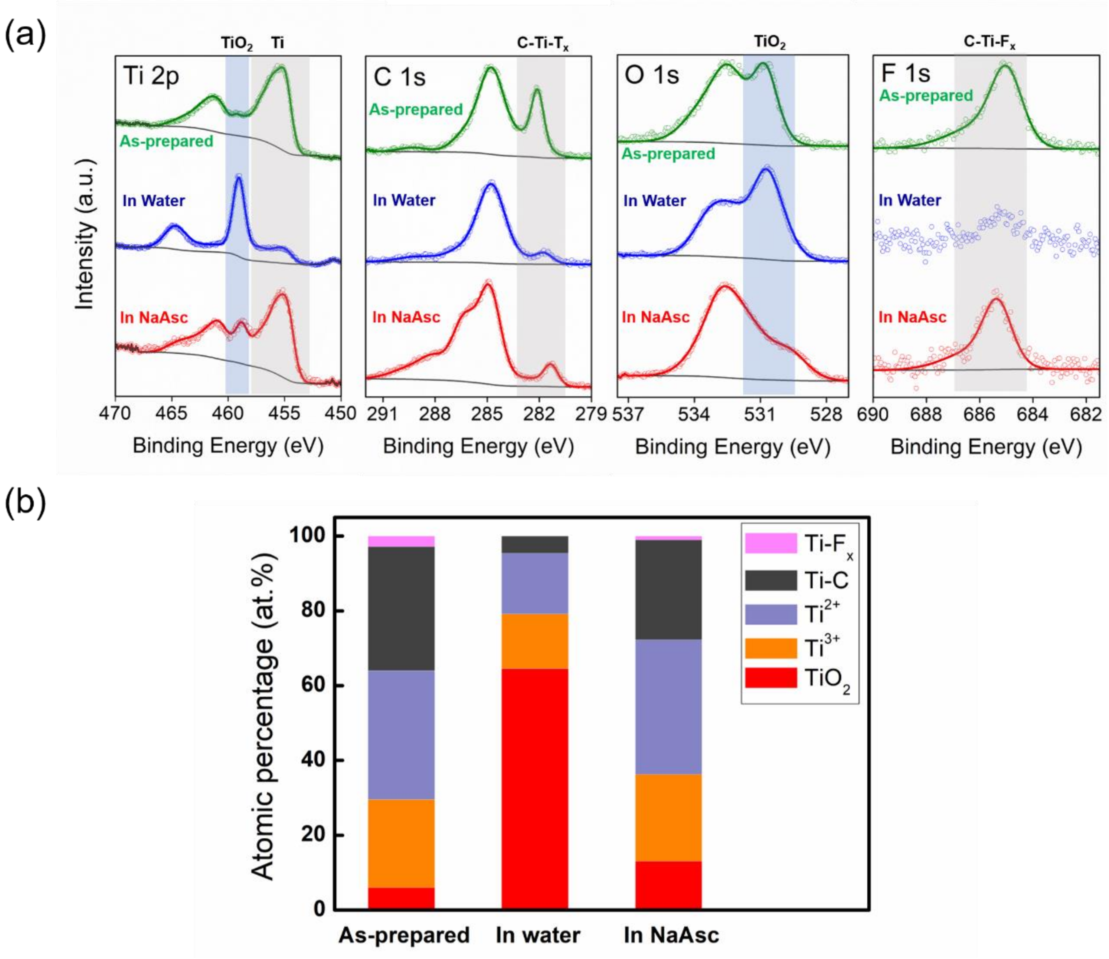

Figure 2-7 Chemical composition of as-prepared $Ti_3C_2T_x$ nanosheets and nanosheets stored after 21 days. (a) XPS spectra of Ti 2p, C 1s, O 1s and F 1s for as-prepared $Ti_3C_2T_x$ nanosheets, nanosheets stored in deionized water and, those stored in 1 mg/mL solution of sodium L-ascorbate after 21 days. Deconvolutions and associated binding energy (B.E.) values are listed in Table 2-1 to 2-3. The Ti 2p spectra shows that the peak corresponding to TiO_2 increased in intensity and that the Ti peak greatly decreased in intensity for the nanosheets dispersed in water when compared to as-prepared MXenes and those stored in NaAsc. This shows that the chemical composition of $Ti_3C_2T_x$ nanosheets was largely retained when sodium L-ascorbate was present. (b) XPS peak fitting results for the Ti 2p region for $Ti_3C_2T_x$ MXenes. The atomic percentages of TiO_2 (Ti^{4+}), Ti^{3+}, Ti^{2+}, Ti-C and C-Ti-F_x obtained from the deconvoluted Ti 2p region for as-prepared and stored $Ti_3C_2T_x$ nanosheets in water and sodium L-ascorbate solution (NaAsc). $Ti_3C_2T_x$ stored in water shows the highest percentage of TiO_2 due to severe oxidation. Sodium L-ascorbate inhibits oxidation; the TiO_2 fraction remains relatively much less-changed when compared to the sample stored in water. Reprinted with permission from reference[75], Copyright 2019 Elsevier Ltd.

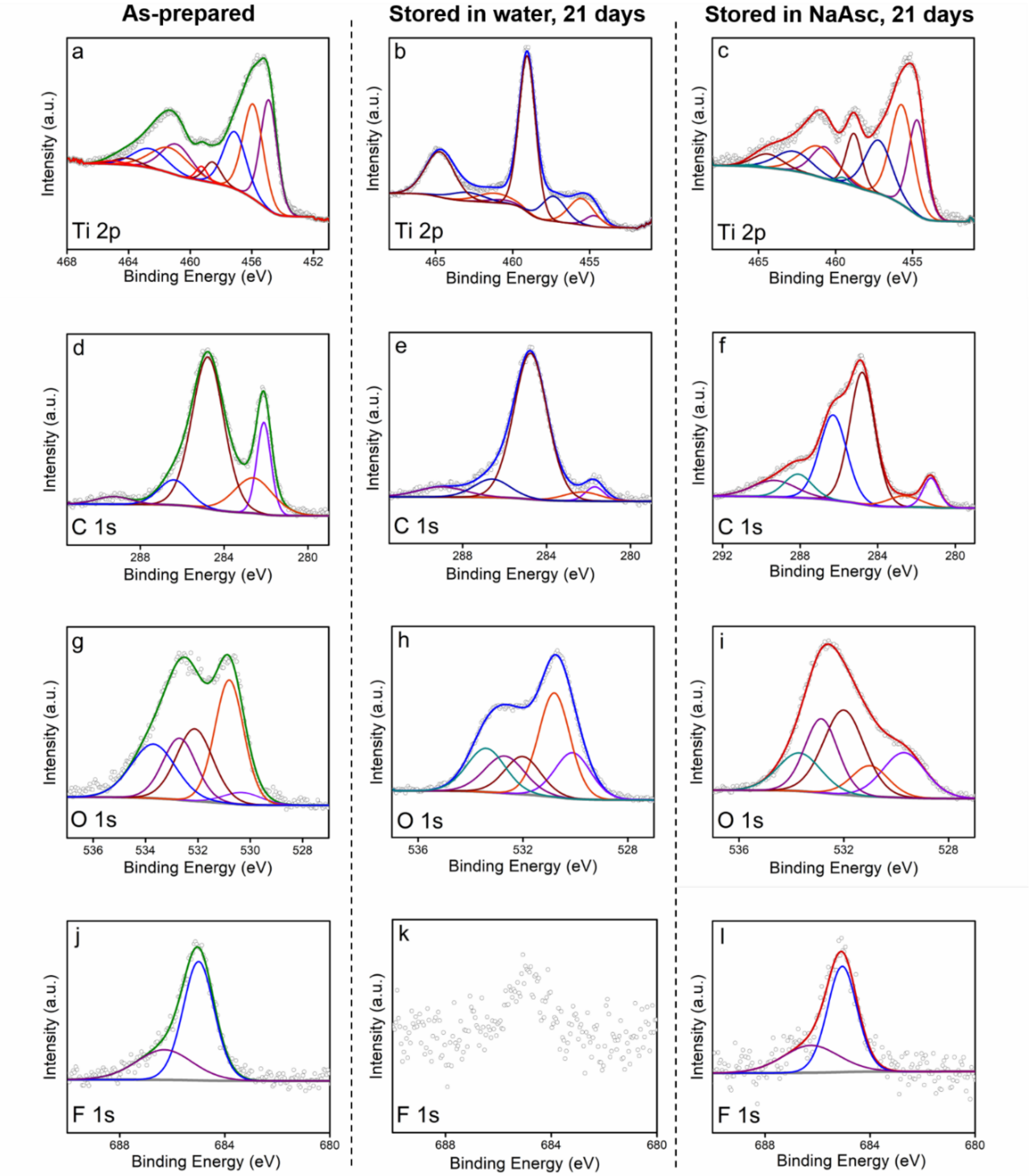

Figure 2-8 Component peak fittings of XPS spectra for as-prepared $Ti_3C_2T_x$ nanosheets and nanosheets after being stored in deionized water and sodium L-ascorbate solution (1 mg/mL) for 21 days. Reprinted with permission from reference[75], Copyright 2019 Elsevier Ltd.

Table 2-1 XPS peak fitting results for as-prepared $Ti_3C_2T_x$ MXenes. Reprinted with permission from reference[75], Copyright 2019 Elsevier Ltd.

Element	Element atomic%	Binding energy (BE) (eV)	Component name	Component atomic%	FWHM
Ti $2p_{3/2}$ ($2p_{1/2}$)	18.5	454.9 (460.9)	Ti-C	33.2	1.3 (2.3)
		455.9 (461.4)	Ti^{2+}	34.4	1.5 (2.9)
		457.1 (462.6)	Ti^{3+}	23.5	1.7 (2.6)
		458.5 (464.1)	TiO_2	6.1	1.2 (1.9)
		459.3 (465.1)	Ti-F_x	2.9	0.9 (1.9)
C 1s	52.3	282.1	C-Ti-T_x[a]	15.3	0.8
		282.6	C-Ti-T_x[a]	16.1	2.2
		284.8	C-C	56.6	1.8
		286.4	CH_x/CO	8.9	1.7
		289.3	COO	3.1	1.9
O 1s	22.4	530.3	TiO_2	4.1	1.7
		530.8	C-Ti-O_x	32.1	1.3
		532.1	C-Ti-$(OH)_x$	23.7	1.6
		532.7	Al_2O_3	18.5	1.5
		533.7	H_2O[b]	21.6	2.0
F 1s	6.8	685.0	C-Ti-F_x	68.9	1.4
		686.3	AlF_x	31.1	2.5

[a] T_x represents the terminal groups grafted on the $Ti_3C_2T_x$ MXene nanosheets. The peak corresponding to this bond is asymmetric, so it is represented by two symmetric peaks.

[b] Water molecules associated with terminal group -OH.

Table 2-2 XPS peak fitting results for $Ti_3C_2T_x$ MXene nanosheets after being stored in deionized water. Reprinted with permission from reference[75], Copyright 2019 Elsevier Ltd.

Element	Element atomic%	Binding energy (BE) (eV)	Component name	Component atomic%	FWHM
Ti $2p_{3/2}$ ($2p_{1/2}$)	14.0	454.7 (460.7)	Ti-C	4.6	1.3 (2.0)
		455.5 (461.1)	Ti^{2+}	16.2	1.9 (2.6)
		457.3 (462.9)	Ti^{3+}	14.6	1.8 (2.6)
		459.0 (464.7)	TiO_2	64.6	1.3 (2.2)
C 1s	40.0	281.7	$C\text{-}Ti\text{-}T_x$[a]	4.0	1.0
		282.3	$C\text{-}Ti\text{-}T_x$[a]	5.0	2.1
		284.8	C-C	73.8	1.9
		286.6	CH_x/CO	9.9	2.0
		289.0	COO	7.3	2.7
O 1s	45.8	530.1	TiO_2	17.2	1.6
		530.8	$C\text{-}Ti\text{-}O_x$	34.4	1.5
		532.0	$C\text{-}Ti\text{-}(OH)_x$	14.6	1.8
		532.7	Al_2O_3	16.1	1.8
		533.4	H_2O[b]	17.7	1.8
F 1s	0.2	N/A	N/A	N/A	N/A

[a] T_x represents the terminal groups grafted on the $Ti_3C_2T_x$ MXene nanosheets. The peak corresponding to this bond is asymmetric, so it is represented by two symmetric peaks.

[b] Water molecules associated with terminal group -OH.

Table 2-3 XPS peak fitting results for $Ti_3C_2T_x$ MXene nanosheets after being stored in sodium L-ascorbate solution (1 mg/mL). Reprinted with permission from reference[75], Copyright 2019 Elsevier Ltd.

Element	Element atomic%	Binding energy (BE) (eV)	Component name	Component atomic%	FWHM
Ti $2p_{3/2}$ ($2p_{1/2}$)	6.9	454.7 (460.7)	Ti-C	26.8	1.3 (2.0)
		455.7 (461.1)	Ti^{2+}	36.0	1.7 (2.8)
		457.2 (462.7)	Ti^{3+}	23.2	1.9 (2.8)
		458.8 (464.4)	TiO_2	13.1	1.2 (2.2)
		459.5 (465.5)	$Ti-F_x$	1.0	0.9 (1.5)
C 1s	63.6	281.2	$C-Ti-T_x$[a]	6.0	1.0
		282.6	$C-Ti-T_x$[a]	4.7	2.0
		284.8	C-C	42.1	1.5
		286.3	CH_x/CO	29.6	1.6
		288.1	C-OH[b]	8.3	1.7
		289.3	COO	9.3	2.6
O 1s	28.1	529.7	TiO_2	18.2	1.9
		531.0	$C-Ti-O_x$	10.7	1.7
		532.0	$C-Ti-(OH)_x$	32.5	1.8
		532.9	Al_2O_3	23.1	1.5
		533.7	H_2O[c]	15.5	1.9
F 1s	1.5	685.1	$C-Ti-F_x$	67.4	1.3
		686.3	AlF_x	32.6	2.5

[a] T_x represents the terminal groups grafted on the $Ti_3C_2T_x$ MXene nanosheets. The peak corresponding to this bond is asymmetric, so it is represented by two symmetric peaks. [b] NaAsc associated with MXene nanosheets. [c] Water molecules associated with terminal group -OH.

The electrical conductivity of the macro-assembly of layered $Ti_3C_2T_x$ nanosheets can also be used as an indicator of the degree of oxidation [46]. **Table 2-4** displays the changes in the electrical conductivities of MXene filtered films made from the as-prepared (day 0) and stored (day 21) $Ti_3C_2T_x$ nanosheets in sodium L-ascorbate solution and deionized water, respectively. The electrical conductivity for the MXene film comprised of as-prepared $Ti_3C_2T_x$ nanosheets ($3.2 \pm 0.3 \times 10^5$ S/m) was consistent with prior studies [90]. After storage in deionized water, the filtered MXene film conductivity dropped below 10^{-6} S/m. In contrast, the film made from $Ti_3C_2T_x$ stored in sodium L-ascorbate solution retained an electrical conductivity of $5.7 \pm 0.5 \times 10^4$ S/m, with a decrease of less than one order of magnitude. The relative electrical conductivity stability is evidence that sodium L-ascorbate protects the $Ti_3C_2T_x$ nanosheets from severe oxidation.

Table 2-4 Electrical conductivities of buckypapers made from as-prepared MXenes and stored $Ti_3C_2T_x$ MXenes in deionized water and 1 mg/mL sodium L-ascorbate solution. Reprinted with permission from reference[75], Copyright 2019 Elsevier Ltd.

No. of days	In deionized water (S/m)	In 1 mg/mL NaAsc (S/m)
0	$3.2 \pm 0.3 \times 10^5$	$2.2 \pm 0.2 \times 10^5$
21	$<10^{-6}$	$5.7 \pm 0.5 \times 10^4$

2.4.2. Oxidation prevention for dried $Ti_3C_2T_x$

Dried MXene nanosheets are also known to undergo oxidization when stored in ambient conditions [46]. With this in mind, we tested whether antioxidant-treated MXenes would resist oxidation in the dry form as powders or films. We prepared vacuum-filtered $Ti_3C_2T_x$ films that were made from colloidal nanosheet dispersions that had been pretreated several antioxidants, including sodium L-ascorbate, tannic acid, and ascorbic acid. **Figure 2-9** shows that the decrease of normalized electrical conductivity (σ/σ_0) can be substantially slowed by the antioxidants introduced in the pre-treatment steps; this indicates that the antioxidants alter oxidation chemistry not only in solution but also in the dried state. (The absolute electrical conductivity values can be found in **Figure 2-10**.) This technique can potentially make shelf-stable MXenes suitable for a variety of applications in the dry environment without substantial oxidation.

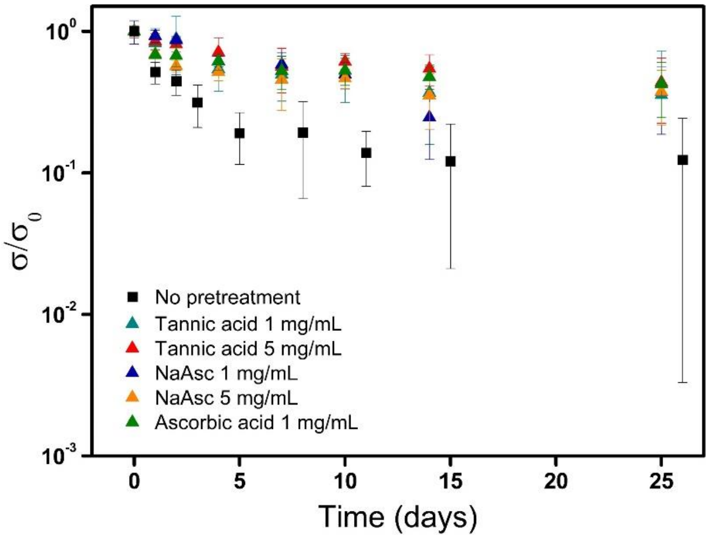

Figure 2-9 Normalized conductivity change over time for buckypaper made from $Ti_3C_2T_x$ pretreated by antioxidants. Conductivity changes were measured for dried filtered films made from $Ti_3C_2T_x$ nanosheets pretreated by various antioxidants. The drastic reduction of normalized electrical conductivity (σ/σ_0) due to oxidation was inhibited by the antioxidants. This acts as an evidence that antioxidants in general prevent oxidation of $Ti_3C_2T_x$ nanosheets in the dried form. (σ is the real-time conductivity (S/m), σ_0 is the initial conductivity of as-prepared $Ti_3C_2T_x$ film.) Reprinted with permission from reference[75], Copyright 2019 Elsevier Ltd.

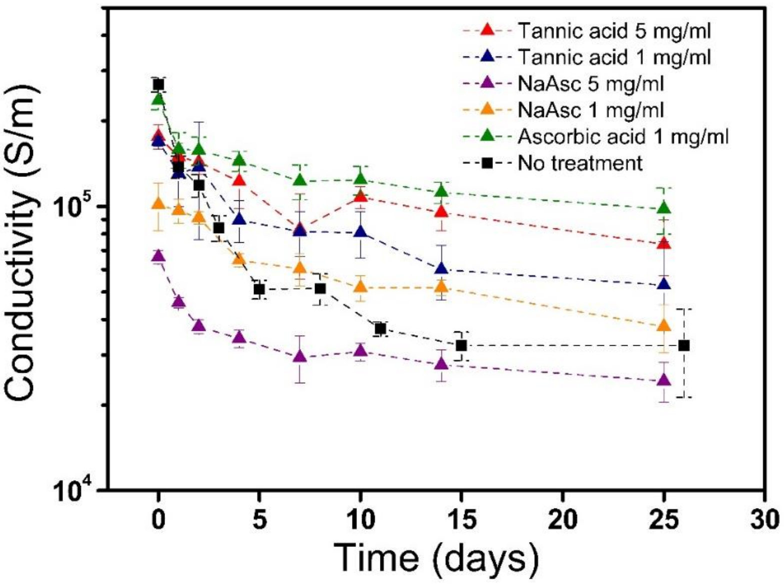

Figure 2-10 Conductivity changes were measured for dried films made from $Ti_3C_2T_x$ nanosheets pretreated by various antioxidants. The decreasing rates of the electrical conductivity for buckypapers made from pretreated nanosheets are much lower than the sample made from pristine nanosheets. The differences among the initial conductivities were possibly caused by the effects of slight antioxidant attachments and antioxidant adsorption due to the electronegativity of $Ti_3C_2T_x$ nanosheets. Reprinted with permission from reference[75], Copyright 2019 Elsevier Ltd.

2.4.3. Molecular simulations show that sodium L-ascorbate associates with $Ti_3C_2T_x$[†]

ReaxFF molecular simulations were performed to elucidate the mechanism for sodium L-ascorbate and $Ti_3C_2T_x$ interactions. Two systems were examined: (i) a $Ti_3C_2T_x$ nanosheet surrounded by water molecules, and (ii) a $Ti_3C_2T_x$ nanosheet with randomly placed sodium L-ascorbate and water molecules. Both systems had a density of ~1 g/cm^3. The starting nanosheet was populated with -OH terminal groups. The -F terminal groups were not considered for simulations because the current force field does not have well-

---

[†] This simulation work was completed by Dr. Aniruddh Vashisth.

defined Na-F interactions. ReaxFF simulations were carried out at 500 °C with 0.25 fs time-steps for 25 ps using Large-scale Atomic/Molecular Massively Parallel Simulator (LAMMPS) [87] and using the ReaxFF force field from Osti *et al.* [86]. It is computationally unfeasible to simulate the chemical kinetics of 21 days, therefore the common method is to carry out the simulations at a higher temperature as compared to the experiments to accelerate the kinetics of the reaction [83].

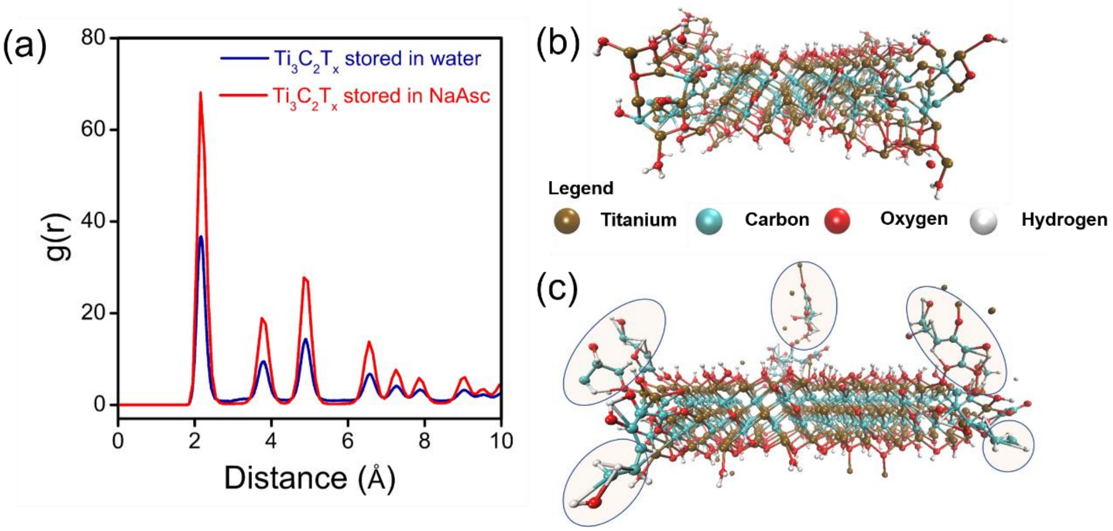

Figure 2-11 Reactive molecular dynamics simulation (ReaxFF) of shelf-stable $Ti_3C_2T_x$ MXenes. (a) The radial distribution functions of Ti-C bonds obtained by ReaxFF are shown for stored $Ti_3C_2T_x$ nanosheets. A higher peak intensity at 2.1 Å was obtained for nanosheets stored in sodium L-ascorbate, suggesting a higher level of stability against oxidation. (b-c) Final molecular configurations of $Ti_3C_2T_x$ nanosheet after 25 ps simulation of oxidation in water and oxidation in the presence of NaAsc and water. L-ascorbate group associates with the nanosheet (highlighted) restricting further reactions between the nanosheets and water molecules. Reprinted with permission from reference[75], Copyright 2019 Elsevier Ltd.

In order to quantify the stability of the $Ti_3C_2T_x$ structures after oxidation, radial distribution function (*rdf*) calculations were carried out for the Ti-C atoms; these only consider the carbon atoms within the MXene structure. The radial distribution function, *g(r)*, gives the probability of finding a particle at a distance *r* from another particle in 3-D space. The *rdf* calculations were carried out for the last 10 ps of the simulations. Our results indicate substantially less oxidation when NaAsc is present in the system. The Ti-C *rdf* calculations show a peak at 2.1 Å (**Figure 2-11a**), which is characteristic for a crystalline $Ti_3C_2T_x$ structure. The Ti-C *rdf* peak intensity at 2.1 Å for the NaAsc system is higher than the water system, suggesting a more stable $Ti_3C_2T_x$ structure in the presence of NaAsc. The experimental XPS results also support this finding (**Table 2-2** and **Table 2-3**), as the atomic percentage of Ti-C is higher in $Ti_3C_2T_x$ stored in NaAsc as compared to $Ti_3C_2T_x$ stored in water.

The stability of the $Ti_3C_2T_x$ nanosheet (**Figure 2-11b** and **2-11c**) can be attributed to the shielding of the $Ti_3C_2T_x$ structure by the ascorbate molecules that associate with the titanium atoms in the nanosheet [86]. The oxidized states of Ti (such as Ti^{3+}, Ti^{2+}, and TiO_2) are far less abundant in $Ti_3C_2T_x$ system simulated with NaAsc compared to $Ti_3C_2T_x$ system simulated with water. During the simulation, the NaAsc loses the Na^+ cation, and the L-ascorbate anion associates with the nanosheet. The Ti-O bonding seen in the simulations primarily forms at the edges of the $Ti_3C_2T_x$ between the nanosheet and L-ascorbate. The L-ascorbate molecules associated with the nanosheet prevent nearby sites from interacting with water molecules, thereby locally shielding the nanosheet from oxidation. This is not true for the case of water oxidation, where water reacts with the nanosheet by breaking Ti-C bonds and forming Ti-O bonds in the process. The reaction between Ti and water subsequently creates more sites for oxidation, thereby reducing the size of the nanosheet. ReaxFF simulations also indicate preferred oxidation along the edges, in accordance with previous experimental observations [64]. This can be attributed to the Ti atoms along the edges of nanosheet, which have significantly high angle strain, as compared to the Ti atoms in the basal plane. The final configurations of the simulation systems are presented in **Figure 2-12**.

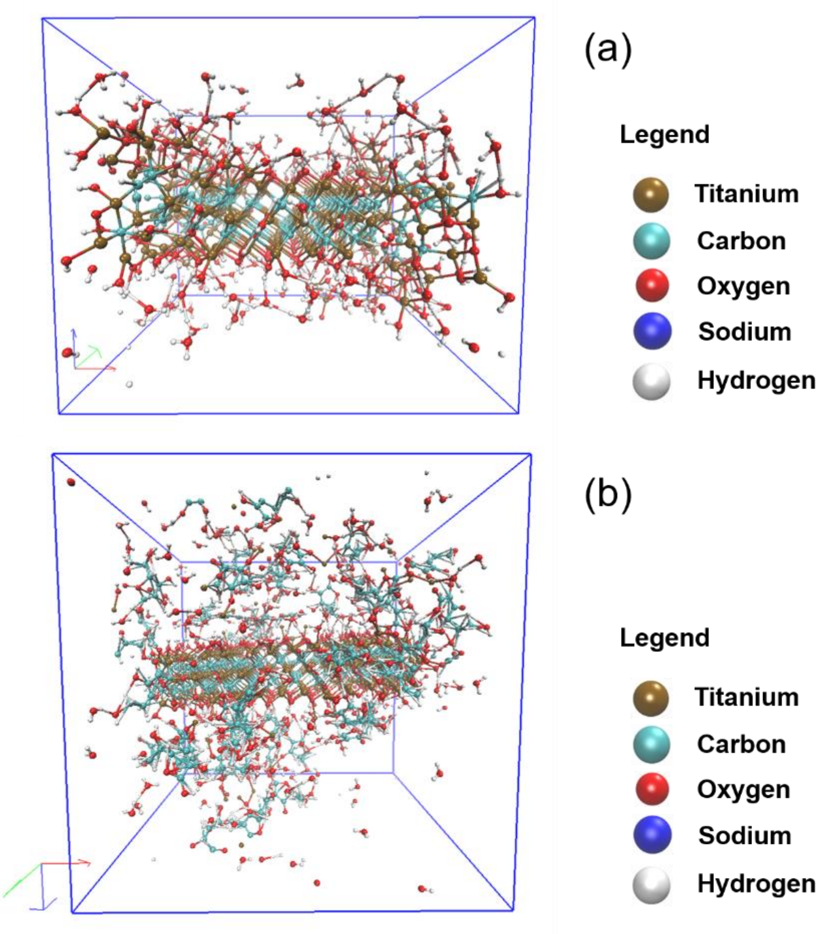

Figure 2-12 Final molecular configuration of molecules after 25 ps of molecular dynamic simulation of systems with (a) $Ti_3C_2T_x$ MXene nanosheet and water, and (b) $Ti_3C_2T_x$ MXene nanosheet, water and NaAsc. The solid line represents the box dimensions for the reaction. Reprinted with permission from reference[75], Copyright 2019 Elsevier Ltd.

2.4.4. Interaction between MXene nanosheets and sodium cations (Na^+)

2.4.4.1. EDS measurements after washing away sodium cations

Here, we assess whether sodium cations can be removed from MXenes in the buckypaper by repeated washing. Stored MXene colloid was vacuum filtered to make films. After that, different amounts of distilled water were used to rinse the film by vacuum filtration. The MXene films were then dried under vacuum for 12 hours. The sodium residues in the dried MXene films were monitored by Energy-dispersive X-ray spectroscopy (EDS). Since all the titanium detected on the film comes from MXene, the weight and atomic ratios between Na and Ti (Na: Ti) are a reasonable metric to quantify the sodium content. A sample made by freeze drying the NaAsc-stabilized MXene colloid was chosen as a reference since no sodium is removed in that case. **Table 2-5** reveals that sodium can be nearly removed in full after adequate washing process. After being washed by 100 ml water, the sodium content became low, so it may be barely detected (the standard deviation is close to the obtained the weight percentage itself, which we did not report it in detail).

Table 2-5 Sodium to titanium ratios, which are measured by Energy-dispersive X-ray spectroscopy (EDS), decreases with the increasing of the washing stages for the NaAsc treated MXenes. Reprinted with permission from references[75], Copyright 2019 Elsevier Ltd.

	Freeze dried with no wash	Vacuum filtration with limited wash (2 ml H_2O)	Vacuum filtration with moderate wash (50 ml H_2O)	Vacuum filtration with adequate wash (100 ml H_2O)
Na: Ti (wt %)	1:2	1:27	1:103	1:163
Na: Ti (at %)	1:1	1:13	1:50	1:80

We believed that most of the sodium and excess ascorbate groups left the MXene samples during the filtration process. This suggests a weak interaction between sodium cation and individual MXene nanosheets, which is consistent with the simulation results. In addition, Ren *et al.* reported that sodium cations carrying a relatively small hydration radii have a fast permeation rate through the 2D nanochannels and layer space in MXene films. In conclusion, the interaction between sodium cations and MXene nanosheets is limited. The strong adsorption and intercalation will not happen in our case for individual nanosheets when the concentration of NaAsc is kept low. In contrast, adequate ascorbate groups will interact with and stabilize the MXene nanosheets. Note that we add NaAsc in excess amount.

2.4.4.2. Simulation of nanosheet-cation interactions

We carried out molecular dynamics simulations to address the interactions of both sodium cations and the dissociated ascorbate group with the nanosheets. The simulations probe a 25 ps timeframe with MXene, NaAsc, and water; the frames from the first and last 0.75 ps of the 25 ps of simulations were used for rdf calculations. While carrying out rdf calculations for Na-O, only the oxygen atoms (O) on the basal plane of nanosheet were considered for the calculations. The oxygen atoms in water and ascorbate molecules were not considered for rdf calculations. **Figure 2-13** shows that the initial 0.75 ps of the simulations do not exhibit a peak at 2 Å (bond length of Na-O bond), suggesting no association between Na+ and O at the beginning of the simulation. A weak peak is seen at the end of the 0.75 ps of the simulation at 2 Å, suggesting minor quantities of association between Na+ and O. To quantify this association, we calculated the number integral

($\int_0^r \rho g(r) r^2 dr$) for all Na-O atomic pairs (where ρ is density, *g(r)* is rdf and r is inter-atomic distance). This number integral of *g(r)* for Na-O is the number of Na cations found within radius r of an O atom, which can also be described as a coordination number for selected bond types. **Figure 2-14** shows int [*g(r)*] for Na-O atom pair, the inset shows the magnified values between 1.5 – 3 Å. From these int [*g(r)*] calculations we observe a very small change in coordination number at ~2 Å, suggesting a very limited degree of Na-O association. It should also be noted that the simulations considered only -OH functionality in MXene (due to limitations of force field parameters), whereas the experiments suggest that other functionalities are also present in the basal plane. Therefore, in experiments, we should potentially observe much smaller Na-O interactions. The simulation results indicate that the majority of Na is free-moving in the water at a low concentration of sodium L-ascorbate during the MXene storage, only the ascorbate groups interact with MXenes.

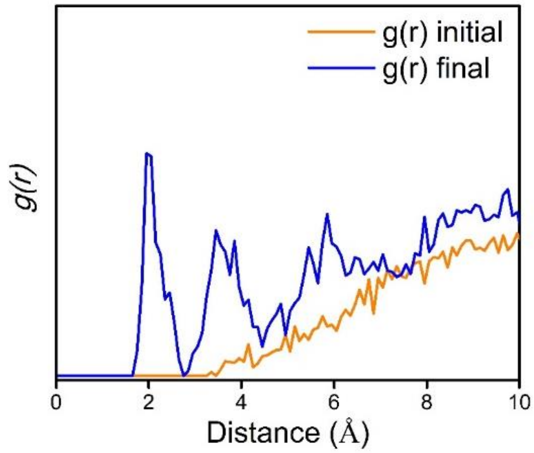

Figure 2-13 RDF calculations of the initial and final 0.25 ps of the MXene/Water/NaAsc simulations. Reprinted with permission from reference[75], Copyright 2019 Elsevier Ltd.

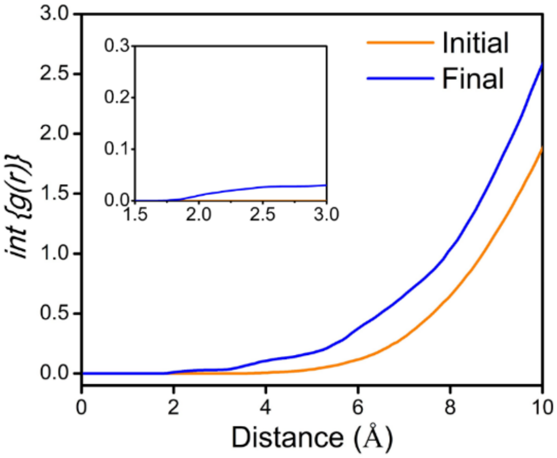

Figure 2-14 Number integral of g(r) for Na-O bond at the initial and final 0.25 ps of the MXene/Water/NaAsc simulations. Reprinted with permission from reference[75], Copyright 2019 Elsevier Ltd.

2.5. Conclusion

This study demonstrates the relatively long-term stabilization of colloidal $Ti_3C_2T_x$ nanosheets in aqueous dispersion using sodium L-ascorbate as the antioxidant. Without this antioxidant, the $Ti_3C_2T_x$ nanosheets rapidly degrade into TiO_2, as shown by large-scale aggregation and a dramatic loss in conductivity of the $Ti_3C_2T_x$ paper made from these samples. In contrast, the antioxidant enables $Ti_3C_2T_x$ nanosheets to retain their crystalline structure, morphology, colloidal stability, chemical composition, and electrical conductivity, even after 21 days in water. The origin of this stability against oxidation is attributed to the association of L-ascorbate anions to the edges of $Ti_3C_2T_x$ nanosheets, which prevent otherwise detrimental oxidation reactions. With these findings, shelf-stable MXenes become possible, and engineering grade MXene-based materials can become a practical reality.

3. PH, NANOSHEET CONCENTRATION, AND ANTIOXIDANT AFFECT THE OXIDATION OF $TI_3C_2T_X$ AND TI_2CT_X MXENE DISPERSIONS[*]

3.1. Summary

The chemical stability of 2D MXene nanosheets in aqueous dispersions must be maintained to foster their widespread application. MXene nanosheets react with water, which results in the degradation of their 2D structure into oxides and carbon residues. The latter detrimentally restricts the shelf life of MXene dispersions and devices. However, the mechanism of MXene degradation in aqueous environment has yet to be fully understood. In this work, the oxidation kinetics is investigated of $Ti_3C_2T_x$ and Ti_2CT_x in aqueous media as a function of initial pH values, ionic strengths, and nanosheet concentrations. The pH value of the dispersion is found to change with time as a result of MXene oxidation. Specifically, MXene oxidation is accelerated in basic media by their reaction with hydroxide anions. It is also demonstrated that oxidation kinetics are strongly dependent on nanosheet dispersion concentration, in which oxidation is accelerated for lower MXene concentrations. Ionic strength does not strongly affect MXene oxidation. The authors also report that citric acid acts as an effective antioxidant and mitigates the oxidation of both $Ti_3C_2T_x$ and Ti_2CT_x MXenes. Reactive molecular dynamic simulations suggest that citric acid associates with the nanosheet edge to hinder the initiation of oxidation.

---

[*] Reprinted with permission from "pH, Nanosheet Concentration, and Antioxidant Affect the Oxidation of $Ti_3C_2T_x$ and Ti_2CT_x MXene Dispersions" by Xiaofei Zhao; Aniruddh Vashisth; Jackson W. Blivin; Zeyi Tan; Dustin E. Holta; Vrushali Kotasthane; Smit A. Shah; Touseef Habib; Shuhao Liu; Jodie L. Lutkenhaus; Miladin Radovic; Micah J. Green. 2020, *Adv. Mater. Interfaces*, 7, 2000845, Copyright 2020 Wiley-VCH GmbH.

3.2. Introduction

As discussed in chapters 1 and 2, MXenes are prone to react with dissolved oxygen and water molecules, which results in the formation of transition metal oxides and carbon residues. [46, 64, 69] Initially, Zhang *et al.* claimed that MXene oxidizes due to the contact with dissolved oxygen in water. [64] However, Huang *et al.* and our group also demonstrated that water molecules, rather than oxygen molecules, play a critical role in MXene degradation. [65, 75] MXenes were reported to oxidize and degrade more rapidly in water rather than in organic solvents, air, or polymer matrixes. [46, 66] Zhang *et al.*, Chae *et al.*, and Habib *et al.* (our group) also found that temperature and humidity have an influence on MXene oxidation. [46, 64, 69] They proposed that low temperatures and low humidity can mitigate the oxidation of MXene nanosheets due to the slower reaction kinetics and reduced exposure to water molecules, respectively. In addition, MXene nanosheets that are single- to few-layered or have smaller lateral size oxidize faster than multilayered MXene clay particles or larger-size nanosheets. MXenes oxidize rapidly when exposed to oxidizers such as hydrogen peroxide or treated by flash-annealing at high temperatures. [91, 92] In addition, elemental composition may influence the oxidation kinetics. [93] VahidMohammadi *et al.* and Huang *et al.* reported that M_2XT_x MXenes, such as V_2CT_x and Ti_2CT_x, oxidize and degrade much faster than the more common $M_3X_2T_x$, such as $Ti_3C_2T_x$. [65, 94] Other aspects may also contribute to the oxidation of MXenes, such as the amount and types of terminal groups, etching conditions, ultraviolet exposure, and the number of defects on the MXene nanosheets.

The shortened shelf life of MXenes due to their oxidation and degradation, has prompted a search for strategies to prevent or mitigate MXene oxidation and degradation. Wu *et al.* developed a carbon nanoplating technique to inhibit oxygen exposure and transport on the surface of $Ti_3C_2T_x$ MXenes. Our group and Natu *et al.* discovered that some antioxidants (such as sodium L-ascorbate) and polyanions (such as polyphosphates) slow the oxidation of $Ti_3C_2T_x$ and significantly extend their shelf-life. [75, 95] Shuck *et al.* reported that $Ti_3C_2T_x$ MXenes derived from MAX phase made from graphite as the carbon source are more stable than that from lampblack and titanium carbide (TiC).[81] However, so far, these studies are limited to $Ti_3C_2T_x$ and have not been applied to any M_2XT_x MXenes. [75, 95]

In this chapter, we investigate the oxidation kinetics of both $Ti_3C_2T_x$ and Ti_2CT_x nanosheets in acid, base, and buffer-adjusted dispersions over a pH range varying from 2 to 10 to elucidate oxidation mechanism in aqueous dispersions. The study aims at how both (i) oxidation affects the pH value of the MXene dispersion and (ii) pH affects the oxidation rate. These relationships markedly differ for $Ti_3C_2T_x$ and Ti_2CT_x. In addition, buffers with different pH are used to separate these inter-related effects from one another by artificially keeping pH constant over time. Even nanosheet concentration can affect oxidation rates, likely due to inter-sheet interactions and steric shielding. In the case of the buffer-adjusted dispersion study, we also discovered an effective antioxidant, citric acid, which mitigates the oxidation of both $Ti_3C_2T_x$ and Ti_2CT_x. In our study, the degree of oxidation of MXenes is mainly evaluated by X-ray photoelectron spectroscopy (XPS) and electrical conductivity changes of dried films made by vacuum filtering the MXene dispersions exposed to oxidation in aqueous dispersions. Colloidal property changes are examined through ζ-potential and dynamic light scattering measurements. Reactive molecular dynamics (ReaxFF)[96] simulations are also used to evaluate the oxidation stability of $Ti_3C_2T_x$ nanosheets in acidic and basic systems, and in the presence of citric acid.

3.3. Experiments and methods

3.3.1. Materials

The parent Ti_3AlC_2 phase was synthesized from the blends of Ti, Al, and graphite powders which were mixed at the ratio of 3.0:1.2:1.9 (Ti: Al: C). The bulk Ti_3AlC_2 was synthesized by heating up the powder mixture in a tube furnace to 1510 °C at 10 °C min^{-1} and being kept for 4 h. The bulk Ti_3AlC_2 was grounded and sieved to the size below 45 µm. $Ti_3C_2T_x$ MXene nanosheets were prepared by the selective acid etching, intercalation, and delamination processes following the prior works, which were also described in detail in prior chapters. [8, 38, 46, 75, 81, 97, 98] Note that in the concentration dependency study on MXene oxidation, to accelerate the experimental timescale, TiC was used as the carbon source in the MAX phase synthesis to replace graphite, which led to relatively faster oxidation kinetics for the nanosheets derived from that source. The blends of Ti, Al, and TiC powders were mixed at a ratio of 1.2:1.2:1.8 (Ti: Al: TiC).

The parent Ti_2AlC MAX phase was synthesized from the blends of Ti, Al, and graphite powders which were mixed with 2.0:1.0:1.0 (Ti: Al: C) ratio. The bulk Ti_2AlC was synthesized by heating the powder mixture in a tube furnace to 1410 °C at 10 °C

min^{-1} and maintaining the temperature for 4 h. Synthesized bulk Ti_2AlC was grounded and sieved to the size below 20 µm. Ti_2CT_x MXenes were prepared by the modified selective acid etching method similar to the $Ti_3C_2T_x$ with the higher etchant concentrations and reduced etching time.

The as-prepared MXene dispersions were first diluted to a concentration of 0.3 mg/ml. Then the pH values of the diluted dispersions were pre-adjusted to higher pH by addition of 0.1 M KOH solution, and to lower pH by addition of 0.1 M HCl, respectively. (The volumes of acid and base added are much smaller than the original volume of the MXene dispersion.) The starting pH values of the pre-adjusted $Ti_3C_2T_x$ dispersion were kept at 10.3, 8.2, 3.6, and 2.6, respectively. The starting pH values of the pre-adjusted Ti_2CT_x dispersion were kept at 10.3, 8.4, 3.5, and 2.6, respectively. For the dispersed MXene nanosheets in buffers, as-prepared MXene dispersions were diluted directly into the concentration of 0.3 mg/ml using strong alkali buffer solution (pH = 10.00 at 25 °C, EMD Millipore, made up of boric acid/ potassium chloride/ sodium hydroxide), weak alkali buffer solution (pH = 8.00 at 25 °C, EMD Millipore, made up of boric acid/ sodium hydroxide/ hydrogen chloride), acidic acetate buffer solution (pH = 3.25 at 25 °C, made up of sodium acetate / acetic acid), acidic buffer solution (pH = 3.00 at 25 °C, EMD Millipore, made up of citric acid/ sodium hydroxide/ hydrogen chloride). In the concentration-dependent study, the as-prepared $Ti_3C_2T_x$ MXene dispersion was diluted with water into concentrations of 7.7 mg/ml, 1 mg/ml, 0.1 mg/ml, 0.05 mg/ml, 0.005 mg/ml. All samples were stored in sealed jars under dark conditions.

3.3.2. Materials characterization

The pH values of the MXene dispersion samples were measured using a pH meter (Mettler Toledo, Switzerland). ζ potential and average hydrodynamic diameter changes of MXene dispersions were measured using a Zetasizer Nano ZS90 from Malvern Instruments, USA. Scanning electron microscope (SEM, JSM-7500F, JEOL, Japan) and atomic force microscope (AFM, Bruker, USA) were used to probe the morphology of dehydrated MXene samples. The morphologies of MAX particle and nanosheets obtained by SEM were shown in **Figure 3-1** and **3-2**. The lateral size of the delaminated $Ti_3C_2T_x$ nanosheets is around 0.5 to 5.0 μm, verified by atomic force microscopy (shown in **Figure 3-3**). Note that it is challenging to image the morphology of pristine Ti_2CT_x nanosheets by AFM due to structural degradation in air caused by the rapid oxidation. The crystalline structures of MAX and MXene nanosheets used in this work were measured by X-ray diffraction (XRD) (shown in **Figure 3-4**). MXene samples used for XRD were prepared by vacuum filtration, followed by vacuum-drying at 40 °C for 12 hours. XRD patterns were acquired using a Bruker D8 powder X-ray diffractometer with CuKα (λ: 1.5418 Å) radiation. The electrical resistance or conductivity was measured using a four-point resistivity probe setup (Keithley Instruments, USA) on MXene films made by vacuum filtration. The thicknesses of the vacuum-filtered film used for conductivity measurements were almost same (1.17 ± 0.05 μm), measured for the cross-sections of each sample by scanning electron microscopy (SEM) (shown in **Figure 3-5)**. The surface chemical states of MXene nanosheets were determined using an Omicron X-ray photoelectron spectrometer (XPS) employing a Mg-sourced X-ray beam. The samples used for XPS analysis were prepared by vacuum filtering the stored MXene dispersions. Before XPS analysis, the samples were dried under vacuum for two days to prevent possible outgassing. XPS accuracy should not be affected by the thickness (>100 nm) of these samples. XPS peak fittings and quantifications were analyzed using CasaXPS software (version 2.3.22). **Figure 3-6** gives the examples of fitting results of Ti 2p and C 1s of $Ti_3C_2T_x$ before and after oxidation.

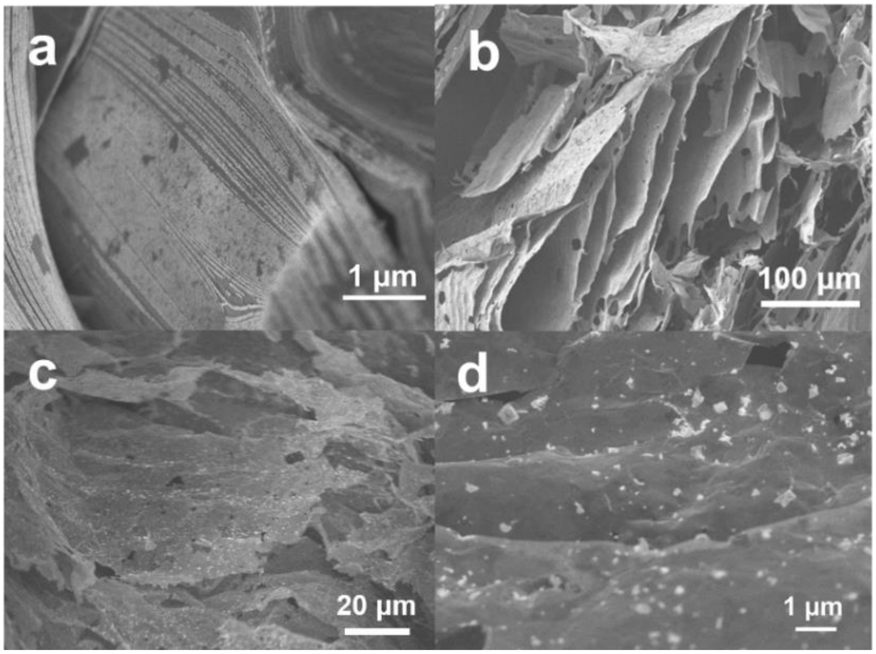

Figure 3-1 Morphology of (a) Ti_3AlC_2 MAX phase powder, (b) delaminated $Ti_3C_2T_x$ MXene nanosheets freeze-dried immediately after exfoliation in DI water. Note that (c) and (d) TiO_2 nanoparticles cover the surface of these MXene flakes indicating that oxidation occurs even during wet acid etching and processing. Reprinted with permission from reference[61], Copyright 2019 WILEY-VCH Verlag GmbH & Co.

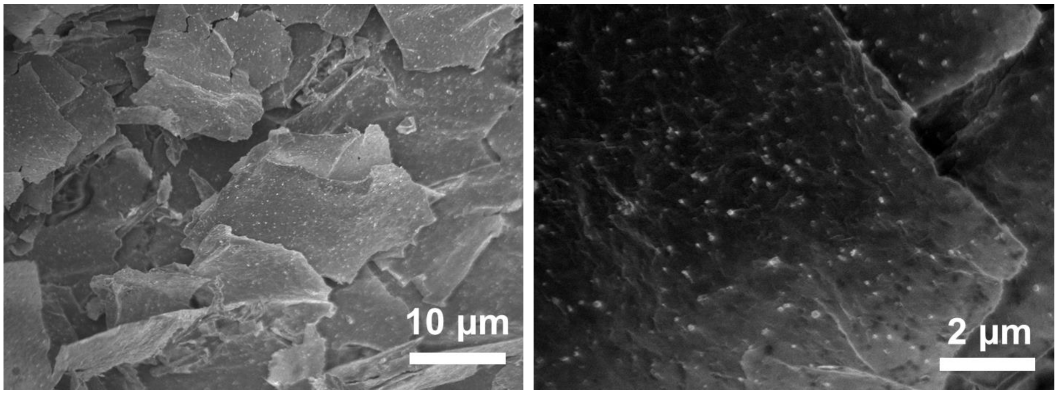

Figure 3-2 Morphology of delaminated Ti_2CT_x MXene nanosheets freeze-dried immediately after exfoliation in DI water at a concentration of 6.0 mg/mL. TiO_2 nanoparticles are observed on the surface of these Ti_2CT_x flakes indicating that oxidation occurs even during wet etching and processing. Reprinted with permission from reference[61], Copyright 2019 WILEY-VCH Verlag GmbH & Co.

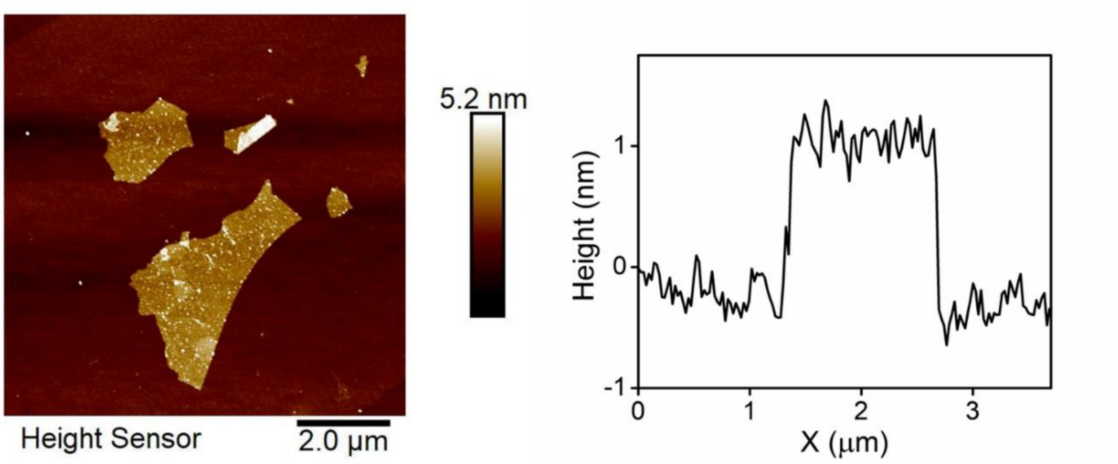

Figure 3-3 An AFM height image of $Ti_3C_2T_x$ MXene nanosheets. The lateral size of the flake is within the range of 0.5 to 3.5 microns. The thickness of the nanosheets is ~1.2 nm. Reprinted with permission from reference[61], Copyright 2019 WILEY-VCH Verlag GmbH & Co.

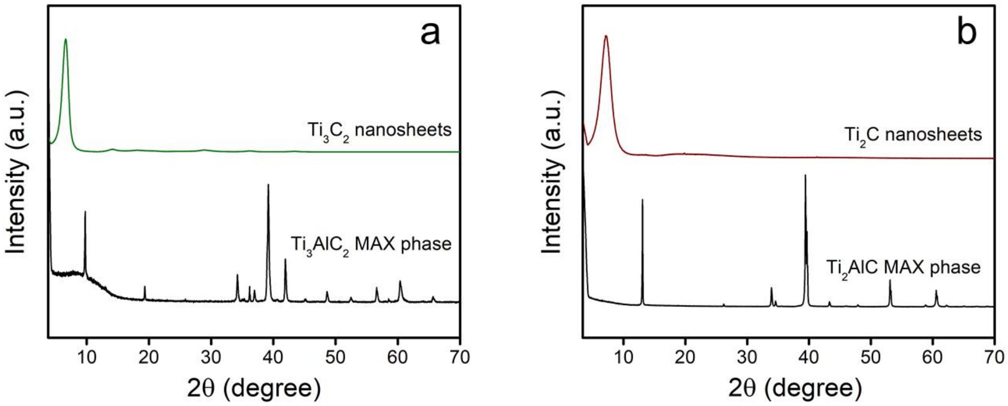

Figure 3-4 Crystalline structural properties of (a) Ti_3AlC_2 and $Ti_3C_2T_x$ and (b) Ti_2AlC and Ti_2CT_x characterized using X-ray diffraction (XRD). MXene samples used for XRD were prepared by vacuum filtration, followed by vacuum-drying at 40 °C for 12 hours. Reprinted with permission from reference[61], Copyright 2019 WILEY-VCH Verlag GmbH & Co.

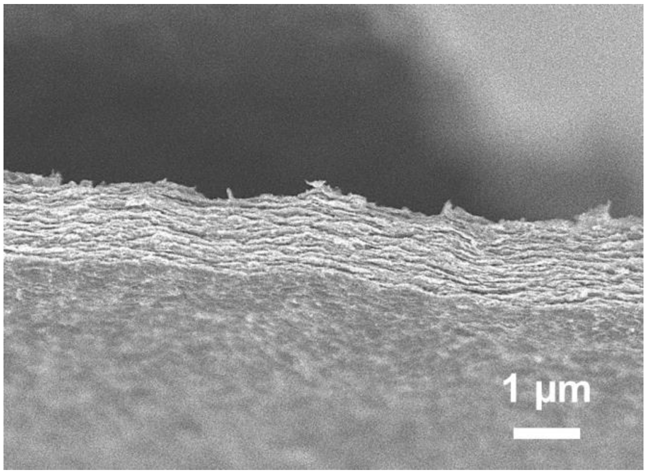

Figure 3-5 SEM image of cross-section of a $Ti_3C_2T_x$ film used in electrical conductivity measurements. Reprinted with permission from reference[61], Copyright 2019 WILEY-VCH Verlag GmbH & Co.

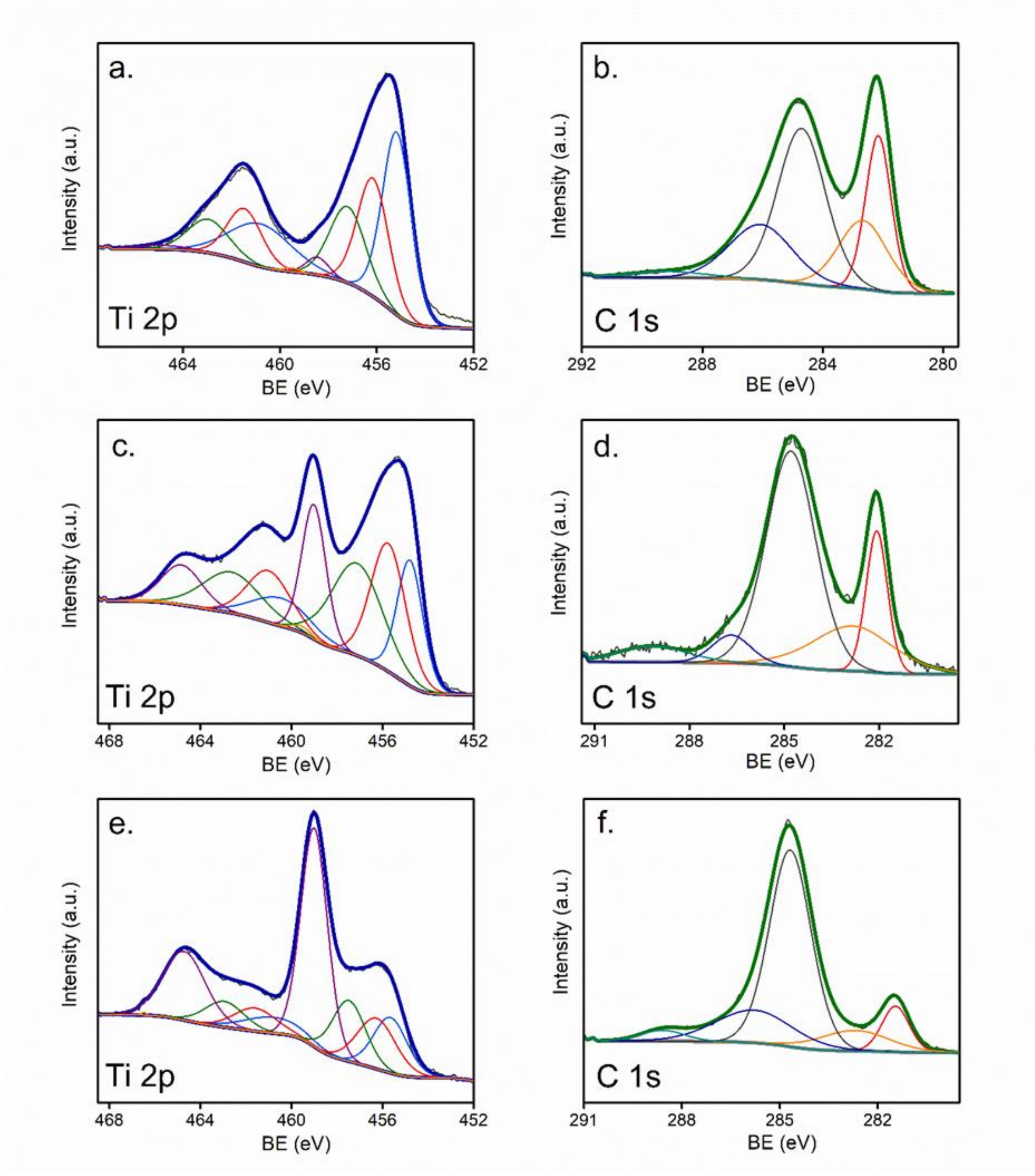

Figure 3-6 Deconvolution and fittings of high-resolution XPS spectra for Ti 2p and C 1s components for (a) and (b): as-prepared, (c) and (d): partially oxidized, and (e) and (f): severely oxidized $Ti_3C_2T_x$ MXene samples. Reprinted with permission from reference[61], Copyright 2019 WILEY-VCH Verlag GmbH & Co.

3.3.3. ReaxFF simulation setup†

ReaxFF is a reactive force field MD simulation technique that uses the bond order concept to calculate the interaction between atoms at each time step [99]. As compared to other non-reactive atomistic simulations, a smooth transition between the non-bonded states and the bonded states is provided by ReaxFF. In ReaxFF, the total energy of the system can be summed up as follows:

$$E_{system} = E_{bond} + E_{over} + E_{under} + E_{val} + E_{tors} + E_{vdW} + E_{Coulomb} + E_{lp} + E_{H\text{-}bond} \tag{1}$$

The total energy of the system (E_{system}) consists of bond-order dependent or covalent interactions and non-bonded interactions. Bond-order-dependent terms include the bond energy (E_{bond}), over-coordination (E_{over}), under-coordination (E_{under}), and hydrogen bond ($E_{H\text{-}bond}$) interactions. Energy penalty terms include torsion angle energy (E_{tor}), valence angle energy (E_{val}), and lone pair energy (E_{lp}), whereas the non-bonded interactions are van der Waals (E_{vdW}) and Coulomb energy ($E_{Coulomb}$). Interatomic distances are calculated and updated at every time step, and bond order is calculated between all pairs of atoms. Non-bonded interactions such as Coulomb energy and van der Waals are considered for all-atom pairs. Quantum mechanics calculations typically optimize force field parameters describing energy terms. The force field used in this study has been fitted for Ti and C based MXene structures and has shown good correlation with experiments [75, 86].

Four systems were generated for ReaxFF molecular dynamics simulations of MXene oxidation under different conditions. The first system had 200 water molecules

---

† This simulation work was completed by Dr. Aniruddh Vashisth.

and a single $Ti_3C_2(OH)$ structure, and second and third systems had an additional 150 OH and H atoms, respectively. The fourth system had 200 water molecules, a single $Ti_3C_2(OH)$ MXene nanosheet and 10 molecules of citric acid ($C_6H_8O_7$). The first three systems were evaluated to examine the effect of pH on the oxidation of MXene nanosheet, whereas the first and the fourth system revealed the improved oxidation stability of MXene in the presence of citric acid. The hydroxide anions, protons, water molecules, and citric acid molecules were randomly distributed around the MXene structure. The density of all the systems was kept at ~1 g/cc. NVT simulations were carried out 500˚C (773 K) with 0.25 fs time-steps for a total time of 25 ps using LAMMPS [87]. Simulations were carried at elevated temperatures as compared to the experiments to accelerate the kinetics of the reactions. Radial distribution function (*rdf*) calculations were carried out using Visual Molecular Dynamics (VMD) [88] for the last 2.5 ps of the oxidation simulations.

3.4. Results and discussion

Titanium carbides $Ti_3C_2T_x$ and Ti_2CT_x are used in this study as the most-studied members of MXenes family. The etching, delamination, and dispersion processes follow the prior works. [46, 75] The as-prepared MXene dispersions were first diluted to a concentration of 0.3 mg/ml. To evaluate the oxidation rate of MXene nanosheets in various pH conditions, the MXene nanosheet dispersions were adjusted to desired pH values by adding 0.1 M potassium hydroxide (KOH) or 0.1 M hydrochloride acid (HCl) solutions as illustrated schematically in **Figure 3-7 a**. Here we also provide a roadmap of the study on the oxidation stability of $Ti_3C_2T_x$ and Ti_2CT_x in dispersions with different initial pH, displayed in **Figure 3-7 b** and **3-7 c**.

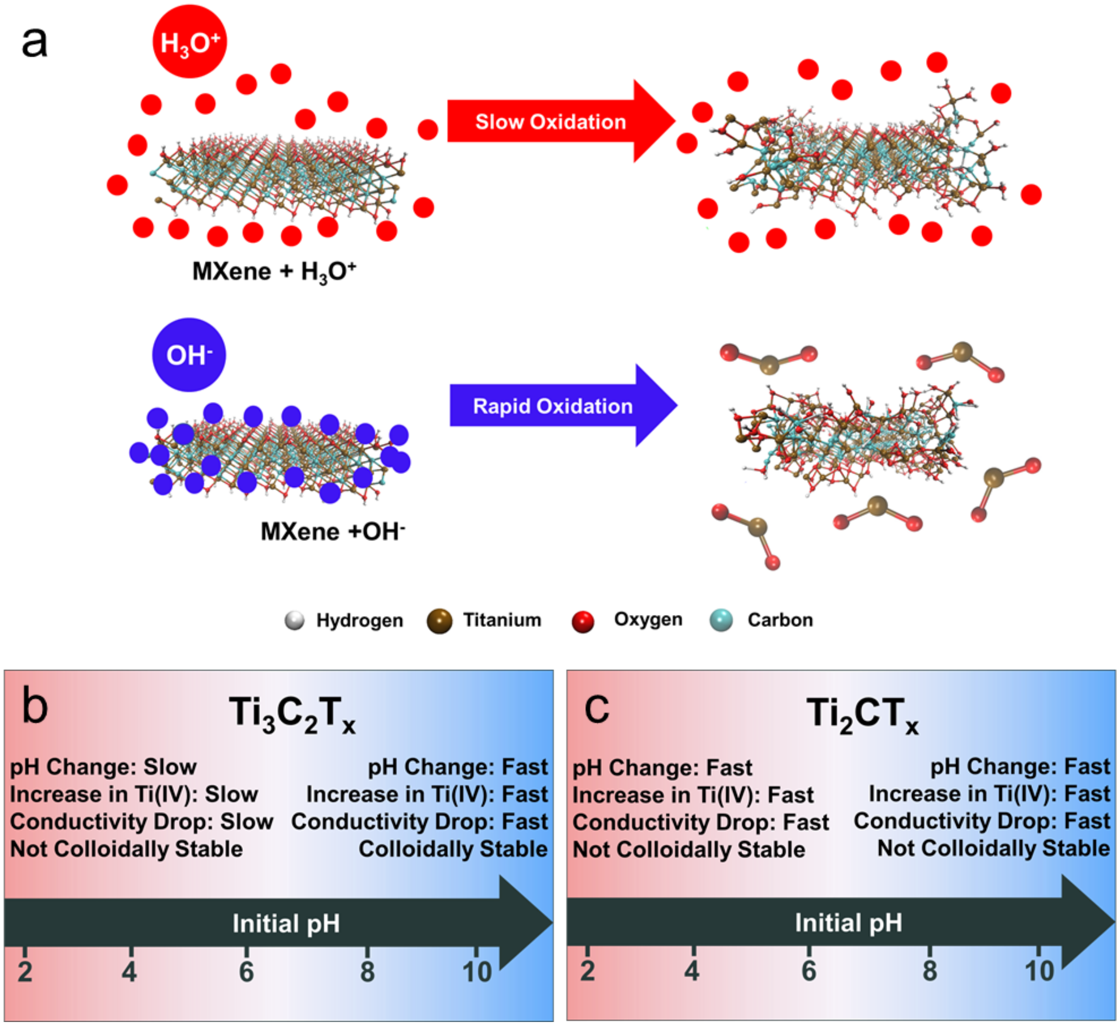

Figure 3-7 (a) Schematic, and (b, c) results for $Ti_3C_2T_x$ and Ti_2CT_x MXene nanosheet oxidation in aqueous dispersions with acidic and alkaline pH. A chemical structure of $Ti_3C_2(OH)$ is used in the schematics. Reprinted with permission from reference[61], Copyright 2019 WILEY-VCH Verlag GmbH & Co.

3.4.1. $Ti_3C_2T_x$ oxidation and pH

The drifts in the pH value of the $Ti_3C_2T_x$ MXene aqueous dispersions were recorded and reported in **Figure 3-8a** for dispersions with varying initial pH values. Rapid decreases in the pH values were observed in the first two days for two initially alkaline dispersions, followed by gradual decreases in pH value. The initially dramatic decreases in pH for the alkaline dispersions are likely due to the rapid uptake of hydroxide ions. A reference dispersion for which the initial pH was not adjusted (natural pH = 4.4) only slightly decreased with time.

The chemical composition changes of $Ti_3C_2T_x$ nanosheets were monitored using X-ray photoelectron spectroscopy (XPS), shown in **Figure 3-9**. The atomic percentage of Ti(IV), as an indicative of TiO_2 content formed due to oxidation, was obtained by analyzing the high-resolution Ti 2p spectra. Examples of spectra deconvolution and fittings for MXene samples with various degrees of oxidation are displayed in **Figure 3-6**. It is clear in **Figure 3-8b** that the initially alkaline $Ti_3C_2T_x$ dispersions show a higher atomic percentage of Ti(IV) component than the initially acidic dispersion, which indicates a faster transition from MXene nanosheets to TiO_2 in alkaline media. Oxidation of MXene nanosheets in acid-adjusted dispersions was similar to the reference dispersion at pH = 4.4. We also observed that the nanosheets in dispersion with initial pH of 2.6 oxidized slightly faster than that in dispersion with initial pH of 3.6. The reason behind this is still not clear and is subject of our further investigation. It is possible that there is some defect formation caused by the MXene surface reacting with a strong acid. This confirms that alkaline conditions promote oxidation of MXene nanosheets in aqueous media.

The colloidal stability of $Ti_3C_2T_x$ MXene dispersions with a specified initial pH was evaluated by characterizing ζ potential over time (shown in **Figure 3-10a**). In the first two days, ζ potential became more positive rapidly for both acidic and basic media MXene dispersions; this can be explained by the adsorption of H^+ and K^+ cations onto the electronegative basal plane of the MXene nanosheets. However, the alkaline dispersions exhibit a relatively slower increase of ζ potential over the 40 days, likely due to induced repulsion from the $-O^-$ described above.

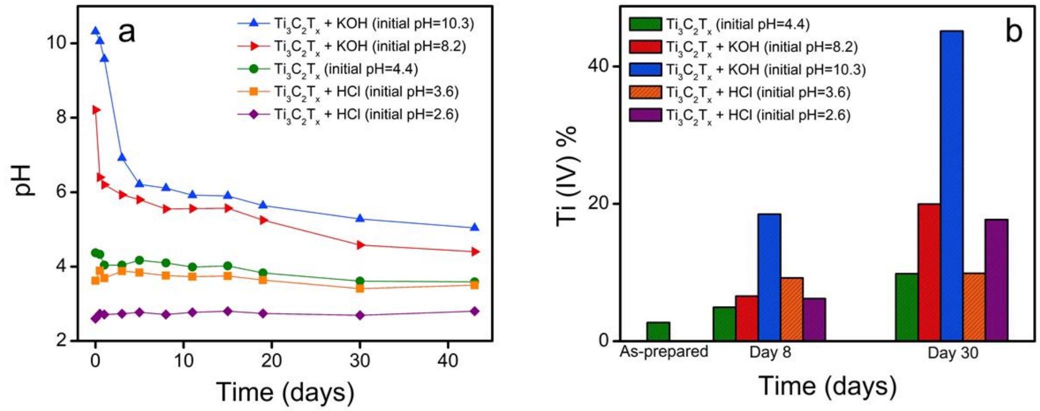

Figure 3-8 (a) the pH of $Ti_3C_2T_x$ MXene aqueous dispersions changes with time; (b) the atomic percentage changes for Ti(IV) component obtained by X-ray photoelectron spectroscopy for $Ti_3C_2T_x$. Reprinted with permission from reference[61], Copyright 2019 WILEY-VCH Verlag GmbH & Co.

Oxidation may also cause the ζ potential value to become more positive. During storage, MXene nanosheets gradually lose colloidal stability due to conversion to TiO_2.[60, 75, 95] For initially acidic media, MXenes colloid stability declines with time, as indicated by the increasingly more positive ζ potential values and the drastic increase in the hydrodynamic size (shown in **Figure 3-10b**). Note that this aggregation of the MXene nanosheets in acidic dispersions may contribute to the slower oxidation rate due to the smaller surface to volume ratio.

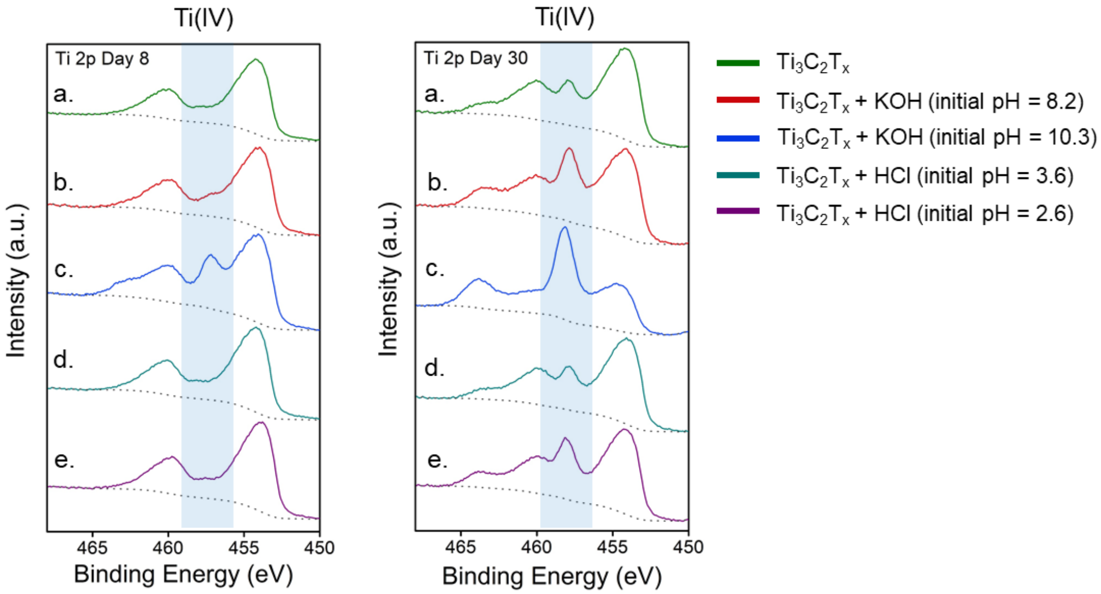

Figure 3-9 Overlays of the high-resolution spectra of Ti 2p obtained by X-ray photoelectron spectroscopy (XPS) for $Ti_3C_2T_x$ nanosheets at day 8 and day 30 of storage in dispersions with pre-specified pH. Reprinted with permission from reference[61], Copyright 2019 WILEY-VCH Verlag GmbH & Co.

The electrical conductivity was measured for vacuum filtered films made from MXene dispersions that had been stored in dispersions with different initial pH for varying times. It has been previously determined that the oxidation of MXenes is correlated with the diminishing electrical conductivity. [46, 60, 69, 75] **Figure 3-10c** confirms that the fast oxidation of $Ti_3C_2T_x$ in alkali environments is correlated with related decreases in the conductivity of $Ti_3C_2T_x$ films. For nanosheets in dispersion with an initial pH of 10.3, the conductivity of the assembled film dropped from $1.6 \pm 0.78 \times 10^5$ S/m to $4.1 \pm 0.1 \times 10^4$ S/m in 18 days and dropped below the measurable limit of 10^{-6} S/m in 30 days.

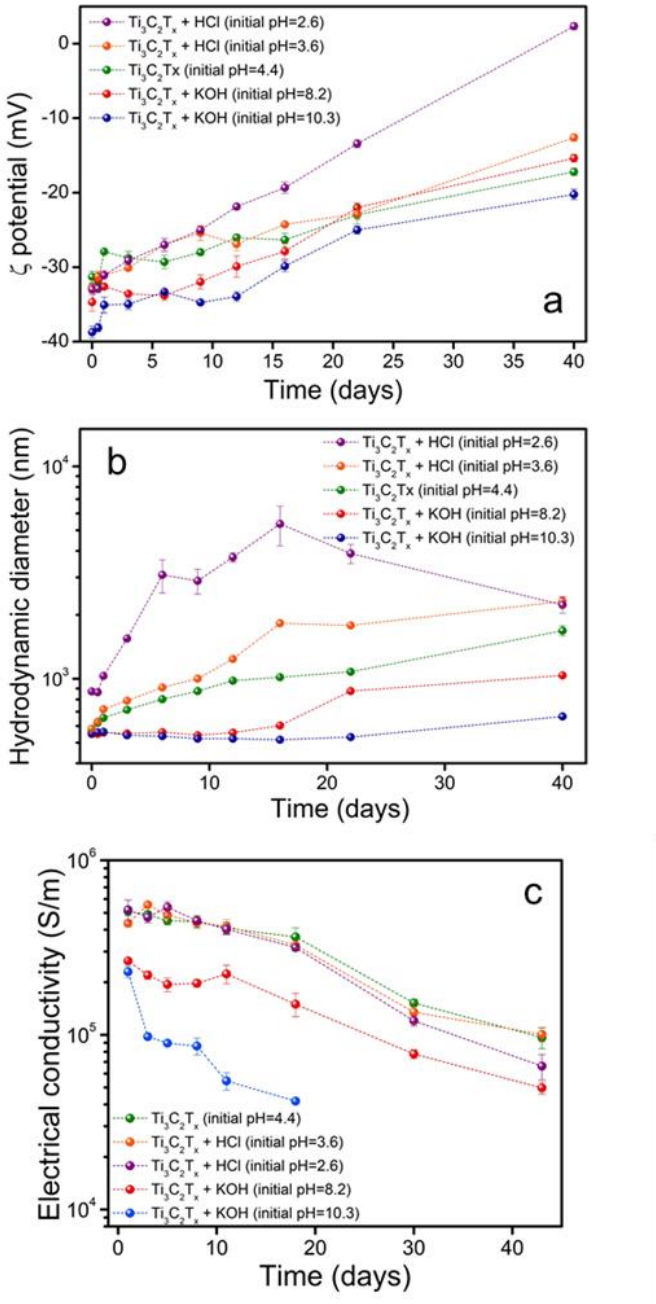

Figure 3-10 (a) ζ potential and (b) hydrodynamic diameter changes for $Ti_3C_2T_x$ dispersions (initial pH indicated in the legend) over the course of 40 days. Dispersions were diluted to ~0.01 mg/ml for ζ potential and size measurements; (c) electrical conductivity of vacuum-filtered films made from $Ti_3C_2T_x$ MXene dispersions of varying ages; conductivity of the film made from an initial pH 10.3 $Ti_3C_2T_x$ dispersion dropped below ~10^{-3} at day 30 measurement (not shown). Reprinted with permission from reference[61], Copyright 2019 WILEY-VCH Verlag GmbH & Co.

The downward pH drifts of MXene dispersions with initially alkaline pH values indicate that the majority of hydroxide ions introduced from the added KOH are consumed within the first two days. On the MXene nanosheet basal plane, OH^- ions react with the protons disassociated from the -OH terminal groups. As a result, the -OH terminal groups are deprotonated to $-O^-$,[60] displayed in the reaction below.

$$Ti_{n+1}C_nOH + OH^- \rightarrow Ti_{n+1}C_nO^- + H_2O$$

Additionally, the pH drift may also stem from negatively charged OH^- ions associating with positively charged nanosheet edges. [60] A counter-hypothesis (from Huang *et al.*) is that acidic carbon derivatives, such as carbonic acid or carbonates, may form because of degradation of MXene nanosheets. [65] However, we argue that the formation of acidic carbon derivatives may not be the reason for the rapid pH decrease because the increased presence of Ti(IV) in $Ti_3C_2T_x$ is not proportional to the rapid pH drop.

Our findings above suggest that the hydroxide ion play an important role in the oxidation of colloidal MXene nanosheets. Two separate mechanisms may be occurring in alkaline conditions. The hydroxide anions play an important role in the deprotonation of -OH terminal groups on MXenes sheets, resulting in the less-stable $-O^-$ groups. We speculate that the deprotonated $-O^-$ groups render the MXene surface more reactive, which leads to faster oxidation. In addition, the OH^- from the base may be uptook by and react with the relatively positive-charged MXene sheet edges resulting in degradation. These findings imply that MXene processing and utilization in basic environments, such as in TMAOH, TBAOH and NaOH, may lead to sub-optimal or declining performance due to oxidation. Specifically, this result suggests that alkaline supercapacitor electrolytes might degrade MXene electrodes over time. As for acidic conditions, MXene sheets have slower oxidation rates indicating an oxidation mechanism similar to the MXene sheets without pH adjustments. The more active MXene edges may first react with OH^- and H_2O. For edge-on degradation, the sheets then become smaller in size and gradually oxidize. In addition, introducing strong acids may cause defect formation, resulting in more reactive spots and a slightly higher oxidation rate.

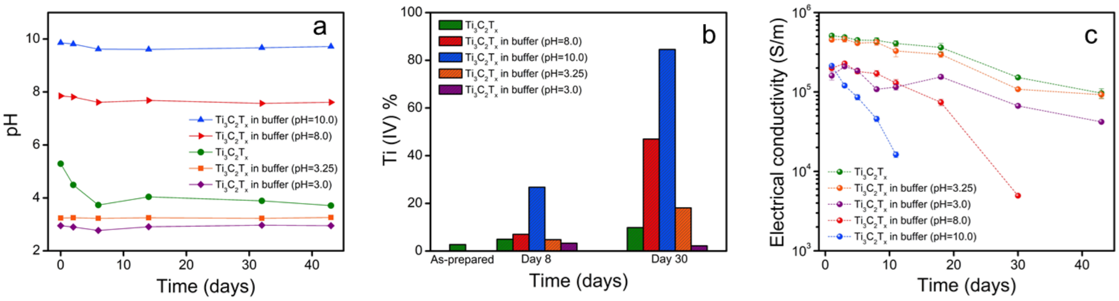

Figure 3-11 (a) pH values change over time for the $Ti_3C_2T_x$ nanosheet buffer dispersions; (b) the atomic percentage changes for the Ti(IV) component obtained by X-ray photoelectron spectroscopy for $Ti_3C_2T_x$; (c) electrical conductivity of vacuum-filtered films made from $Ti_3C_2T_x$ MXene in buffer solutions of varying ages. Each sample was maintained at a specified pH in buffer solutions. The dispersions in the study were kept at a concentration of 0.3 mg/ml. Reprinted with permission from reference[61], Copyright 2019 WILEY-VCH Verlag GmbH & Co.

To study the effect of continuously supplying hydroxide anions on MXene oxidation, $Ti_3C_2T_x$ nanosheets were dispersed in various buffer solutions and their oxidation stability was evaluated. **Figure 3-11a** shows that the pH of the buffered MXene dispersions barely changes (in contrast to un-buffered analogs in **Figure 3-8a**). The films produced from buffered alkaline dispersions indicate more rapid formations of TiO_2 (shown in **Figure 3-11b**, and **Figure 3-12**) than the alkaline dispersions with specified initial pH values. Consistent with this finding, the electrical conductivity of vacuum-filtered MXene films created from the buffered alkaline dispersions (**Figure 3-11c**) shows faster declines. We conclude that the alkaline buffers accelerate MXene oxidation to a greater extent because of the higher amount or “nearly unlimited” supply of hydroxide anions.

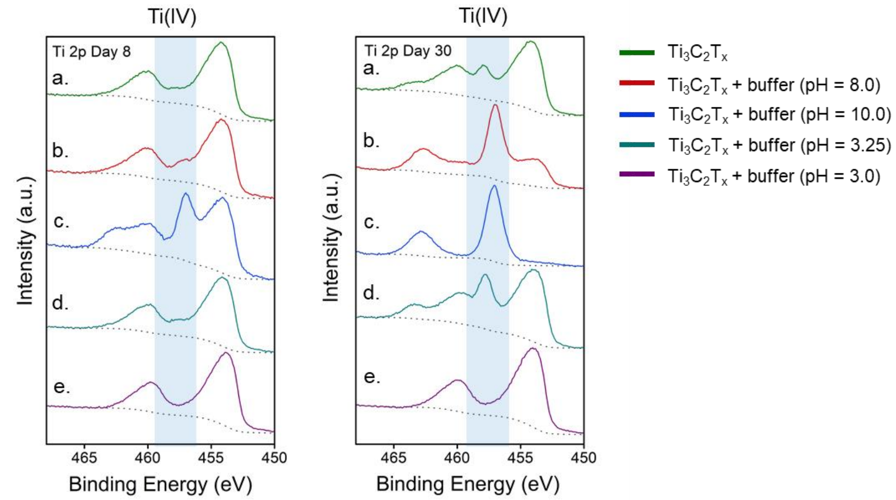

Figure 3-12 Overlays of the high-resolution Ti 2p spectra obtained by X-ray photoelectron spectroscopy (XPS) for $Ti_3C_2T_x$ nanosheets at day 8 and day 30 of storage in buffer solutions. Reprinted with permission from reference[61], Copyright 2019 WILEY-VCH Verlag GmbH & Co.

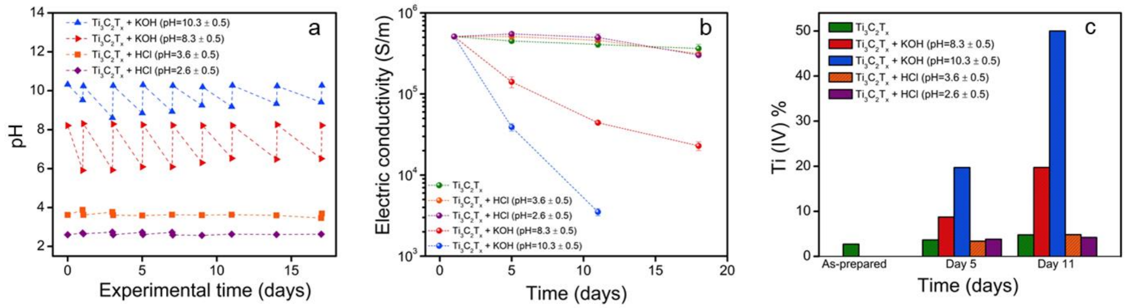

Figure 3-13 (a) Observed pH for $Ti_3C_2T_x$ dispersions with time; the pH of the dispersion was adjusted periodically to a desired value by supplying extra KOH or HCl; (b) conductivity of films made from $Ti_3C_2T_x$ dispersions described in panel (a); (c) atomic percentages for the Ti(IV) component obtained by X-ray photoelectron spectroscopy for $Ti_3C_2T_x$ films prepared from the dispersions described in (a). Reprinted with permission from reference[61], Copyright 2019 WILEY-VCH Verlag GmbH & Co.

In order to rule out any possible side effects brought by the salt ions in the commercial buffer solutions as we evaluated the role of OH^- and H^+ ions, we further investigated the oxidation kinetics of $Ti_3C_2T_x$ nanosheets in dispersions periodically supplied with 0.1 M KOH or HCl to maintain relatively constant pH values (shown in **Figure 3-13**). Both the increase in TiO_2 formation and the rapid conductivity decline of subsequently vacuum-filtered films indicate that $Ti_3C_2T_x$ oxidizes rapidly when hydroxide ions are supplied continuously. In contrast, vacuum-filtered films produced from the acidic dispersions showed a fairly stable electrical conductivity (~ 4.0 x 10^5 S/m over the course of 18 days).

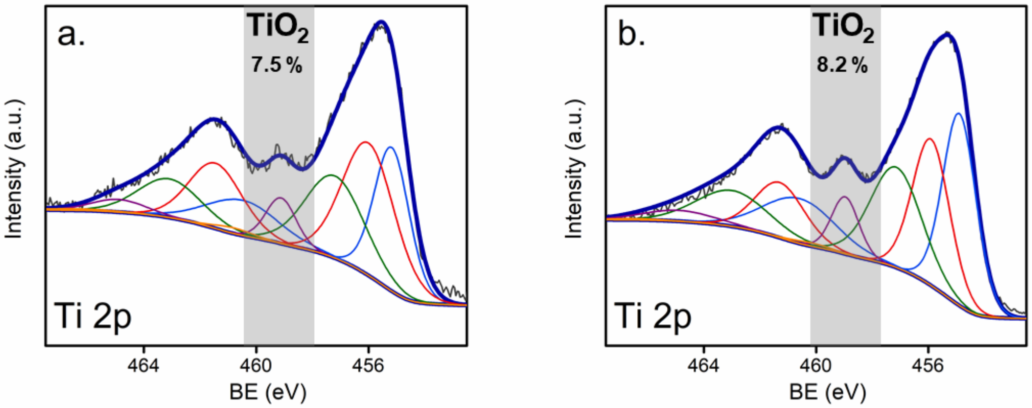

Figure 3-14 Component peak fittings of XPS spectra for (a) $Ti_3C_2T_x$ nanosheets stored in water and (b) in 0.1 M KCl solution for 10 days. The atomic percentages for TiO_2 are similar. Reprinted with permission from reference[61], Copyright 2019 WILEY-VCH Verlag GmbH & Co.

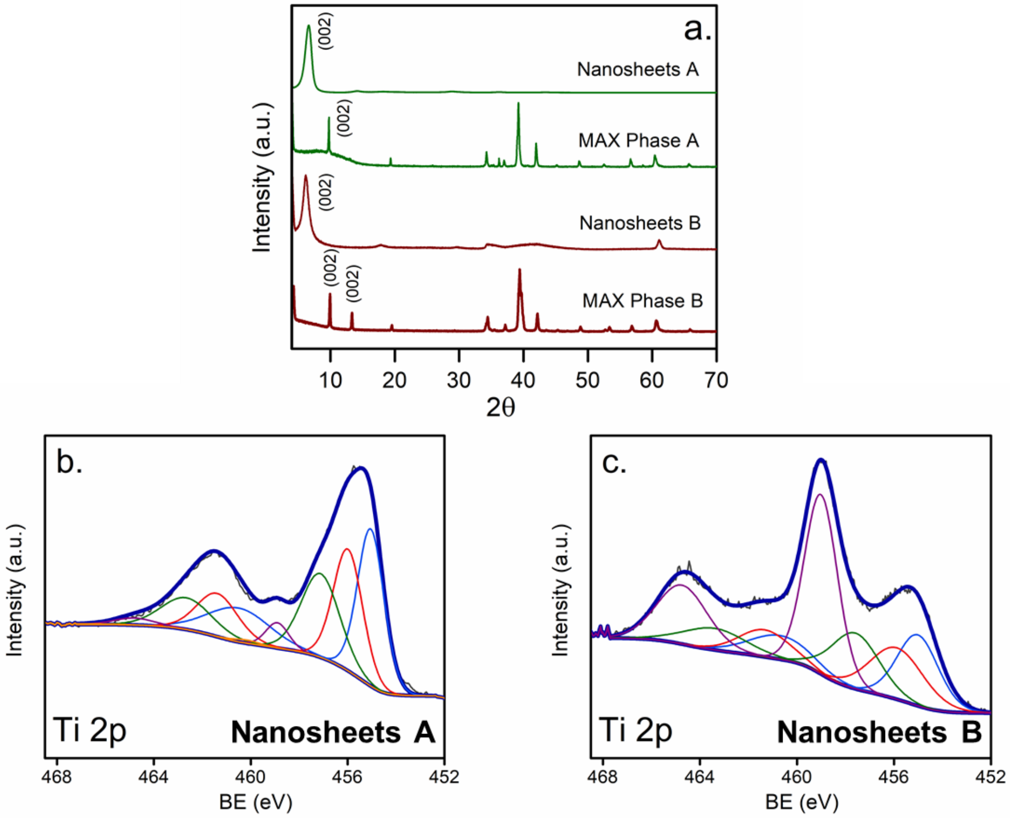

Figure 3-15 The oxidation stability of $Ti_3C_2T_x$ MXene nanosheets derived from Ti_3AlC_2 MAX phases with different purity was investigated after 8 days of storage in water. (a) MAX phase A (Ti_3AlC_2) is considered purer in phase than B (Ti_3AlC_2 mixed with impurity Ti_2AlC grains) since there is only one (002) peak was observed at 9.5°. In MAX phase B, the (002) peak at around 13.5° indicates the presence of Ti_2AlC phase. This is likely due to the incomplete reaction and phase transformation during sintering; (b) and (c) suggest that the MXene nanosheets synthesized from MAX phase A exhibit higher stability; this may be caused by the defects derived after the rapid degradation of Ti_2CT_x impurities during etching and processing. Reprinted with permission from reference[61], Copyright 2019 WILEY-VCH Verlag GmbH & Co.

In addition, we examined the oxidation of $Ti_3C_2T_x$ nanosheets in sodium chloride and potassium chloride solution with an ionic strength of 0.1 M. The similarities in the degree of oxidation to the reference dispersion without any added salt (indicated by the similar TiO_2 percentages shown in **Figure 3-14**) suggest that the addition of salt ions, such as K^+ and Cl^-, has minimal effect on MXene oxidation. However, the addition of salt can disrupt the colloidal stability of MXene dispersions because of the reduced Debye screening length. Observed agglomerates of MXene nanosheets precipitated and settled down entirely within only a few hours in 0.1 M KCl.

We also discovered that oxidation stabilities are different for $Ti_3C_2T_x$ nanosheets derived from the Ti_3AlC_2 MAX phases with and without Ti_2AlC impurities. The Ti_2AlC phase, considered as an impurity phase here, was indicated by (002) plane detected using X-ray diffraction, as shown in **Figure 3-15a**. From **Figure 3-15b** and **3-15c**, X-ray photoelectron spectroscopy suggests that nanosheets derived from the Ti_3AlC_2 MAX phase with Ti_2AlC impurities bear much faster oxidation. This may result from defects on $Ti_3C_2T_x$ nanosheet resulting from the degraded Ti_2CT_x grains. These defects may provide more edges for initializing oxidation.

3.4.2. Ti_2CT_x oxidation and pH

We also investigated the effects of initial pH of aqueous dispersion on the oxidation stability of Ti_2CT_x nanosheets. At high pH, the pH drift for the Ti_2CT_x dispersions exhibited trends similar to that of $Ti_3C_2T_x$, shown in **Figure 3-16a**. However, for the Ti_2CT_x dispersion, its pH value declined far more rapidly due to the swift Ti_2CT_x oxidation as compared to $Ti_3C_2T_x$. On the other hand, initially acidic dispersions maintained relatively stable pH values over time for both Ti_2CT_x and previously studied $Ti_3C_2T_x$ dispersions. The chemical composition changes of Ti_2CT_x nanosheets were monitored by XPS, shown in **Figure 3-16b**. Unlike the more rapid increase in the atomic percentage of Ti(IV) component in initially alkaline dispersions for $Ti_3C_2T_x$, oxidation is uniformly rapid in both alkaline and acidic environments for Ti_2CT_x. In addition, more rapid drops of electrical conductivities are observed for Ti_2CT_x, as shown in **Figure 3-16c**. Films made from Ti_2CT_x dispersions generally lost their conductivity much faster (dropping below 10^{-6} S/m in 6 hours) than films made by $Ti_3C_2T_x$.

The oxidation stability of Ti_2CT_x nanosheets were also evaluated in various buffer solutions, shown in **Figure 3-17**. It is interesting to see that the oxidation is initially fast in the alkaline buffer (pH = 10.0); however, in the later stage of observation, the Ti(IV) percentages become highest for Ti_2CT_x dispersed in the water and in the acetate buffer (pH =3.25).

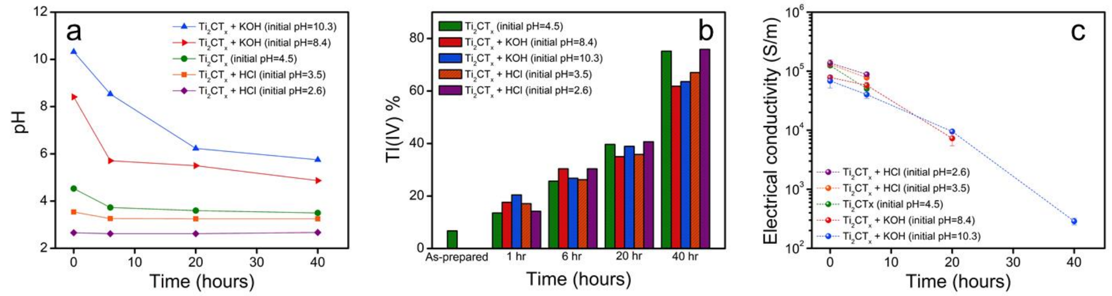

Figure 3-16 (a) the pH of Ti_2CT_x MXene dispersions changes with time; (b) the atomic percentage changes for Ti(IV) component obtained by X-ray photoelectron spectroscopy for Ti_2CT_x; (c) electrical conductivity of vacuum-filtered films made from Ti_2CT_x MXene dispersions of varying ages; conductivities of Ti_2CT_x films made from the reference and acidic dispersions dropped below ~10^{-3} in less than 10 hours after being made (not shown). Reprinted with permission from reference[61], Copyright 2019 WILEY-VCH Verlag GmbH & Co.

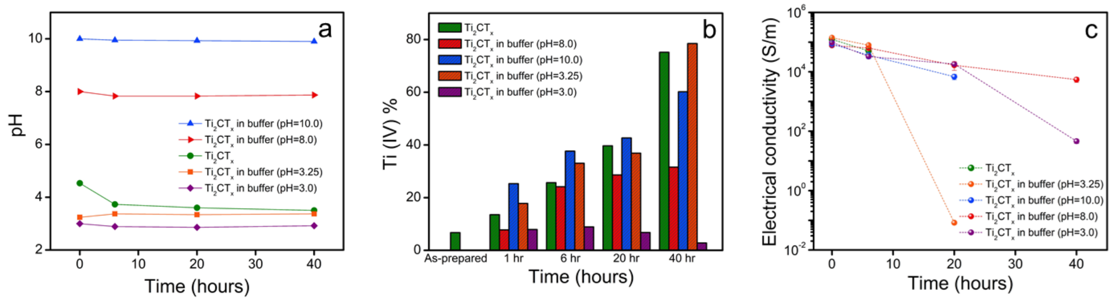

Figure 3-17 (a) pH values change over time for the Ti_2CT_x nanosheet buffer dispersions; (b) the atomic percentage changes for the Ti(IV) component obtained by X-ray photoelectron spectroscopy for Ti_2CT_x; (c) electrical conductivity of vacuum-filtered films made from Ti_2CT_x MXene in buffer solutions of varying ages. Each sample was maintained at a specified pH in buffer solutions. The dispersions in the study were kept at a concentration of 0.3 mg/ml. Reprinted with permission from reference[61], Copyright 2019 WILEY-VCH Verlag GmbH & Co.

3.4.3. Concentration effects on oxidation

In a separate study, we found that oxidation kinetics of MXene nanosheets depend heavily on the colloidal concentration. $Ti_3C_2T_x$ dispersions with five different concentrations were examined periodically for the signs of oxidation. **Figure 3-18** suggests that $Ti_3C_2T_x$ oxidizes much faster in dilute dispersions as compared to higher concentrations, as indicated by (i) the accelerated formation of TiO_2 and (ii) the decline in the electrical conductivity of the vacuum-filtered film. The reason for the slow kinetics of MXene oxidation in high-concentration dispersions can be attributed to the capping and steric shielding effects among MXene nanosheets in close proximity; this restricts water's access to the MXene sheet edges, where oxidation initiates.

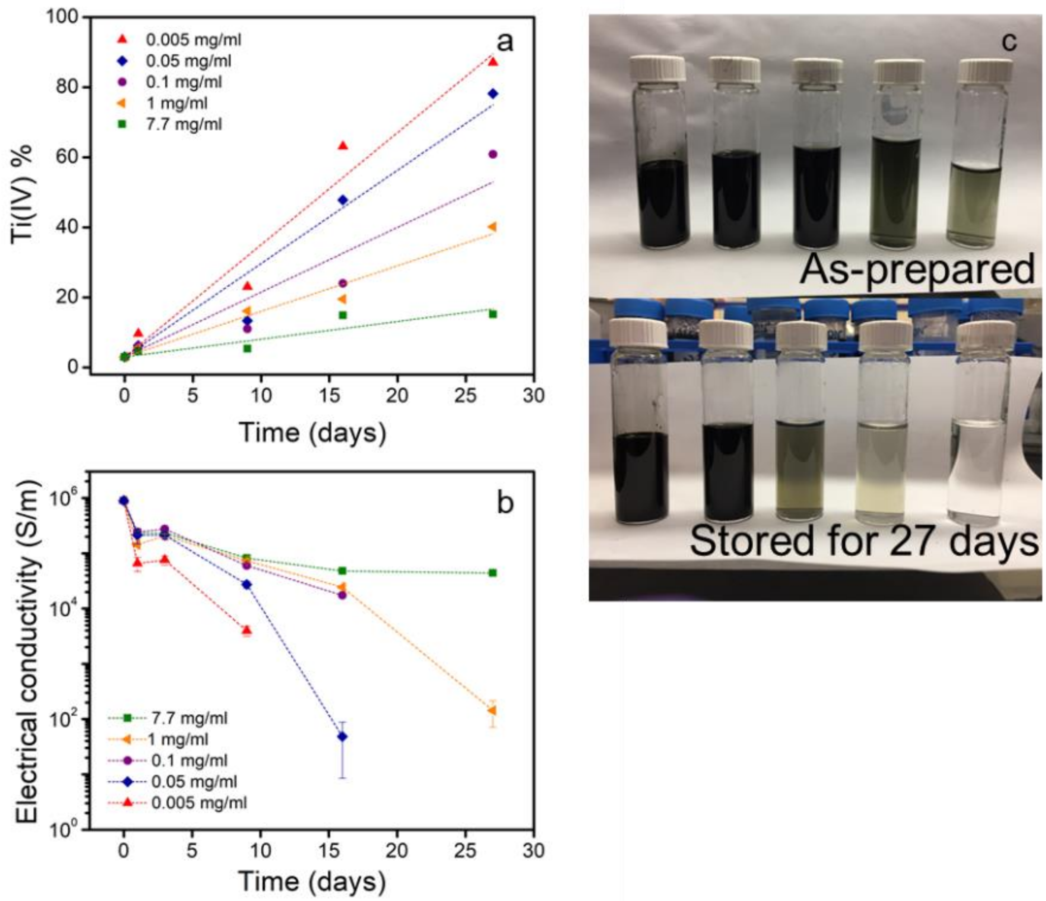

Figure 3-18 Oxidation kinetics of $Ti_3C_2T_x$ changes for MXene dispersions of varying concentrations indicated by (a) the increase of Ti(IV) atomic percentage obtained using X-ray photoelectron spectroscopy and (b) the drop in electrical conductivity of vacuum-filtered films; (c) the color of as-prepared MXene nanosheet dispersions and the same dispersions on the 27th day (from left to right: 7.7 mg/ml, 1 mg/ml, 0.1 mg/ml, 0.05 mg/ml, 0.005 mg/ml). Reprinted with permission from reference[61], Copyright 2019 WILEY-VCH Verlag GmbH & Co.

The relevant concentrations can be estimated by considering an individual nanosheet as a circular disk with a diameter of *D* and a thickness of *t*. The semi-dilute transition volume fraction φ* for any anisotropic disc can be determined from the ratio of the disc volume to the volume that the disc sweeps out during rotational Brownian motion, expressed as

$$\varphi^* = \frac{V_{disc\ MXene}}{V_{sphere}} = \frac{3t}{2D}$$

$Ti_3C_2T_x$ MXenes have a density around 3.7 g cm^{-3};[100] and the volume fraction can be related to concentration as

$$\varphi = \frac{c}{\rho_{MXene}}$$

Based on images taken by atomic force microscopy (shown in **Figure 3-3**), we assume that MXene nanosheets have an average lateral size of 1.5 µm and an average thickness of 1.2 nm. The critical concentration (c^*) at which the nanosheets will start affecting each other can be estimated as 4.4 mg/mL by

$$c^* = \rho_{MXene}\varphi^*$$

This suggests that at dispersion concentrations higher than c*, as in **Figure 3-18a**, the edge-edge interactions of nanosheets will prevent edge oxidation. Accordingly, the MXene dispersion having the highest concentration of 7.7 mg/mL exhibited the least oxidation.

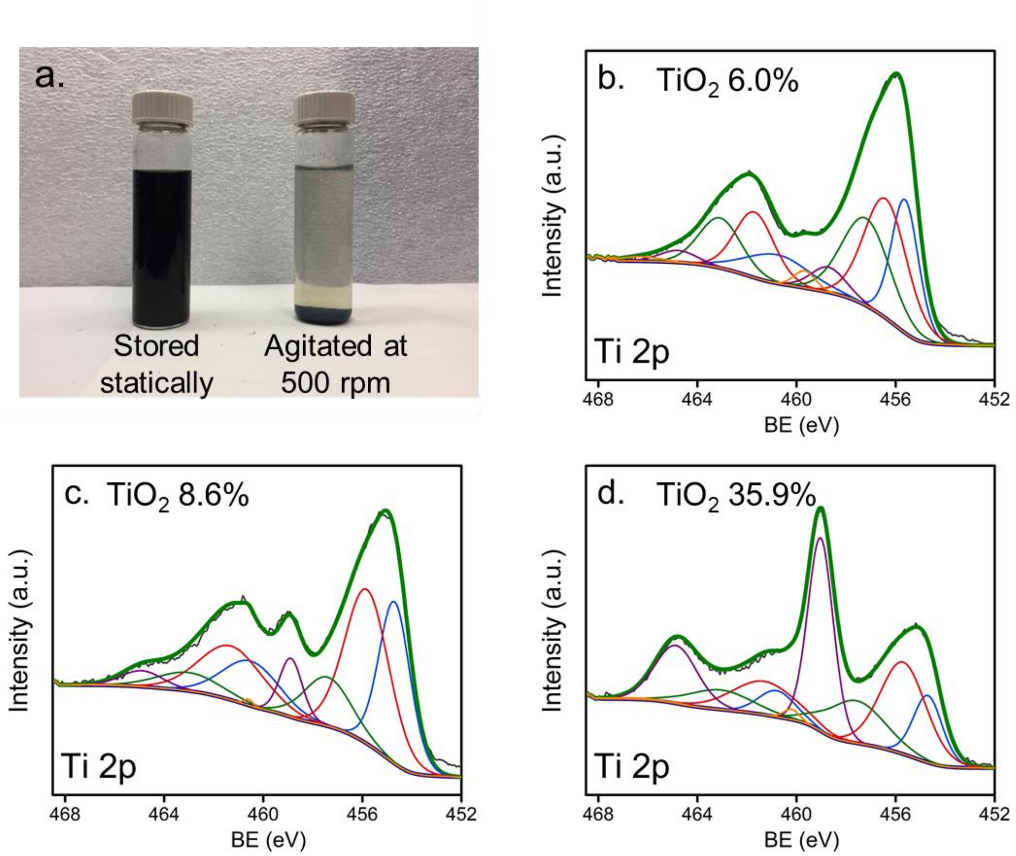

Figure 3-19 (a) A dispersion of $Ti_3C_2T_x$ MXene nanosheets at a concentration of 3.6 mg/ml was agitated at 500 rpm using a magnetic stir bar. After 20 days, the stirred dispersion (right vial) shows more oxidation indicated by the corresponding color change and loss of colloidal stability in comparison to a reference sample kept statically at identical environment (left vial). (b) to (d) X-ray photoelectron spectroscopy (XPS) spectra for Ti 2p for the as-prepared sample, sample kept statically, and sample agitated at 500 rpm, respectively. From this figure, it can be found that agitation will accelerate the oxidation of MXene nanosheets due to the enhanced mobility of water molecules. Reprinted with permission from reference[61], Copyright 2019 WILEY-VCH Verlag GmbH & Co.

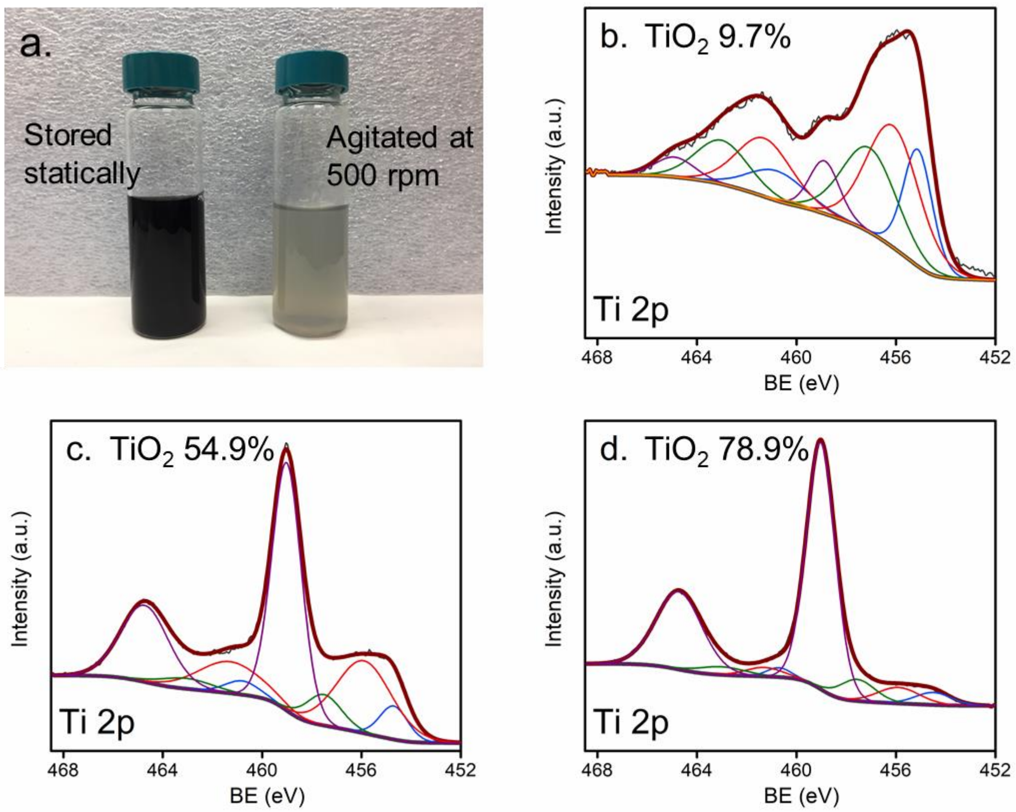

Figure 3-20 (a) A dispersion of Ti_2CT_x MXene nanosheets at a concentration of 6.0 mg/ml was agitated at 500 rpm using a magnetic stir bar. After 40 hours, the stirred dispersion (right vial) shows more oxidation and corresponding color change in comparison to a reference sample kept statically at identical environment (left vial). (b) to (d) X-ray photoelectron spectroscopy (XPS) spectra for Ti 2p for the as-prepared sample, sample kept for 40 hours with agitation at 500 rpm, and sample kept statically for 40 hours. From this figure, it is found that agitation will accelerate the oxidation of MXene nanosheets due to the enhanced mobility of water molecules. Reprinted with permission from reference[61], Copyright 2019 WILEY-VCH Verlag GmbH & Co.

To further understand the role of particle-particle interactions (determined by nanosheet concentration) on oxidation, as-prepared $Ti_3C_2T_x$ aqueous dispersion (3.6 mg/ml) and Ti_2CT_x aqueous dispersion (6.0 mg/ml) were stirred at 500 rpm for 20 days and 40 hours respectively at room temperature in the dark. The stirred MXenes were severely oxidized. The atomic percentage of Ti(IV) increased dramatically from 6.0 % to 35.9 % for stirred $Ti_3C_2T_x$, as shown in **Figure 3-19** For stirred Ti_2CT_x, the Ti(IV) percentage increased dramatically from 9.7 % to 78.9 %, as shown in **Figure 3-20**. In contrast, reference dispersions kept statically under the same conditions reached a final Ti(IV) percentage of 8.6 % for $Ti_3C_2T_x$ and 54.9 % for Ti_2CT_x, respectively. The agitation disrupts the particle-particle steric shielding leading to accelerated oxidation. This observation (stirring vs. not stirring) confirms the idea of edge-to-edge interactions impacting oxidation.

3.4.4. Citric acid prevents degradation of $Ti_3C_2T_x$ and Ti_2CT_x MXenes

Interestingly, we discovered that a weak organic tricarboxylic acid - citric acid (CA), which is one of the components of the acidic buffer solution (pH = 3), is an effective antioxidant for protecting MXenes from oxidation and degradation. Both $Ti_3C_2T_x$ and Ti_2CT_x MXene in this acidic buffer did not show much oxidation, as indicated by the relatively stable electrical conductivities and small changes in the Ti(IV) percentage shown in **Figure 3-11** for $Ti_3C_2T_x$ and **Figure 3-17** for Ti_2CT_x. Compared to the previously reported antioxidants such as a polyphosphate reported by Natu *et al.* [95] and L-ascorbate anion reported by our group, [75] citric acid enables MXene nanosheets to have a much higher and longer stability in terms of chemical composition (shown in **Figure 3-21** and **Figure 3-22**). It is surprising to see from **Figures 3-21a** and **3-21b** that the Ti(IV) percentage does not rise at all for $Ti_3C_2T_x$ vacuum-filtered films made from nanosheets protected by citric acid after even 5 months and longer, while severe oxidation and nearly complete degradation were observed after just 50 days for $Ti_3C_2T_x$ dispersed in a water-only reference system. In addition, citric acid can be used to mitigate the oxidation of Ti_2CT_x, as shown in **Figures 3-21c, 21d,** and **21e**, which was not reported in prior studies. The later can enable the widespread applications of Ti_2CT_x, which have been limited because of their rapid oxidation. To further demonstrate the antioxidation performance of citric acid in the citric acid buffer (pH = 3.0), MXene nanosheets were stored in an acetate buffer with a similar pH of 3.25. We found that the acetate buffer (pH = 3.25) does not protect MXenes from oxidation like the buffer containing citric acid, as shown in **Figure 3-11b** and **Figure 3-17b**. In both buffers, the MXene sheets tend to aggregate; hence, the aggregation of nanosheets is the not the main factor that accounts for the $Ti_3C_2T_x$ stabilization in the citric acid-containing buffer.

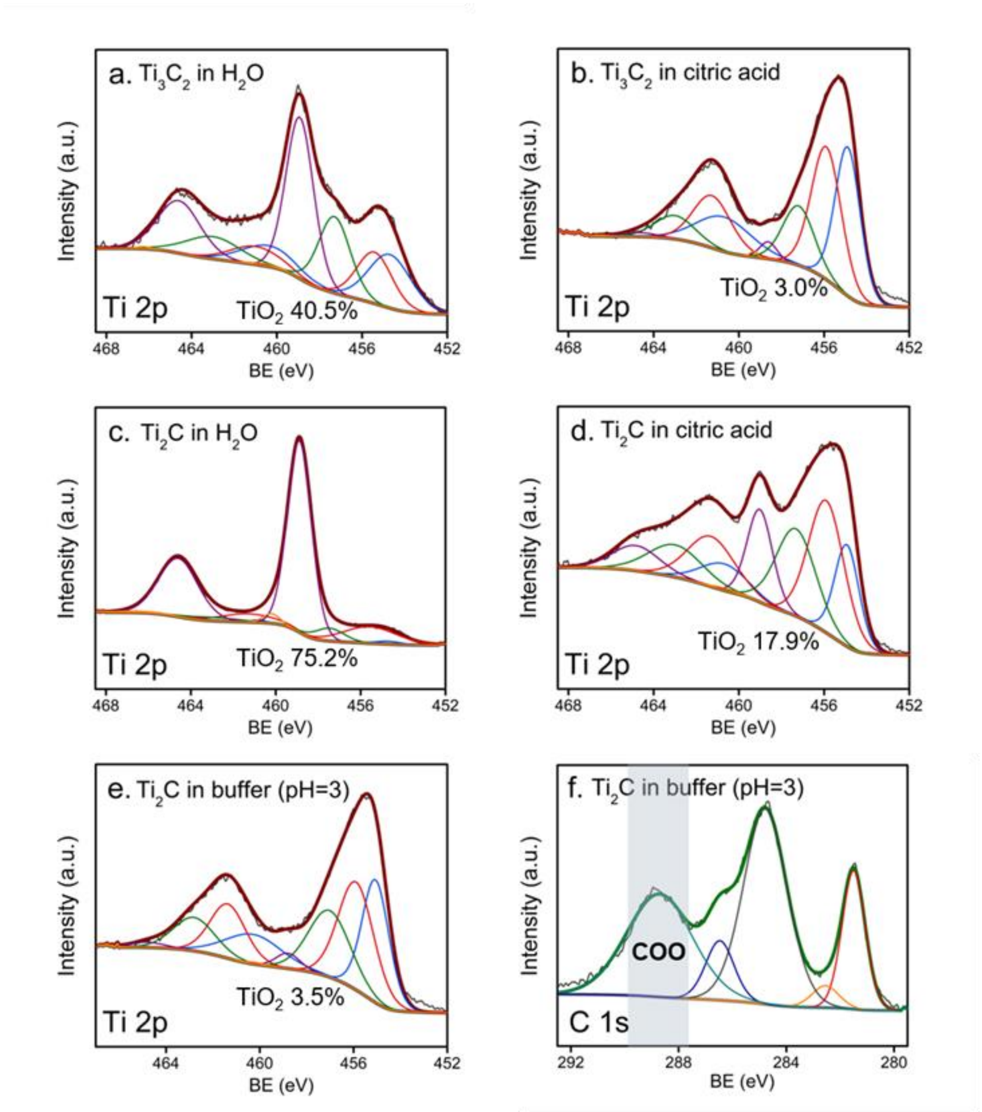

Figure 3-21 X-ray photoelectron spectroscopy (XPS) spectra of Ti 2p for $Ti_3C_2T_x$ vacuum filtered films that had been stored at a concentration of 0.3 mg/ml (a) after 50 days in water and (b) after 5 months in 1.5 mg/ml citric acid solution; Ti_2CT_x films stored at a concentration of 0.3 mg/ml after 40 hours in (c) water, (d) 1.5 mg/ml citric acid, and (e) EMD Millipore buffer (pH=3, made up of citric acid, sodium hydroxide, hydrogen chloride); the buffer solution shows better performance in mitigating the oxidation of Ti_2CT_x due to the interaction between citric acid molecules and nanosheets indicated by the high content of COO^- component (COO^- % = 32.5%) shown in (f) the C 1s spectrum for MXene that had been stored in buffer solution. Reprinted with permission from reference[61], Copyright 2019 WILEY-VCH Verlag GmbH & Co.

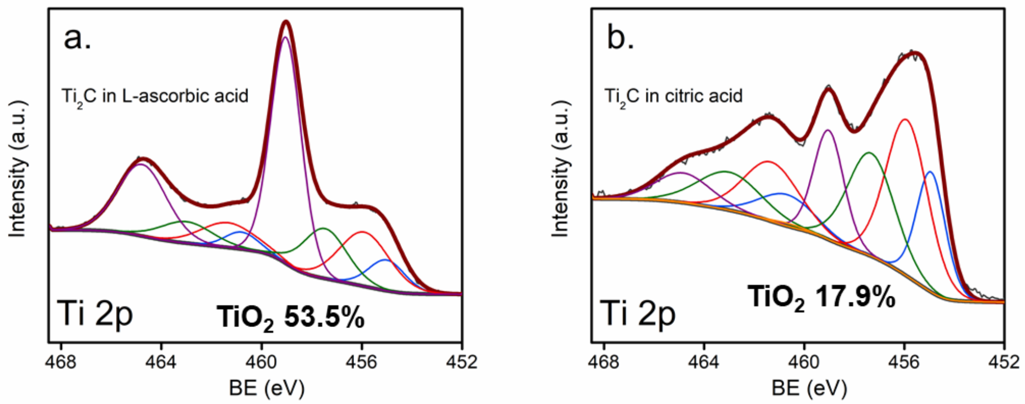

Figure 3-22 X-ray photoelectron spectroscopy (XPS) spectra for Ti 2p in Ti_2CT_x MXene nanosheets protected in (a) L-ascorbic acid solution, and (b) citric acid solution; it is found that citric acid is much more effective than the L-ascorbic acid in preventing Ti_2CT_x oxidizing. Reprinted with permission from reference[61], Copyright 2019 WILEY-VCH Verlag GmbH & Co.

Similar to other antioxidants such as ascorbate and polyphosphate ions, it is reasonable to infer that citric acid protects MXene oxidation through edge capping and shielding. Interestingly, citric acid in the acidic buffer showed better protection for Ti_2CT_x than citric acid in its aqueous solution, indicated by the low Ti(IV) percentage presented. To gain a better understanding of this, the performance of citric acid as an antioxidant was examined in acidic and alkaline environments, respectively. **Figure 3-23** suggests that citric acid is not effective in MXene protection in alkaline environment, in which the citric acid molecules are deprotonated (citric acid is a tricarboxylic acid with three different values of pKa = 3.1, 4.7, and 6.4 [101]). This can be explained by the electrostatic repulsion between the deprotonated citric acid anions and the overall negatively charged MXene nanosheets, which prevents the anion from approaching the MXene basal surfaces and edges for protection. In acidic environments, the antioxidative effect may be achieved by shielding interactions between citric acid molecules and MXene edges as the repulsion barrier is removed, and citric acid molecules are able to approach the nanosheets. In addition, it may also be a result of the hydrogen bonding interactions between MXene functional groups and the protonated citric acid carboxylic groups.

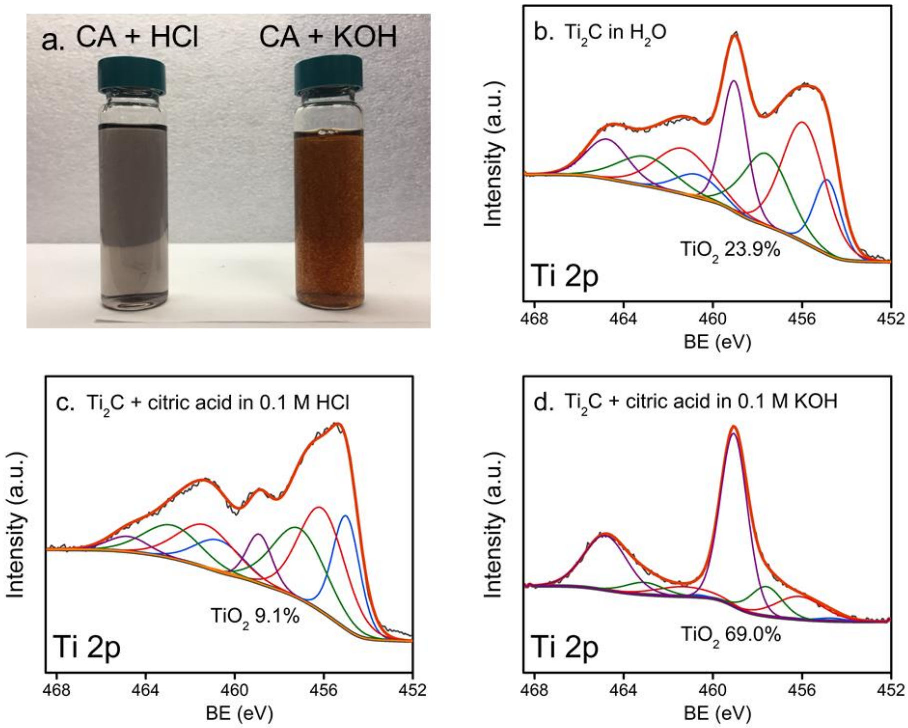

Figure 3-23 Ti_2CT_x nanosheets were dispersed together with citric acid in 0.1 M HCl and 0.1 M KOH solutions, respectively. (a) mixtures of Ti_2CT_x dispersed with citric acid in HCl and KOH after 3 days. (b)-(d) X-ray photoelectron spectroscopy (XPS) spectra for Ti 2p for Ti_2CT_x nanosheets dispersed at a concentration of 0.3 mg/ml after 15 hours in (b) water, (c) 0.1 M HCl solution with citric acid (1.5 mg/ml), and (d) 0.1 M KOH solution with citric acid (1.5 mg/ml); it is found that citric acid is effective in preventing Ti_2CT_x from oxidizing only in neutral or acidic environments. Reprinted with permission from reference[61], Copyright 2019 WILEY-VCH Verlag GmbH & Co.

3.4.5. ReaxFF simulations[‡]

Visualizing and understanding how the dispersed nanosheets interact with ionic species is a task best suited to molecular simulations. To further elucidate the mechanism of how pH affects the oxidation stability of MXene, ReaxFF molecular simulations were performed to examine a single-layer $Ti_3C_2T_x$ MXene nanosheet in systems with altered pH (acidic and alkaline). Three systems were examined: (i) $Ti_3C_2T_x$ nanosheet surrounded by water molecules, (ii) $Ti_3C_2T_x$ nanosheet surrounded by hydroxide ions and water molecules, and (iii) $Ti_3C_2T_x$ MXene nanosheet surrounded with protons and water molecules. In addition, a fourth system with a MXene nanosheet surrounded by water and citric acid molecules was also evaluated to examine the improved stability of nanosheets in the presence of this antioxidant. ReaxFF simulations were carried out at 500 °C for 25 ps using Large-scale Atomic/Molecular Massively Parallel Simulator (LAMMPS) [87] and using the ReaxFF force field from Osti *et al.* [86] To accelerate the kinetics of the reactions, simulations were carried out at a higher temperature as compared to the experiments, which is a common method. [83]

In order to quantify the stability of the $Ti_3C_2T_x$ structures after oxidation, radial distribution functions (*rdf*) were computed for the Ti-C atoms for the last 2.5 ps of each simulation. Only the carbon atoms in the MXene structure were considered for the *rdf* calculations. The radial distribution function, *g(r)*, provides the probability of finding a particle at a distance *r* from another particle in 3-D space. Our results indicate substantially

---

[‡] This simulation work was completed by Dr. Aniruddh Vashisth.

less oxidation in the acidic system as compared to the basic system shown in **Figure 3-24**. A peak at 2.1 Å is observed in the Ti-C bond (the backbone of MXene structure) *rdf* calculations, which is characteristic of a crystalline $Ti_3C_2T_x$ structure. The *rdf* peak intensity at 2.1 Å for the acidic system is the highest, followed by the system with just water, and then the basic system. These simulations support the experimental measurements, as the Ti(IV) percentage of MXene stored in basic medium increases more rapidly as compared to acidic systems due to oxidation in the presence of hydroxide anions. The final frames of the oxidation simulations in acidic and basic systems are shown in **Figure 3-25**.

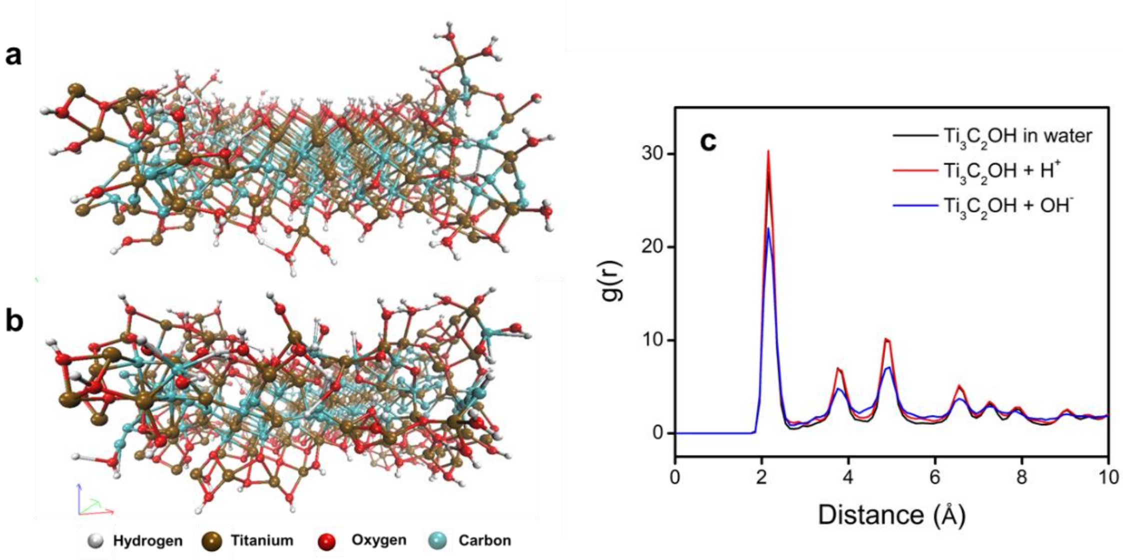

Figure 3-24 Final molecular configuration of $Ti_3C_2T_x$ nanosheet after 25 ps ReaxFF molecular dynamic simulation of systems with (a) $Ti_3C_2T_x$ MXene nanosheet, water and protons (acidic environment), and (b) $Ti_3C_2T_x$ MXene nanosheet, water, and hydroxide ions (alkaline environment). (c) The radial distribution functions of Ti-C bonds obtained by ReaxFF are shown for acidic, alkaline, and water-only systems. A higher peak intensity at 2.1 Å was obtained for nanosheets stored in the acidic system, suggesting a higher level of stability against oxidation. Reprinted with permission from reference[61], Copyright 2019 WILEY-VCH Verlag GmbH & Co.

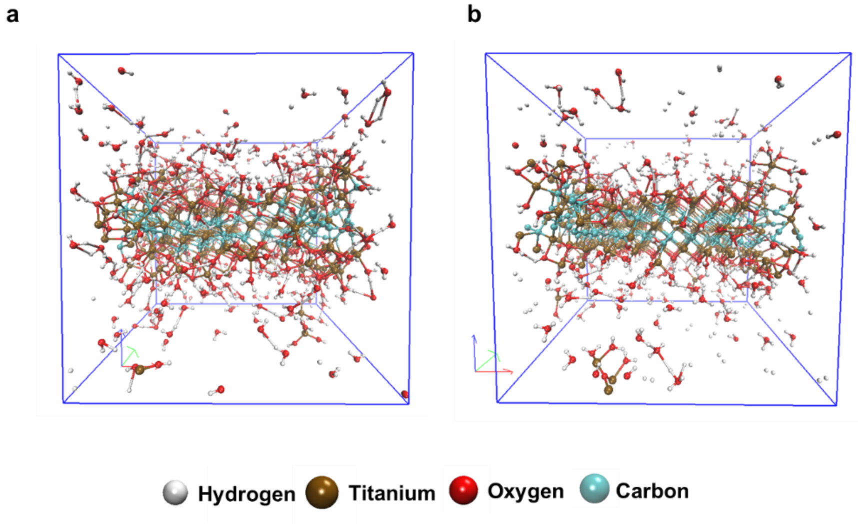

Figure 3-25 Final molecular configuration of molecules from molecular dynamic simulation of systems with (a) $Ti_3C_2T_x$ MXene nanosheet, water and hydroxide ions, and (b) $Ti_3C_2T_x$ MXene nanosheet, water, and protons. Reprinted with permission from reference[61], Copyright 2019 WILEY-VCH Verlag GmbH & Co.

To understand the mechanism driving the higher stability in acidic systems as compared to basic systems, we carried out a frame-by-frame examination of the simulation trajectories. As detailed in our previous publication, [75] oxidation starts along the nanosheet edges in the system with only water and the $Ti_3C_2T_x$ nanosheet. For the acidic system, we observe that protons interact with water molecules to form H_3O^+ intermediate species. These intermediate species as well as the MXene nanosheet edges are positively charged, therefore we observe minimal oxidation in the acidic system (**Figure 3-24a)**. The MXene nanosheet stored in the basic system is primarily attacked by the highly reactive hydroxide anions, with oxidation starting from the edges, and later affecting the basal plane as well (**Figure 3-24b**). The simulation results indicate that the MXene nanosheet stored in the basic system loses Ti atoms in the form of TiO_2 and other complex species with Ti, O, and

H atoms. Overall, MXene stored in basic system show much faster oxidation due to the aggressive nature of hydroxide ions.

Simulations of the effect of citric acid on the oxidation stability of MXene nanosheets show improved stability, mainly due to the steric shielding effect of citric acid along the edges. The final structure of a $Ti_3C_2T_x$ MXene nanosheet after 25 ps is shown in **Figure 3-26a**. The *rdf* calculations show a higher peak intensity at 2.1 Å as compared to just water and MXene system, suggesting less oxidation in the presence of citric acid (**Figure 3-26b**).

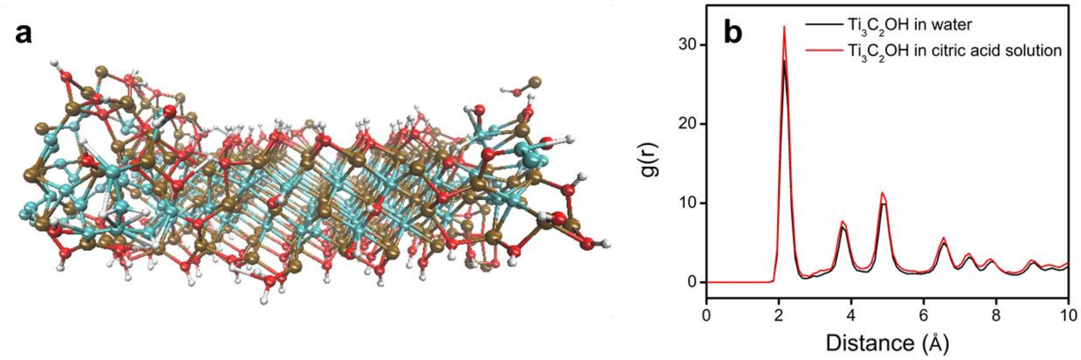

Figure 3-26 (a) Final molecular configuration of $Ti_3C_2T_x$ nanosheet after 25 ps ReaxFF molecular dynamic simulation of systems with $Ti_3C_2T_x$ MXene nanosheet, water and citric acid. (b) The radial distribution functions of Ti-C bonds obtained by ReaxFF are shown for MXene in water, and citric acid. The peak intensity at 2.1 Å represents the higher stability of the nanosheet in citric acid. Reprinted with permission from reference[61], Copyright 2019 WILEY-VCH Verlag GmbH & Co.

3.5. Conclusion

Our study demonstrates that the oxidation kinetics of $Ti_3C_2T_x$ and Ti_2CT_x MXenes are dependent on the pH and concentration of the dispersions. MXene nanosheets in the aqueous phase can interact with hydroxide anions rapidly, then become more prone to oxidation due to the unstable terminal group $-O^-$. Meanwhile, the pH value drops rapidly in the initially alkaline MXene dispersion. Hence, MXene processing and applications in alkaline environments may lead to sub-optimal or declining performance due to the rapid oxidation. The oxidation of MXene nanosheets in various buffers were also examined, and the results suggest that the highest oxidation rate occurs when hydroxide anions are continuously available. In addition, an effective antioxidant, citric acid, was discovered, which can effectively prevent or mitigate the oxidation of both “312” $Ti_3C_2T_x$ and “211” Ti_2CT_x. We also demonstrated that the oxidation rate decreases when the MXene dispersion concentration is high due to steric shielding effect among the nanosheets. With these new findings, we recommend that MXene dispersions be formulated to have a high concentration, acidic pH, and citric acid to minimize their oxidation.

4. MOLECULAR STRUCTURE AND OXIDATION STABILITY: INTERACTIONS BETWEEN ANTIOXIDANTS AND $TI_3C_2T_X$ AND TI_2CT_X MXENES

4.1. Introduction

MXenes are a fast-growing family of two-dimensional transition metal carbides, nitrides, and carbonitrides.[1-3, 5, 40] MXenes have a general formula of $M_{n+1}X_nT_x$, where n+1 layers (n is from 1 to 4) of transition metal atoms ('M' element) are interleaved and covalently bonded with n layers of carbon or nitrogen atoms ('X' element). T_x represents the functional groups attached to the MXene layer surface resulting from the wet chemical synthesis methods (-OH, =O, -F, and -Cl). The majority of known carbide MXenes, such as $Ti_3C_2T_x$, Ti_2CT_x, V_2CT_x, and Nb_2CT_x, are synthesized from their ceramic MAX phase (with a formula of $M_{n+1}AX_n$, where A is a group 13 or 14 element) by the top-down selective acid etching method in hydrofluoric acid (HF) or fluorinated aqueous solutions, followed by intercalation and delamination steps.[8, 44, 102-104]

MXenes are known for a combination of excellent functional properties such as high electrical conductivity, good aqueous processability, and a variety of surface terminal groups. Extensive studies have focused on the practical applications of MXenes, especially in energy storage,[13-15, 105-107] electromagnetic wave shielding,[18, 108-110] layer-by-layer functional coatings,[16, 17, 20] nanocomposites,[19, 22, 33] optoelectronic devices,[111, 112] sensors,[17, 113] catalysis,[114] and biomedical applications[115, 116].

However, MXenes are generally not stable against oxidation, especially in their commonly-used aqueous colloidal state. Prior studies have demonstrated that MXenes are prone to react with water and strong oxidants, resulting in structural and chemical degradation over time.[46, 65] This phenomenon and issue of rapid MXene oxidation and degradation is still not well-understood and is often missing from prior reports on MXene applications. Low oxidation stability threatens to restrict both the shelf life of MXene dispersions and the product lifetime for MXene-based devices.

Multiple studies have discovered that oxidation results in the degradation of the MXene's 2D structure and loss of functional properties. $Ti_3C_2T_x$ and Ti_2CT_x nanosheets in their aqueous colloidal state and in functional films can react with water molecules, resulting in the formation of titanium dioxides (TiO_2) and amorphous carbon.[46, 65, 69, 71] Oxidation rates of MXene nanosheets dispersed in water were found to be a function of dispersion temperature, pH, exposure to laser and UV light, and the presence of oxidants such as hydroxide anions, hydrogen peroxide, and ozone.[46, 61, 68, 117] In addition to dispersed nanosheets, storage or usage of dried MXene nanosheet powders and MXene-based devices in conditions with high humidity or elevated temperatures in an oxidizing atmosphere may also result in structural degradation and declined electrical performance .[46, 74, 89] Naguib *et al.* and others reported that MXene oxidation starts from nanosheet edges so that large nanosheets may have better oxidation stability than the small ones.[45, 51] MXene oxidation is also dependent on intrinsic nanosheet properties such as defective vacancies and surface functionalization.[70, 74] Furthermore, MXenes with small *n* oxidize much more rapidly than their high *n* counterparts; for example, oxidation rates show the following trend: $Ti_4C_3T_x < Ti_3C_2T_x < Ti_2CT_x$.[61]

Several investigations have focused on developing methods to prevent or mitigate oxidation during storage in the colloidal state and prolong the usage life of MXene-based devices. Early studies recommended preserving MXene dispersions under extremely low temperatures (for example, at -80 °C) and oxidant-free conditions such as argon-filled vials.[46, 64, 77] However, these methods restrict the usage conditions of MXene-based devices and lower the MXene processability in ambient environment. MXene oxidation stability can also be improved by reducing the amount of reactive oxygen-containing groups, which may be achieved by thermal annealing under inert or reductive environments.[74, 80]

Both our team and Natu *et al.* discovered an approach to prevent the oxidation of $Ti_3C_2T_x$ and Ti_2CT_x in their colloidal form by introducing antioxidants such as sodium L-ascorbate, ascorbic acid, citric acid, and polyphosphate anions.[61, 75, 95] The shelf life of MXene colloid can be significantly improved with this method. For example, $Ti_3C_2T_x$ can be stored in an aqueous solution of citric acid for over 5 months without seeing any transformation of its chemical composition, which has a much longer storage life for $Ti_3C_2T_x$ in water.[61] However, the protection mechanism of the antioxidant is still not very clear. Molecular simulations were used to investigate the interaction between the $Ti_3C_2T_x$ nanosheets and antioxidants. The simulation results suggest that the stabilization of $Ti_3C_2T_x$ is achieved by edge-capping and/or steric shielding caused by the association of the antioxidant molecules with the nanosheets, although the nature of the association remains somewhat elusive. This interaction restricts water molecules from reacting with the MXene surface. Even so, this protection mechanism still remains elusive, particularly in understanding how other antioxidants would interact with MXene surfaces.

In this study, we carry out an investigation on the oxidation stability of $Ti_3C_2T_x$ and Ti_2CT_x dispersed in aqueous solutions of antioxidants from groups such as α-hydroxy acids, polycarboxylic acids, and phenolic acids. The oxidation stability of the MXene nanosheets was determined by X-ray photoelectron microscopy (XPS) after 14-day storage for $Ti_3C_2T_x$ and 31-hour storage for Ti_2CT_x. This study reveals that MXene nanosheets interact differently with each of the organic compounds. We discovered that $Ti_3C_2T_x$ and Ti_2CT_x MXene nanosheets can be stabilized by multiple antioxidants, including citric acid, tartaric acid, and oxalic acid. However, some antioxidant candidates actually accelerate MXene oxidation and degradation. Here we analyze the relationship between an antioxidant's chemical structure and its effectiveness in protecting $Ti_3C_2T_x$ and Ti_2CT_x. This work proposes that a chelation effect induced by antioxidants with polydentate ligands helps to prevent or eliminate MXene oxidation. These results represent a significant improvement in understanding the stabilization of MXene nanosheets in aqueous dispersion, and this paper is the first to report the various effects of organic acids on the oxidation stability of MXenes.

4.2. Materials and methods

4.2.1. Synthesis of MAX precursor particles

Elemental powder mixtures of Ti, Al, and TiC were used as starting materials to synthesize the precursor Ti_3AlC_2 and Ti_2AlC MAX phase. The mixtures were sintered using the Pulsed Electric Current System (PECS). The high-purity MAX powder was made by drill-milling and being sieved to obtain powder with particle sizes below 44 μm for Ti_3AlC_2 and below 20 μm for Ti_2AlC.

4.2.2. Synthesis of $Ti_3C_2T_x$ and Ti_2CT_x nanosheets

$Ti_3C_2T_x$ nanosheets were synthesized by etching aluminum from the MAX phase following the selective acid etching method reported in prior literatures.[8, 35, 38] 50 mL of 6 M HCl solution was made by diluting concentrated hydrochloric acid (HCl, ACS reagent, 37% w/w Sigma-Aldrich) with DI water. 3.5 grams of lithium fluoride (LiF, 98+% purity, Alfa Aesar) was dissolved into the HCl solution. 5 grams of Ti_3AlC_2 MAX powder was slowly added to the HCl+LiF solution to prevent overheating. The mixture was stirred and kept at 40 ºC for 40 hours. After etching, several washing cycles were implemented to remove HF and Li cations until pH of the mixture reached a value of above 6. $Ti_3C_2T_x$ clay was then intercalated with dimethyl sulfoxide (DMSO) (ReagentPlus, >99.5%, Sigma-Aldrich) for 20 hours. Excess DMSO was removed by multiple cycles of solvent exchanges with DI water and centrifugation at 9000 rpm. The intercalated $Ti_3C_2T_x$ clay particles in DI water were bath sonicated for 1 hour at room temperature followed by centrifugation at 3500 rpm for 1 hour to separate the heavier components. The synthesize $Ti_3C_2T_x$ nanosheet dispersion has a concentration of 8.8 mg/mL.

Ti_2CT_x nanosheets were synthesized by a similar method with $Ti_3C_2T_x$ but with a reduced etching duration of 12 hours and a lower etching temperature at 36 ºC. The as-prepared Ti_2CT_x nanosheet dispersion was measured to have a concentration of 10.0 mg/mL.

4.2.3. Sample preparation

Before introducing the MXene nanosheets, 250 mL aqueous solutions of organic compounds in groups of α-hydroxy acids, polycarboxylic acids, and phenolic acids were prepared at a concentration of 1.5 mg/mL. 0.5 mL of the as-prepared dispersion of MXene nanosheets was then introduced and diluted individually into each of the target solutions. The dispersions of $Ti_3C_2T_x$ in each solution of organic substances were stored in closed bottles for 14 days at ambient conditions. The dispersions of Ti_2CT_x were stored in closed bottles for 31 hours.

4.2.4. Characterization

Scanning electron microscope (SEM, JSM-7500F, JEOL, Japan) and atomic force microscope (AFM, Bruker, USA) were used in the morphology study of dehydrated MAX, clay particle, and MXene nanosheets. The degree of MXene oxidation was determined by using an Omicron X-ray photoelectron spectrometer (XPS) employing a Mg-sourced X-ray beam. The films used for XPS analysis were prepared by vacuum filtration of the stored MXene dispersions. Prior to XPS, the films were dried under vacuum for 20 hours to prevent possible outgassing. XPS peak fittings and quantifications were analyzed using CasaXPS software (version 2.3.22). ζ potential and hydrodynamic size changes of MXene dispersions were measured and monitored using a Zetasizer Nano ZS90 from Malvern Instruments, USA.

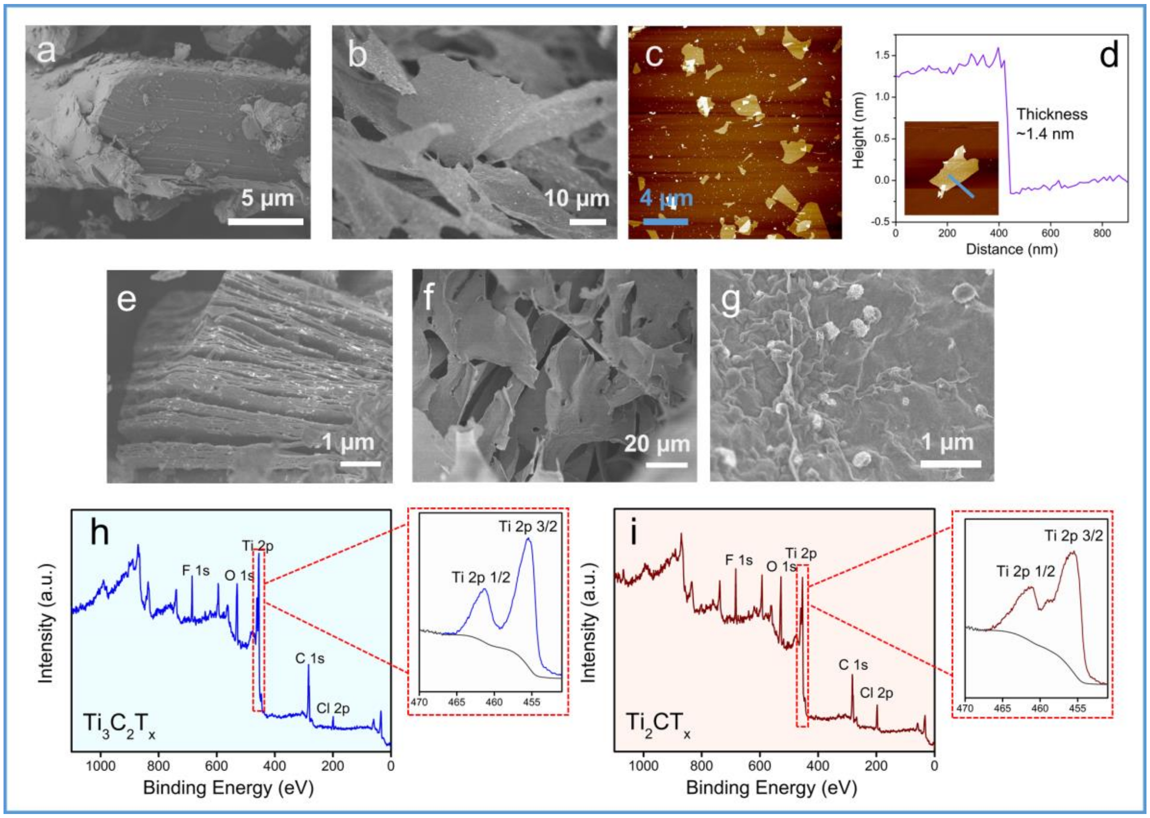

Figure 4-1 (a) Scanning electron microscopy (SEM) image of the Ti_3AlC_2 MAX precursor particles; (b) morphology of freeze-dried $Ti_3C_2T_x$ 2D nanosheets imaged by SEM; (c) atomic force microscopy (AFM) image and (d) height profile of $Ti_3C_2T_x$ nanosheets. Sample was prepared by drop-casting dispersion on a mica disk; (e) SEM image of the multilayered Ti_2CT_x MXene clay particle; (f) morphology of freeze-dried Ti_2CT_x 2D nanosheets imaged by SEM; (g) TiO_2 nanoparticles shown on as-prepared Ti_2CT_x nanosheets made by freeze-drying the colloidal dispersion, imaged by SEM; X-ray photoelectron microscopy (XPS) spectra of as-prepared (h) $Ti_3C_2T_x$ and (i) Ti_2CT_x MXene nanosheets. Sample used for XPS analysis was made by vacuum filtration. Split peaks of Ti 2p spectra were also displayed in the inserted figures.

4.3. Results and discussion

$Ti_3C_2T_x$ and Ti_2CT_x MXene nanosheets were synthesized via the selective acid etching method used in prior literatures.[8, 35, 38] Morphologies of bulk Ti_3AlC_2 MAX particle and freeze-dried $Ti_3C_2T_x$ nanosheets are shown in SEM images in **Figure 4-1a**

and 1b. AFM images indicate that $Ti_3C_2T_x$ nanosheets have a size distribution from 0.5 to 5 µm and a thickness of ~1.4 nm (**Figure 4-1c and 1d)**. For the Ti_2CT_x samples, the morphologies of both the clay and the delaminated Ti_2CT_x nanosheets are shown as well (**Figure 4-1e, 4-1f,** and **4-1g)**. Even for measurements taken right after exfoliation, TiO_2 nanoparticles were already observed on Ti_2CT_x nanosheet surface, indicating that these nanosheets have very poor oxidation stability. XPS confirms the presence of titanium, carbon, oxygen, and fluorine elements on the as-prepared $Ti_3C_2T_x$ and Ti_2CT_x surfaces (**Figure 4-1h** and **4-1i**).

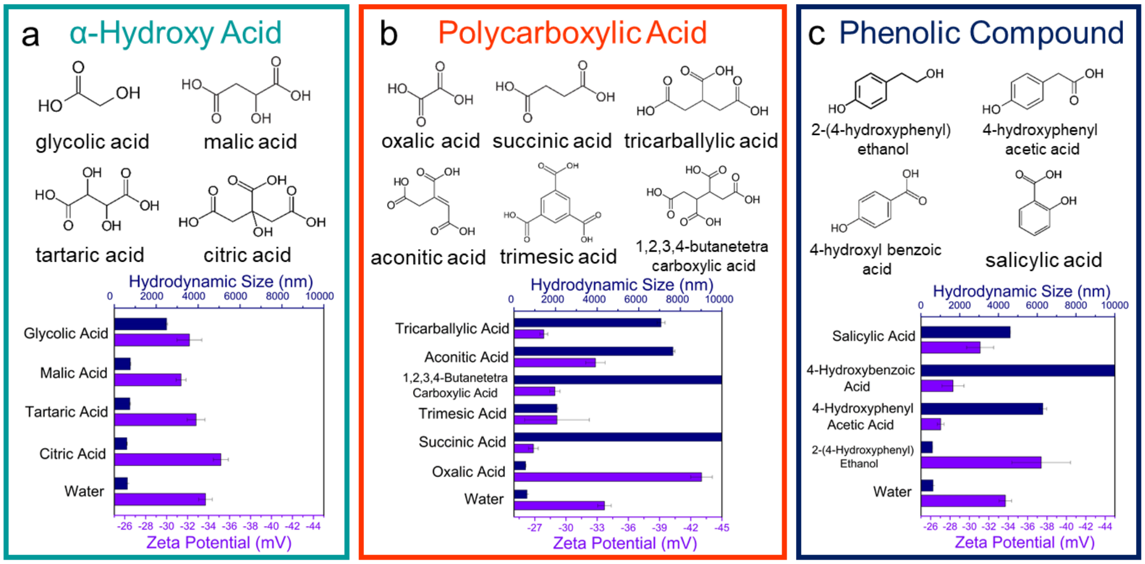

Figure 4-2 Molecular structures of studied organic compounds in the three antioxidant classes. $Ti_3C_2T_x$ nanosheet dispersions were mixed with antioxidant solutions; after 3 hours, the zeta potential and hydrodynamic size were measured all three classes of antioxidants: (a) α-hydroxy acids, (b) polycarboxylic acids, and (c) phenolic compounds.

For the antioxidant study, as-prepared nanosheet dispersions were introduced and diluted individually into distilled water and each of the 1.5 mg/mL aqueous solutions of the antioxidant candidates. The mixtures were stored in closed bottles for 14 days at ambient conditions. We utilized the following characterization techniques to assess oxidation: XPS determines the extent of $Ti_3C_2T_x$ oxidation by Ti(IV) atomic percentage in each dispersion before and after the storage. The colloidal stability of dispersed $Ti_3C_2T_x$ MXenes in each solution were investigated by measuring the zeta-potential and hydrodynamic size average using the dynamic light scattering technique (DLS). Ti_2CT_x nanosheets were assessed as well, over a much shorter time frame of 31 hours due to their rapid oxidation.

We have grouped the antioxidant candidates into three major categories based on their molecular structures (displayed in **Figure 4-2**): α-hydroxy acids, polycarboxylic acids, and phenolic compounds. After 3 hours of storage, the $Ti_3C_2T_x$ nanosheet dispersions with additives already exhibited different colloidal behaviors. $Ti_3C_2T_x$ nanosheets in the α-hydroxy acid solutions and water maintained their colloidal stability, showing stronger zeta potential values (less than -30 mV) and generally small hydrodynamic sizes (**Figure 4-2a**). However, the polycarboxylic acids (except oxalic and trimesic acid) rapidly induced aggregation, resulting in the formation of nanosheet clusters with large hydrodynamic sizes (over 6000 nm) (**Figure 4-2b**). Natu *et al.* reported that at low pH, there are few deprotonated hydroxyl ($-O^-$) terminal groups, leading to decreased electrostatic repulsion and eventual aggregation.[60] However, we find that $Ti_3C_2T_x$ in oxalic acid solution showed a stronger zeta potential value, even though oxalic acid is a stronger acid than the other polycarboxylic acids (with a low pK_a of around 1.2). Finally, the addition of phenolic acids leads to weaker zeta potential values and increased hydrodynamic size, shown in **Figure 4-2c**.

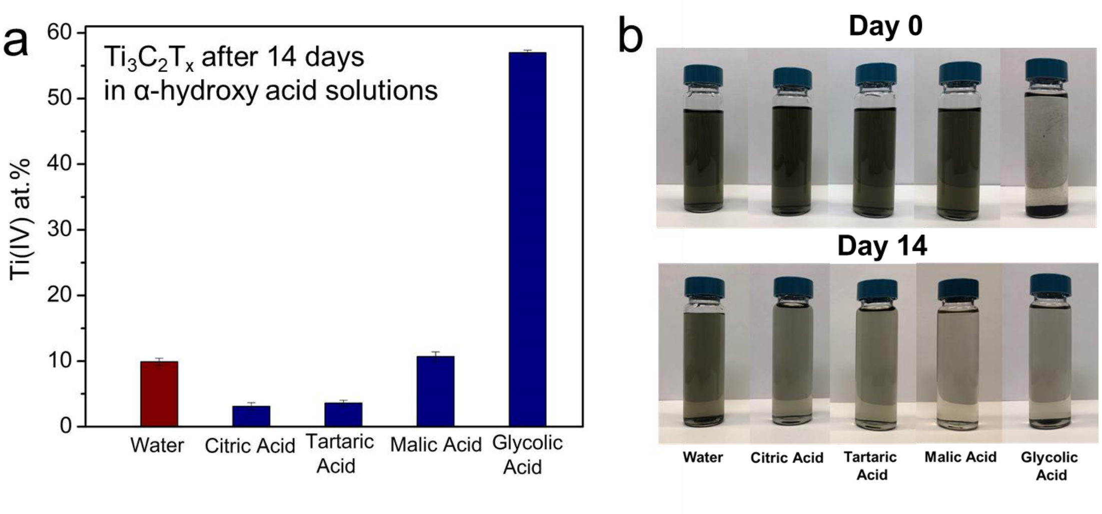

Figure 4-3 (a) Atomic composition of Ti(IV) measured by X-ray photoelectron microscopy (XPS) for $Ti_3C_2T_x$ nanosheets dispersed in water and 1.5 mg/mL aqueous solutions of α-hydroxyl acids after 14-day storage; (b) visual appearance of $Ti_3C_2T_x$ dispersions before and after storage. Samples used for XPS were made by vacuum filtration, followed by a 24-hour dehydration process under vacuum.

In prior studies, our group demonstrated that citric acid, which is a tricarboxylic acid in the α-hydroxy acid group, can effectively enhance the oxidation stability of dispersed $Ti_3C_2T_x$ nanosheets. Here we generalize these findings to other types of α-hydroxyl acids, including glycolic acid, malic acid, and tartaric acid. XPS analysis indicates that $Ti_3C_2T_x$ nanosheets stored in citric acid and tartaric acid solutions were the most stable after 14 days, yielding low Ti(IV) atomic percentages (reflecting the formed TiO_2 content) of 3.1 ± 0.6 at.% and 3.6 ± 0.4 at.%, significantly lower than samples stored in water (**Figure 4-3a**). (The full XPS spectra of $Ti_3C_2T_x$ in hydroxyl acids are summarized in **Figure 4-4**.) Malic acid showed behavior similar to that of water, but glycolic acid actually appeared to accelerate the oxidation of $Ti_3C_2T_x$. These findings are consistent with changes in visual appearance of the $Ti_3C_2T_x$ dispersions over time (**Figure 4-3b)**. The effective antioxidants not only prevent TiO_2 formation, but they also maintain zeta potential and hydrodynamic size after 14 days in storage (**Figure 4-5)**.

We also investigated the interactions of several polycarboxylic acids with $Ti_3C_2T_x$ nanosheets. In contrast to α-hydroxyl acids, polycarboxylic acids contain two or more carboxyl groups in their molecular structures but do not have an α-hydroxy group adjacent to the carboxyl groups. Oxalic acid, which is the simplest dicarboxylic acid, was discovered to be an effective antioxidant for $Ti_3C_2T_x$ in this study, showing a Ti(IV) content of 1.7 ± 0.3 at.% after storage, which is much lower than that of water (**Figure 4-6a**). However, succinic acid, trimesic acid, 1,2,3,4-butanetetra carboxylic acid, aconitic acid, and tricarballylic acid were observed to accelerate the oxidation of $Ti_3C_2T_x$, displaying much higher TiO_2 content after the testing period. (The full XPS spectra of $Ti_3C_2T_x$ in polycarboxylic acids are displayed in **Figure 4-7**). In addition, oxalic acid retained the colloidal stability of $Ti_3C_2T_x$ dispersion after 14-day storage (**Figure 4-6b**) while the dark green/black aggregated $Ti_3C_2T_x$ in other polycarboxylic acid solutions turned into brownish-gray sediments, confirming the degradation of $Ti_3C_2T_x$.

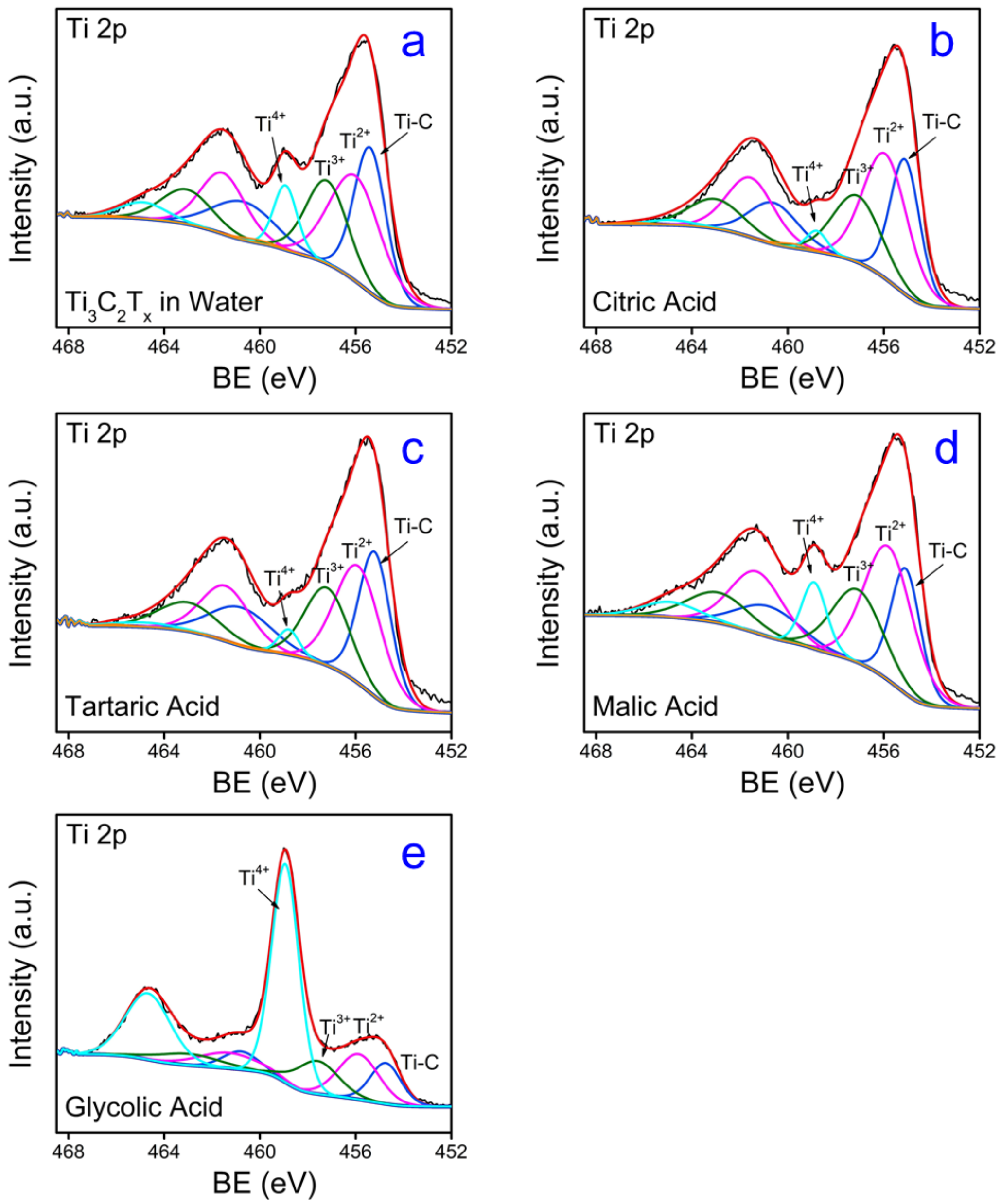

Figure 4-4 X-ray photoelectron microscopy (XPS) spectra for $Ti_3C_2T_x$ nanosheets after 14-day storage dispersed in (a) water and 1.5 mg/mL aqueous solutions of (b) citric acid, (c) tartaric acid, (d) malic acid, and (e) glycolic acid.

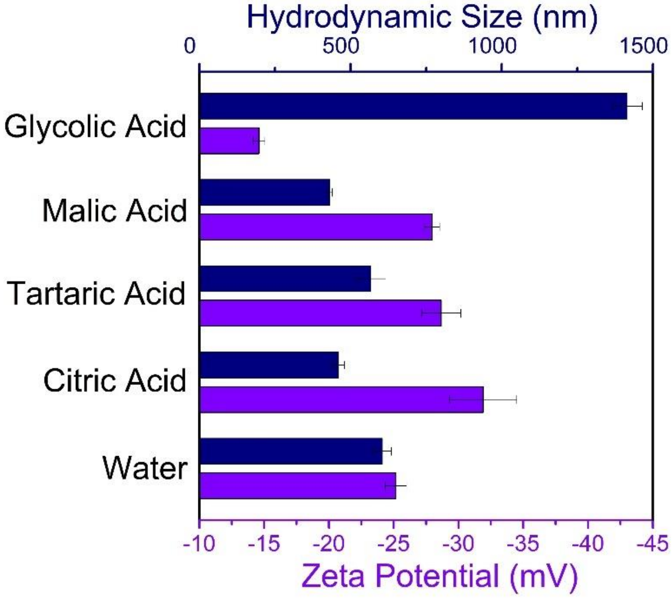

Figure 4-5 Zeta potential and hydrodynamic size of $Ti_3C_2T_x$ nanosheets dispersed in water and α-hydroxyl acid aqueous solutions after the 14-day storage.

Several phenolic compounds were investigated in this study as well. 2-(4-Hydroxyphenyl) ethanol (tyrosol) is a phenylethanoid which has been used in other settings as a naturally occurring antioxidant. After 14-day storage, tyrosol did not exhibit any major effect on the oxidation and colloidal stability of $Ti_3C_2T_x$ nanosheets. However, 4-hydroxyphenyl acetic acid, in which the -OH group in tyrosol's side chain is substituted by -COOH group, actually accelerates the oxidation of $Ti_3C_2T_x$ (**Figure 4-8a**). We also compared 4-hydroxybenzoic acid (para-hydroxybenzoic acid) and salicylic acid (2-hydroxybenzoic acid or ortho-hydroxybenzoic acid). After the testing period, salicylic acid did not show much impact on the Ti(IV) content in the sample. However, 4-hydroxybenzoic acid can completely oxidize the $Ti_3C_2T_x$, as indicated by a high Ti(IV) content of 81.5 ± 0.7 at.%. The XPS spectra of $Ti_3C_2T_x$ in polycarboxylic acids after storage are summarized in **Figure 4-9**. Note that in all cases, acids (not the tyrosol) caused visual aggregation of $Ti_3C_2T_x$ even in the as-prepared dispersions (**Figure 4-8b**).

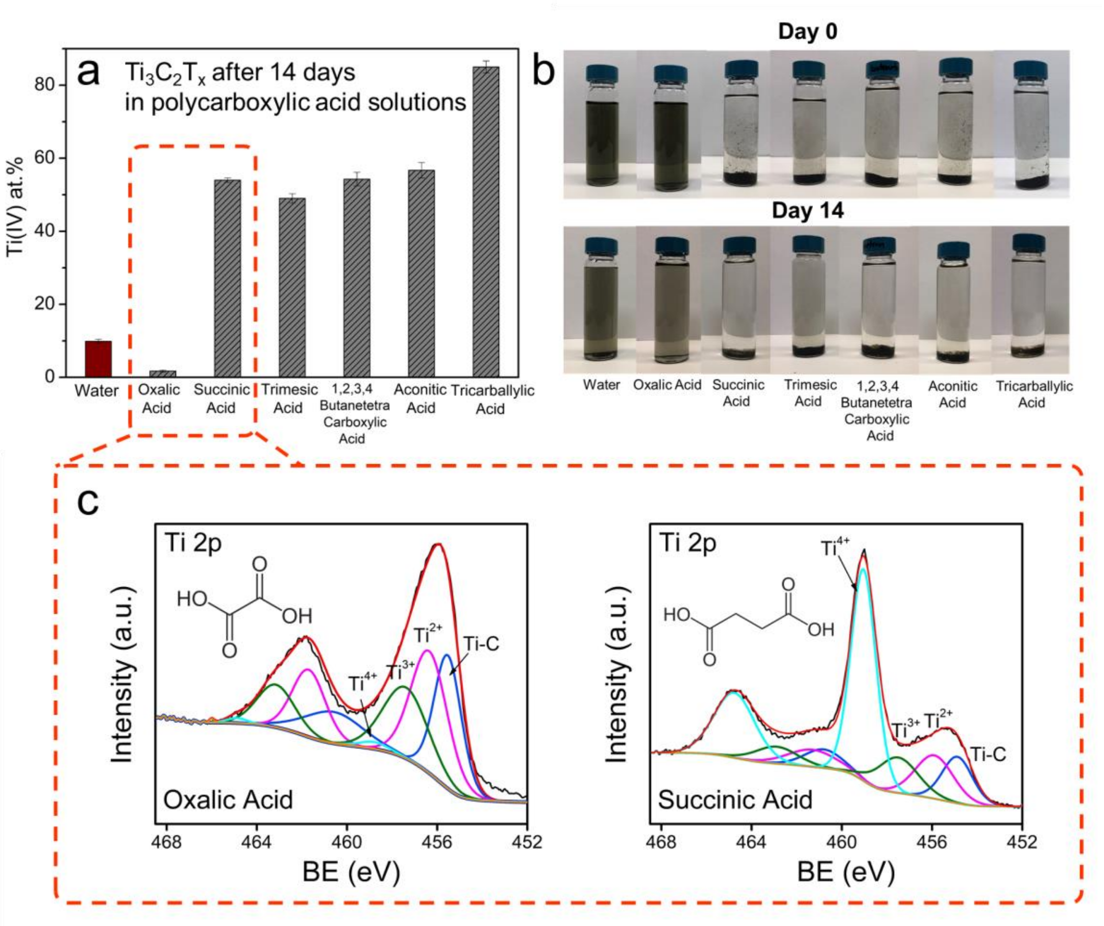

Figure 4-6 (a) Atomic contents of Ti(IV) measured by X-ray photoelectron microscopy (XPS) for $Ti_3C_2T_x$ nanosheets dispersed in water and 1.5 mg/mL aqueous solutions of polycarboxylic acids after 14-day storage; samples used for XPS were made by vacuum filtration, followed by a 24-hour dehydration process under vacuum. (b) $Ti_3C_2T_x$ dispersions before and after storage in aqueous solutions of polycarboxylic acids. (c) Comparison of XPS spectra of $Ti_3C_2T_x$ in dispersions in aqueous solutions of oxalic acid and succinic acid.

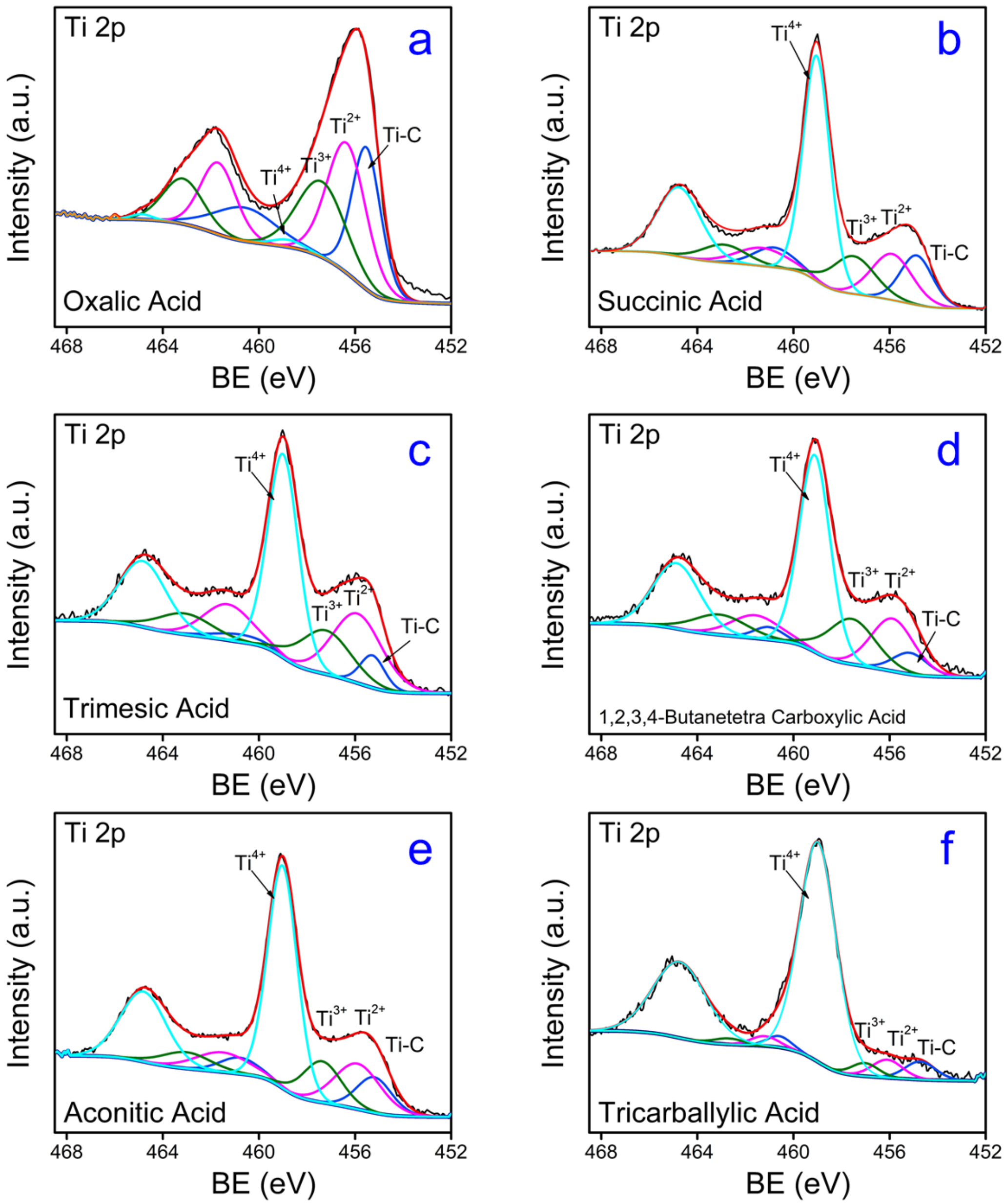

Figure 4-7 X-ray photoelectron microscopy (XPS) spectra for $Ti_3C_2T_x$ nanosheets after 14-day storage dispersed in 1.5 mg/mL aqueous solutions of (a) oxalic acid, (b) succinic acid, (c) trimesic acid, (d) 1,2,3,4-butanetetra carboxylic acid, (e) trans-aconitic acid, and (f) tricarballylic acid.

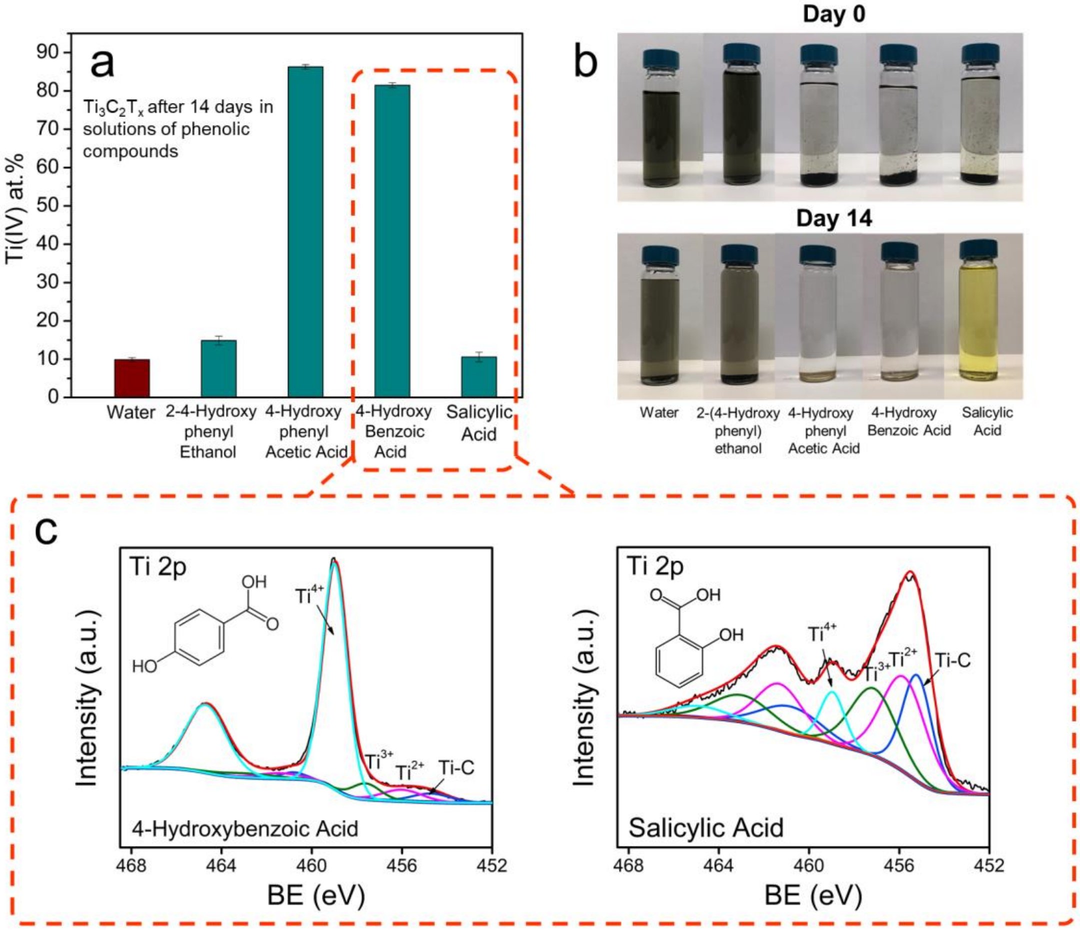

Figure 4-8 (a) Atomic contents of Ti(IV) measured by X-ray photoelectron microscopy (XPS) for $Ti_3C_2T_x$ nanosheets dispersed in water and 1.5 mg/mL aqueous solutions of phenolic compounds after 14-day storage; samples used for XPS were made by vacuum filtration, followed by a 24-hour dehydration process under vacuum. (b) $Ti_3C_2T_x$ dispersions before and after storage in aqueous solutions of phenolic compounds. (c) Comparison of XPS spectra of $Ti_3C_2T_x$ in dispersions in aqueous solutions of 4-hydroxybenzoic acid and salicylic acid.

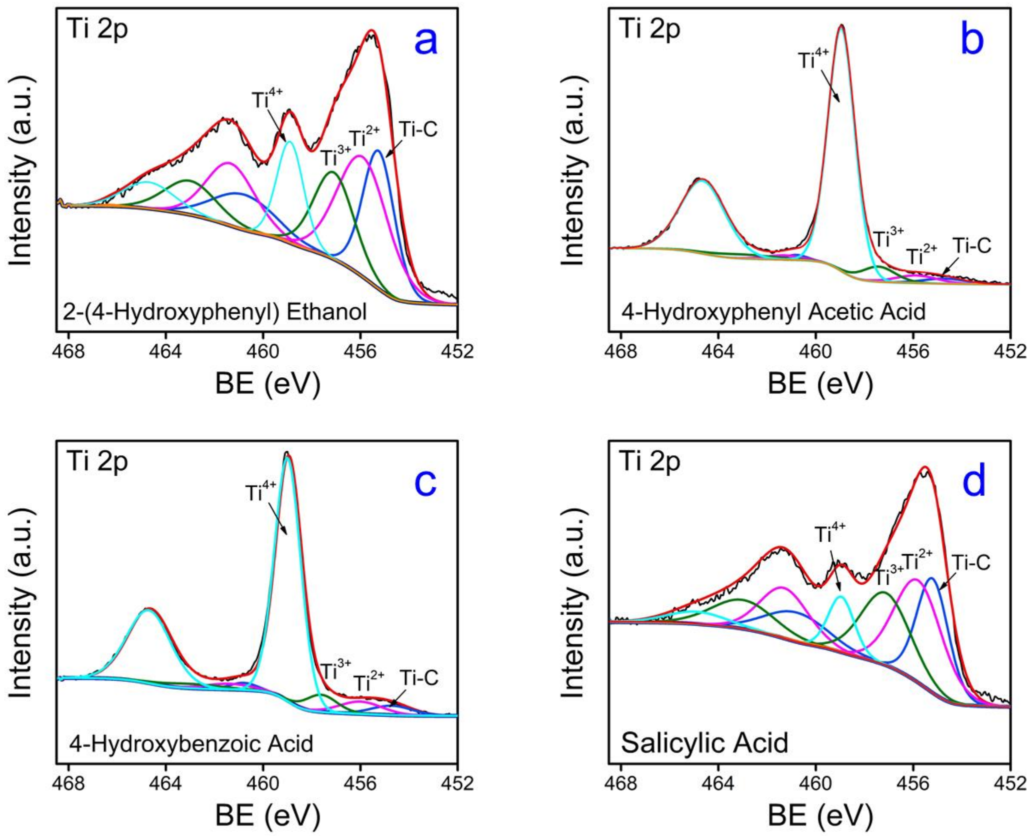

Figure 4-9 X-ray photoelectron microscopy (XPS) spectra for $Ti_3C_2T_x$ nanosheets after 14-day storage dispersed in 1.5 mg/mL aqueous solutions of (a) 2-(4-hydroxyphenyl) ethanol, (b) 4 hydroxyphenyl acetic acid, (c) 4-hydroxybenzoic acid, and (d) salicylic acid.

The antioxidant performance of α-hydroxy acids, polycarboxylic acids, and phenolic compounds is summarized in **Figure 4-10a**. The data indicate that citric acid, tartaric acid, and oxalic acid can effectively protect $Ti_3C_2T_x$ from oxidation; however, other antioxidant candidates have limited or even deleterious effects on the nanosheets. The effective antioxidants not only prevented the transformation of $T_3C_2T_x$ structures into TiO_2, but also retained stable negative zeta potential values and hydrodynamic size (**Figure 4-10b**). In contrast, the poor antioxidants, such as malic acid and glycolic acid, cause the $Ti_3C_2T_x$ dispersion to have weaker zeta potential values and increased hydrodynamic size (associated with nanosheet aggregation).

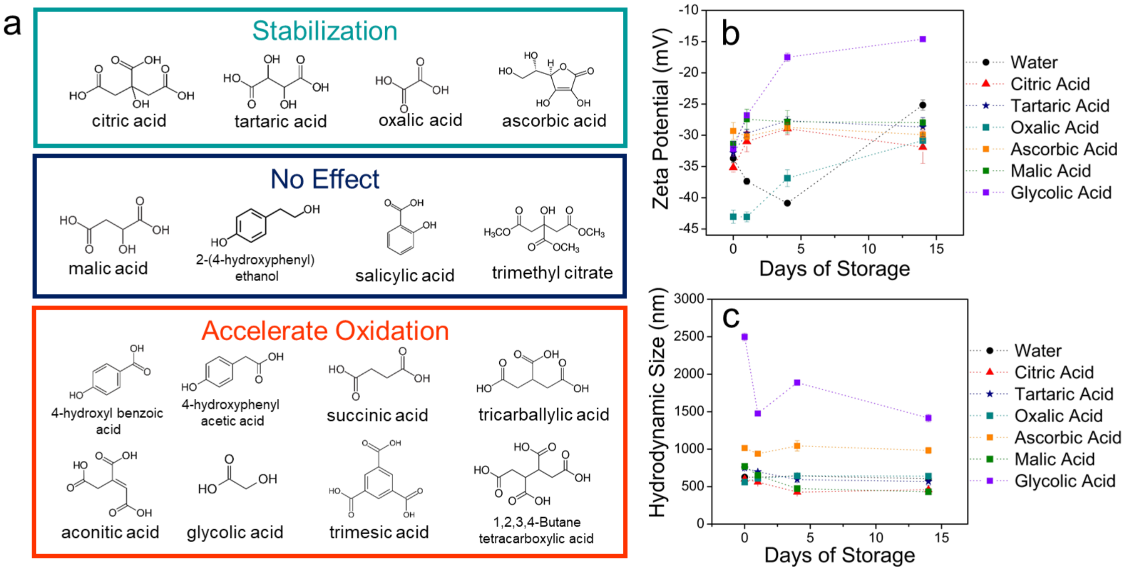

Figure 4-10 (a) The antioxidants may be classified based on their antioxidant performance in protecting $Ti_3C_2T_x$; (b) zeta potential and (c) hydrodynamic size changes of $Ti_3C_2T_x$ nanosheets dispersed in water and studied organic acid aqueous solutions over the 14-day storage.

Antioxidants, defined in biological, pharmaceutical, and food sciences, are often categorized as radical scavengers. They tend to react with radicals, which prevents the damage to cell and tissues from radical oxidants. However, antioxidants for MXenes may function via mechanisms other than radical scavenging. In the current work, certain strong radical scavenging antioxidants were investigated, such as 2-(4-hydroxyphenyl) ethanol,[118-120] but these molecules did not strongly affect the oxidation stability of $Ti_3C_2T_x$. Hence, we argue that the radical scavenging ability of antioxidants is not the key role that they play for preventing oxidation of MXenes. (Note that prior studies of MXene-radical interactions relied on external factors such radiation from an external source or the introduction of radical-forming chemical agents, such as hydrogen peroxide (H_2O_2) or ozone (O_3).[46, 91, 117, 121] Note that MXenes still oxidize without these factors present.[46, 65])

We conducted an additional comparative study with several variants of citric acid, with slightly modified chemical structures to elucidate which aspects of this highly effective antioxidant are important. Specifically, we examined the oxidation stability of $Ti_3C_2T_x$ in solutions of trimethyl citrate, which is an ester of citric acid, and tricarballylic acid, which is a tricarboxylic acid, but not a hydroxy acid. XPS analysis indicates that the introduction of trimethyl citrate or tricarballylic acid cannot protect $Ti_3C_2T_x$ as effectively as citric acid (**Figure 4-11**). Instead, the use of tricarballylic acid leads to more severe oxidation of $Ti_3C_2T_x$. In addition, tricarballylic acid caused the $Ti_3C_2T_x$ to lose colloidal stability, indicated by a weaker zeta potential and large hydrodynamic size average (**Figure 4-12**).

Given the data above, there are a few possible mechanisms that may explain $Ti_3C_2T_x$ stabilization by certain antioxidants: (i) In chelation, a polydentate ligand forms two or more coordinate bonds with a single metal atom. (ii) Another possible effect is induction. Induction occurs when an electron-withdrawing or donating group is present near an ionic group within a molecule, which affects the electron density of the molecule and can enhance or inhibit dissociation depending on charge sign. In the case of carboxylic acids, the enhanced dissociation of hydrogen by adding an electron-withdrawing group can lower the pK_a of a molecule. (iii) Finally, intermolecular, or even intra-molecular hydrogen bonding may have an effect on the ability of antioxidants to stabilize MXenes.

These mechanisms, and pairs of effective and ineffective antioxidants that possibly demonstrate them, are discussed in the following paragraphs.

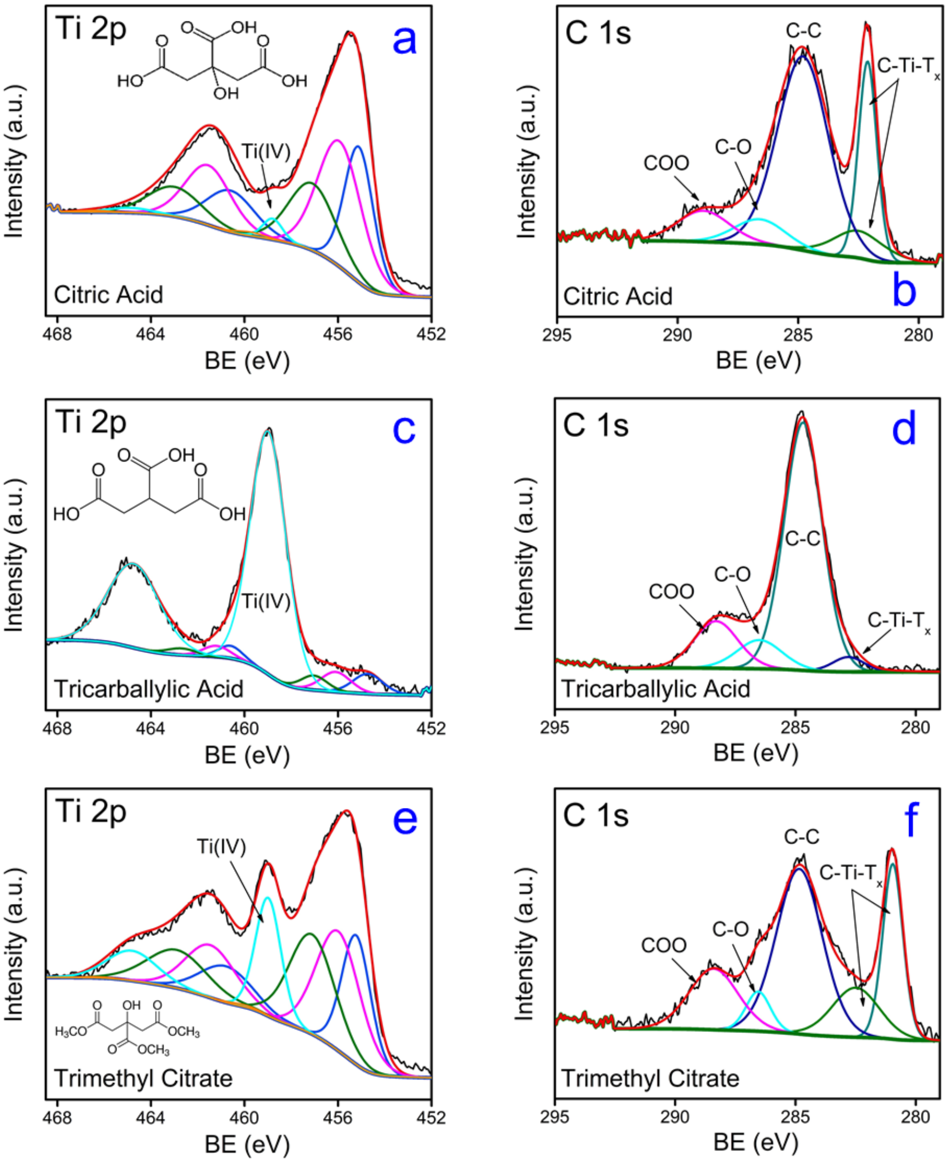

Figure 4-11 X-ray photoelectron spectroscopy (XPS) spectra and fittings of Ti 2p and C 1s peaks for (a), (b) $Ti_3C_2T_x$ nanosheets stored in water after 14 days; (c), (d) $Ti_3C_2T_x$ nanosheets stored in 1.5 mg/mL tricarballylic acid solution after 14-day storage; (e) and (f) $Ti_3C_2T_x$ nanosheets stored in 1.5 mg/mL trimethyl citrate solution after 14 days. Samples used for XPS analysis were made by vacuum filtration, followed by a 24-hour dehydration process under vacuum.

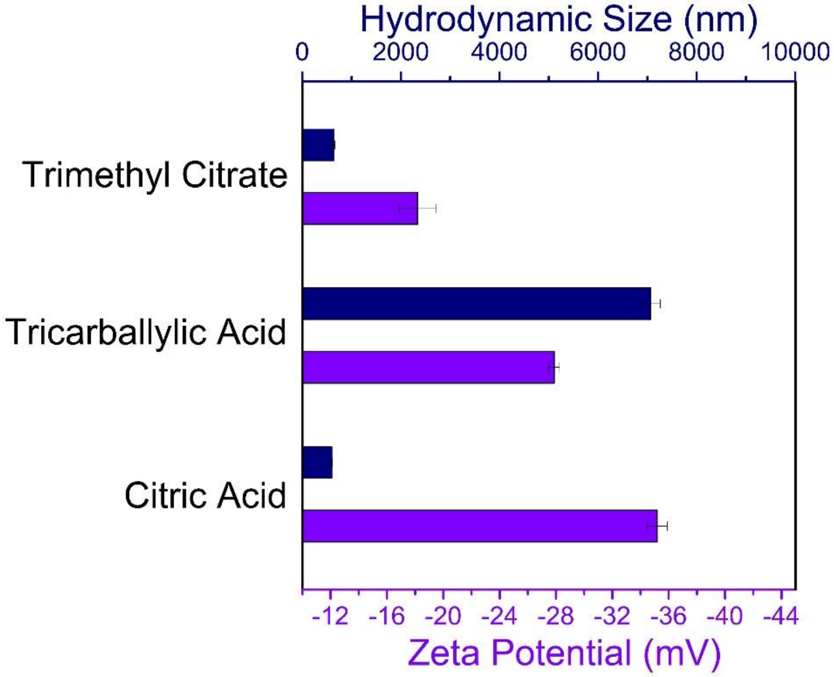

Figure 4-12 Zeta potential and hydrodynamic size measured after introducing $Ti_3C_2T_x$ nanosheets in citric acid, tricarballylic acid, and trimethyl citrate aqueous solutions.

Chelation complexes formed between the citric acid molecules and surface Ti atoms are a likely candidate for the observed oxidation trends. In a citric acid molecule, oxygen atoms in the hydroxy and nearby carboxy groups tend to share unpaired electrons with a positively-charged Ti atom on the $Ti_3C_2T_x$ surface, forming coordination bonds. The six-membered ring complex formed by chelation effects (**Figure 4-13a**) is chemically stable, which may prevent the oxidation of $Ti_3C_2T_x$ structure from reacting with water. In contrast, without the hydroxy group, tricarballylic acid cannot form coordination bonds with Ti atoms. Instead, the carboxy groups pull electrons away from Ti atoms because they are a strong electron-withdrawing group. Trimethyl citrate, another tested antioxidant, is like citric acid except that the hydroxy in the carboxy groups is replaced with a methoxy group (-OCH_3). Oxidation stability of $Ti_3C_2T_x$ was found to be unaffected by trimethyl citrate.

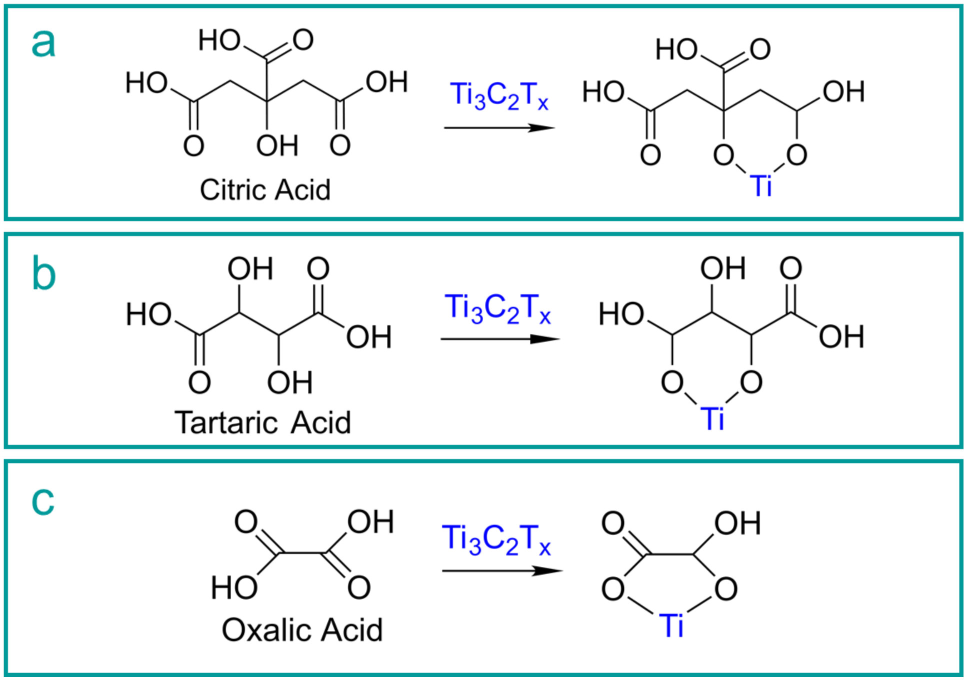

Figure 4-13 Chelation reaction between the Ti atoms on $Ti_3C_2T_x$ surface and molecules of (a) citric acid, (b) tartaric acid, and (c) oxalic acid.

Tartaric acid, similar to citric acid, can also form a chelation complex with Ti atoms on nanosheets, which is indicated by its good performance in oxidation prevention (**Figure 4-13b**). Both citric acid and tartaric acid are polydentate ligands, which means that there are multiple electron-donating oxygen atoms that can form coordination bonds with Ti atoms on $Ti_3C_2T_x$. However, malic acid and glycolic acid, both α-hydroxy acids, do not have the same good performance in protecting $Ti_3C_2T_x$ from oxidation. The denticity of malic acid and glycolic acid is less than citric acid and tartaric acid based on their structure. In addition, because of the shorter chain, glycolic acid cannot form five- or six-membered rings with Ti atoms on the surface, which is necessary for a stable chelation complex.

The chelation effect can also be observed between oxalic acid and $Ti_3C_2T_x$. Oxalic acid was found to be an effective antioxidant for $Ti_3C_2T_x$. The deprotonated form of oxalic acid, the oxalate ion, is well-known as a chelating agent (**Figure 4-13c**). In contrast, succinic acid, which is also a dicarboxylic acid, is not effective. Because of its longer molecular chain, the -COOH groups are too far from each other within the molecule to form chelation complex with MXenes. The mechanism that is most likely responsible to antioxidant protection is the chelation effect. This mechanism features the most significant interaction between MXene and the antioxidants compared with the other potential mechanisms.

By comparing how 4-hydroxybenzoic acid and salicylic acid interact with $Ti_3C_2T_x$, we also note that the distance between the -COOH and -OH groups can affect the interactions with $Ti_3C_2T_x$ nanosheets. In the 4-hydroxybenzoic acid molecule, the -COOH is distant from the -OH, and the $Ti_3C_2T_x$ in 4-hydroxybenzoic acid was oxidized after storage. However, for salicylic acid, the -OH is adjacent to the -COOH on the benzene ring. Intramolecular hydrogen bonding may occur between the hydrogen atom in hydroxy group and =O in carboxy group, restricting the electron-withdrawing ability of -COOH. In addition, the benzene ring in the salicylic molecules is an electron-withdrawing group that prevents the chelation effect with $Ti_3C_2T_x$. As a result, salicylic acid has limited interaction with $Ti_3C_2T_x$, showing little effect on $Ti_3C_2T_x$ oxidation.

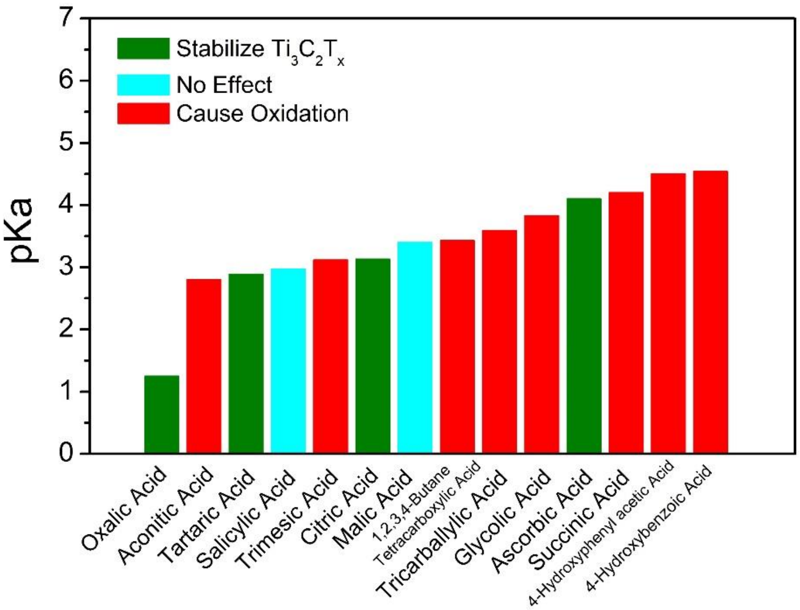

Figure 4-14 Correlations between pK_a values of studied chemicals and their interactions with $Ti_3C_2T_x$ nanosheet.

The close proximity of -OH and -COOH in salicylic acid is correlated with a lower pK_a than 4-hydroxybenzoic acid due to an induction effect. We have summarized the pK_a of the studied compounds and their performance in protecting $Ti_3C_2T_x$ in **Figure 4-14** and **4-15**. However, we did not observe any clear trend that indicates a correlation between pK_a and antioxidant effectiveness in protecting $Ti_3C_2T_x$.

Note that the carboxyl group (-COOH) may actually accelerate oxidation of $Ti_3C_2T_x$. We observed that interactions between 2-(4-hydroxyphenyl) ethanol or 4-hydroxyphenyl acetic acid with $Ti_3C_2T_x$ are different because of the presence of -COOH in the latter compound. $Ti_3C_2T_x$ has accelerated oxidation rates in solutions of polycarboxylic acids as well, such as succinic acid, trimesic acid and 1,2,3,4-butanetetra carbolic acid, which contain -COOH groups that do not form chelation complexes.

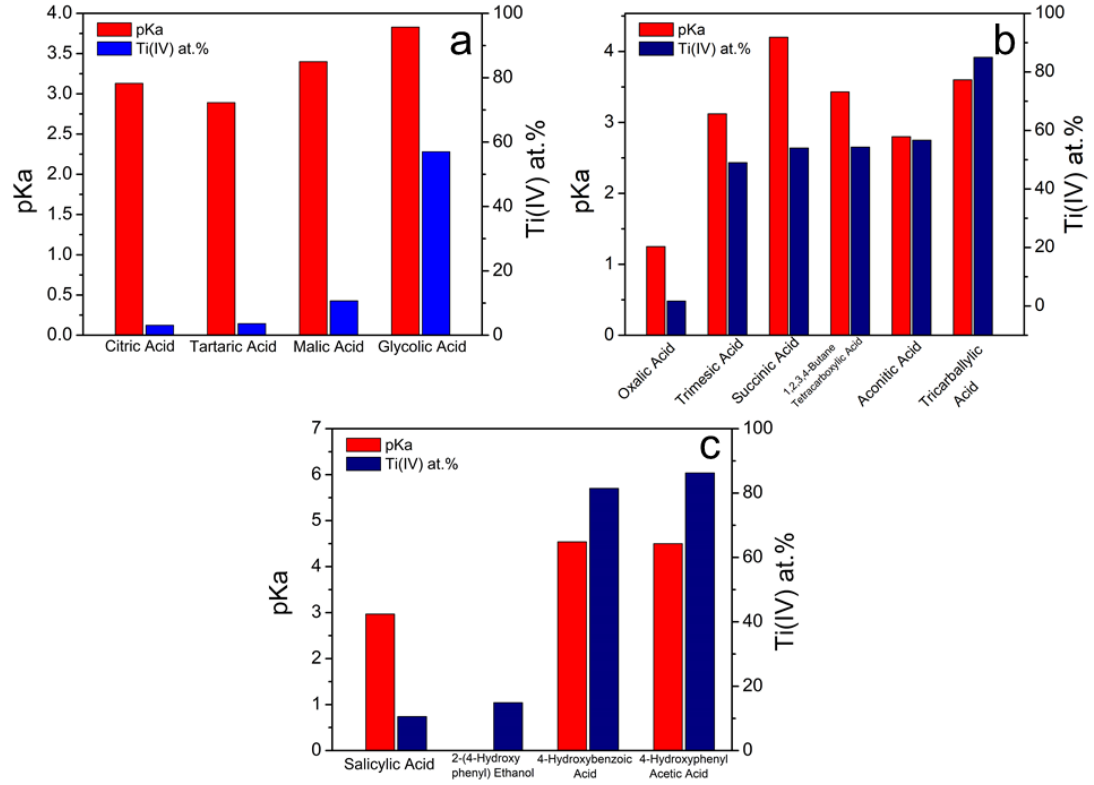

Figure 4-15 Correlations between pK$_a$ values and atomic percentages of Ti(IV) measured by XPS for $Ti_3C_2T_x$ nanosheets stored after 14 days in aqueous solutions of (a) α-hydroxy acids; (b) polycarboxylic acids, and (c) phenolic compounds.

We have also investigated the effectiveness of the antioxidant candidates in protecting "211" Ti_2CT_x nanosheets from oxidation. Citric acid, tartaric acid, and oxalic acid were also confirmed to be effective antioxidants, as shown in **Figure 4-15** and **Figure 4-16**. The α-hydroxy acids exhibit a similar trend of oxidation protection effectiveness for Ti_2CT_x as with $Ti_3C_2T_x$. However, we discovered in this work that the Ti_2CT_x nanosheets oxidize faster in water than in organic acid solutions. Protons provided by the disassociation of organic acids may mitigate the oxidation of Ti_2CT_x, but the same findings were not observed for $Ti_3C_2T_x$, as noted above. The mechanism behind these differences is still unclear. **Figure 4-17** illustrates that the addition of phenolic compounds with lower pK_a values may help to retard the oxidation of Ti_2CT_x. For instance, we observed that Ti_2CT_x in salicylic acid with a low pK_a of 2.97 exhibits lower Ti(IV) content than in water, 2-(2-hydroxyphenyl) ethanol, 4-hydroxyphenyl acetic acid, and 4-hydroxybenzoic acid.

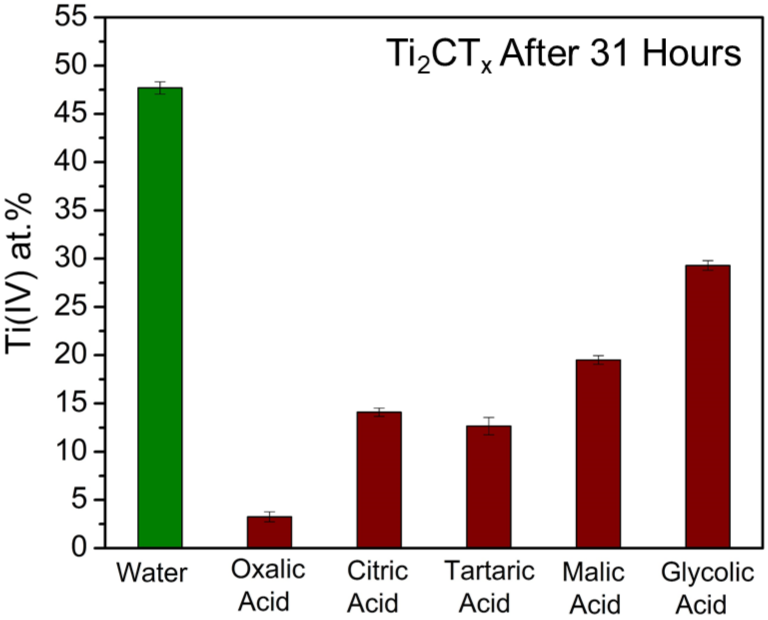

Figure 4-16 Atomic compositions of Ti(IV) measured by X-ray photoelectron microscopy (XPS) for Ti_2CT_x nanosheets dispersed in water and 1.5 mg/mL aqueous solutions of oxalic acid, citric acid, tartaric acid, malic acid, and glycolic acid after 31-hour storage.

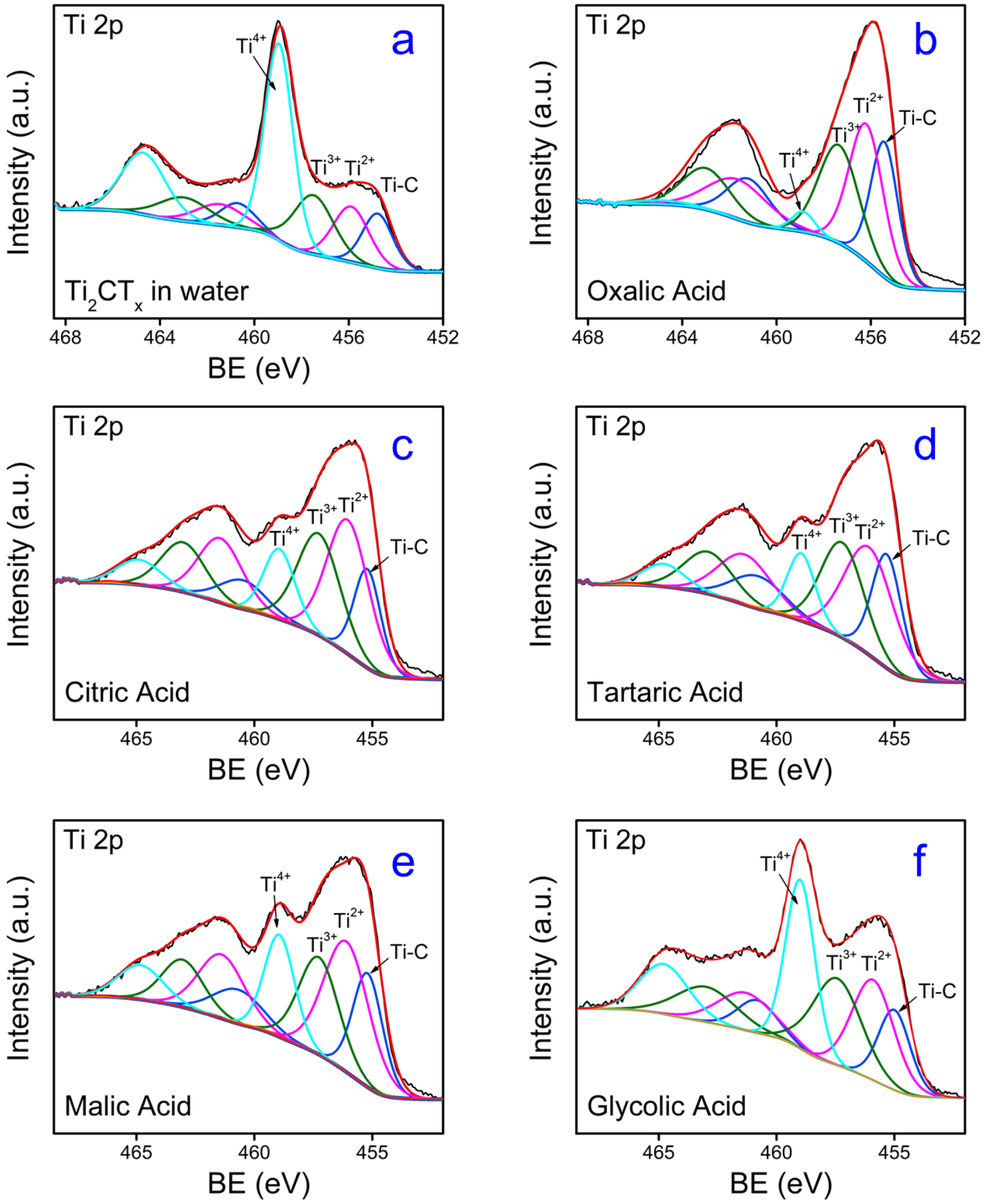

Figure 4-17 X-ray photoelectron microscopy (XPS) spectra for Ti_2CT_x nanosheets after 31-hour storage dispersed in (a) water, and 1.5 mg/mL aqueous solutions of (b) oxalic acid, (c) citric acid, (d) tartaric acid, (e) malic acid, and (f) glycolic acid.

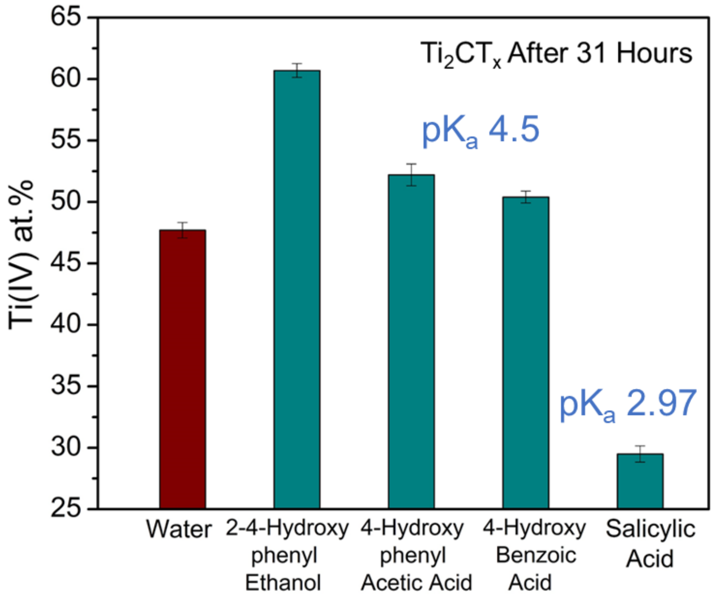

Figure 4-18 Atomic compositions of Ti(IV) measured by X-ray photoelectron microscopy (XPS) for Ti_2CT_x nanosheets dispersed in water and 1.5 mg/mL aqueous solutions of phenolic compounds after 31-hour storage.

4.4. Conclusion

Here, we demonstrated that several organic acids can be used to improve the oxidation stability of $Ti_3C_2T_x$ and Ti_2CT_x MXene nanosheets. A systematic study on the antioxidant performance of several organic compounds with similar structures was conducted to illustrate that the chelation effect between antioxidant molecules and $Ti_3C_2T_x$ surface atoms may be the main cause of the stabilization effect. These findings address one of the major challenges in using 2D MXene nanomaterials by identifying the key characteristics of effective antioxidants for mitigating oxidation and degradation of MXene nanosheets. The interactions we discovered in this work between organic compounds and MXenes in aqueous solutions, such as the chelation effect, may also suggest new pathways in tuning the nanosheet surface functionality.

5. ANNEALED $TI_3C_2T_Z$ MXENE FILMS FOR OXIDATION-RESISTANT FUNCTIONAL COATINGS[*]

5.1. Summary

2D transition metal carbide and nitride nanomaterials, known as MXenes, exhibit low chemical stability in aqueous environments; they tend to oxidize and react with water molecules, resulting in structural degradation and decreased electrical conductivity. This significantly limits their storage lifetime and potential use in the presence of water, particularly in nanosheet-assembled films for battery electrodes and functional coatings. Here we demonstrate that thermal annealing of $Ti_3C_2T_z$ films at elevated temperatures (~ 600 °C) causes changes in the termination distribution as well as the formation of a protective layer of TiO_2 on the outermost layer of films. The induced chemical and structural changes during thermal treatment arrest MXene oxidation and enable the MXene films to be stable in aqueous solutions for over 10 months.

5.2. Introduction

MXenes are a family of 2D layered transition metal carbides, carbonitrides, and nitrides with the general chemical formula of $M_{n+1}X_nT_z$, where M represents an early transition metal such as Ti, V, Nb, Cr, and Mo, X is C and/or N, T refers to terminal

---

[*] Reprinted with permission from "Annealed $Ti_3C_2T_z$ MXene Films for Oxidation-Resistant Functional Coatings" by Xiaofei Zhao; Dustin E. Holta; Zeyi Tan; Ju-Hyun Oh; Ian J. Echols; Muhammad Anas; Huaixuan Cao; Jodie L. Lutkenhaus; Miladin Radovic; Micah J. Green. 2020, *ACS Appl. Nano Mater.*, 3, 11, 10578–10585, Copyright 2020 American Chemical Society.

groups, n ranges from 1 to 5, and z reflects the number of terminal groups. [2-4, 122, 123] MXenes with a multilayered structure (MXene clay) are typically synthesized by a top-down selective etching step in fluoride-containing acid (i.e.. HF) to dissolve and extract A layer from their MAX counterpart, where A refers to a group 13 or 14 element, such as Al and Si. [8, 44] Single or few-layered MXene nanosheets, which are one to a few nanometers thick, can be further derived by exfoliation of these multilayered MXene structures by agitation or sonication. [5, 8, 10, 35, 36] One of the most-studied members in the family of MXenes, $Ti_3C_2T_z$, is terminated with numerous functional groups (-OH, -O-, -F, -Cl) during etching and exfoliation in the aqueous phase. Terminal groups such as -OH and -O- enable MXene nanosheets' hydrophilicity and surface electronegativity, making them readily dispersible in water and certain polar organic solvents. Free-standing films made from $Ti_3C_2T_z$ have shown promise in flexible energy storage devices such as supercapacitors, [3, 30, 94] portable electronics, [108] electromagnetic interference shielding coatings, [18] and gas-separation membranes. [124] The wide range of applications are enabled by MXenes' excellent electrical conductivity, abundant surface functionalities, metallic properties, in-plane stiffness, and large-scale processability by filtration, blade coating, spray coating, layer-by-layer coating, and drop-casting methods. [8, 20, 46, 125]

However, MXene nanosheets oxidize rapidly in aqueous and humid environments, resulting in the degradation of the 2D structure into transition metal oxides and carbon residues, which precludes many of the properties that make MXenes-made devices attractive. [46, 65, 69] Early reports claimed that $Ti_3C_2T_z$ nanosheets react with dissolved oxygen in water and fully oxidize within just 15 days. [64] More recent studies, including our own, revealed that MXenes are prone to react with water molecules rather than dissolved oxygen. [46, 65] In addition, free-standing MXene thin films also suffer from oxidation and loss of functional performance, but at a slower rate than in the dispersed form. Rapid decreases in the electronic conductivity and growth of TiO_2 nanocrystals were observed on $Ti_3C_2T_z$ films stored in humid air. [46, 52, 80]

This limited lifetime for MXene devices has prompted a search for strategies to mitigate MXene oxidation and degradation. A number of studies have focused on slowing down MXene oxidation by controlling the storage conditions and restricting the exposure of MXenes to water and oxygen. [46, 64, 66, 69, 78, 126] In addition, oxidation can be mitigated by introducing antioxidants such as ascorbate and polyphosphoric anions. [75, 95] Lee *et al.* reported that reducing $Ti_3C_2T_z$ by H_2 annealing can mitigate the oxidation of MXene film. [80] They reported that the TiO_2 formed by MXene oxidation could be reduced by H_2 gas at elevated temperatures. They also found that the fresh MXene films annealed in H_2 environment have even slower oxidation rates in humid environments. However, the enhanced stability of MXene films was solely attributed to its reaction with H_2; the effect of structural alterations brought up by thermal annealing on film stability was not addressed. In addition, the long-term stability of annealed MXene films that are immersed in water has not been discussed in prior studies.

In this study, we demonstrate that thermally annealing free-standing MXene films under inert argon gas can induce surface and structural modifications which increase the chemical stability of the films and extend their storage life in water. Through annealing, a sandwich-like film structure was developed, with the formation of a protective TiO_2 layer on the films' surfaces and more compact nanosheet stacking that prevents water ingress and degradation of the interior structure, shown schematically in **Figure 5-1**. As-prepared $Ti_3C_2T_z$ films were annealed at 300 °C and 600 °C respectively to address the differences in stability caused by low and high annealing temperatures. In contrast to the fully degraded untreated $Ti_3C_2T_z$ film and films annealed at 300 °C, almost no changes in chemical structure and composition were observed in films annealed at 600 °C, even after 10-month storage in water. This method allows MXene thin films to have an extended lifetime and be used in a range of environments.

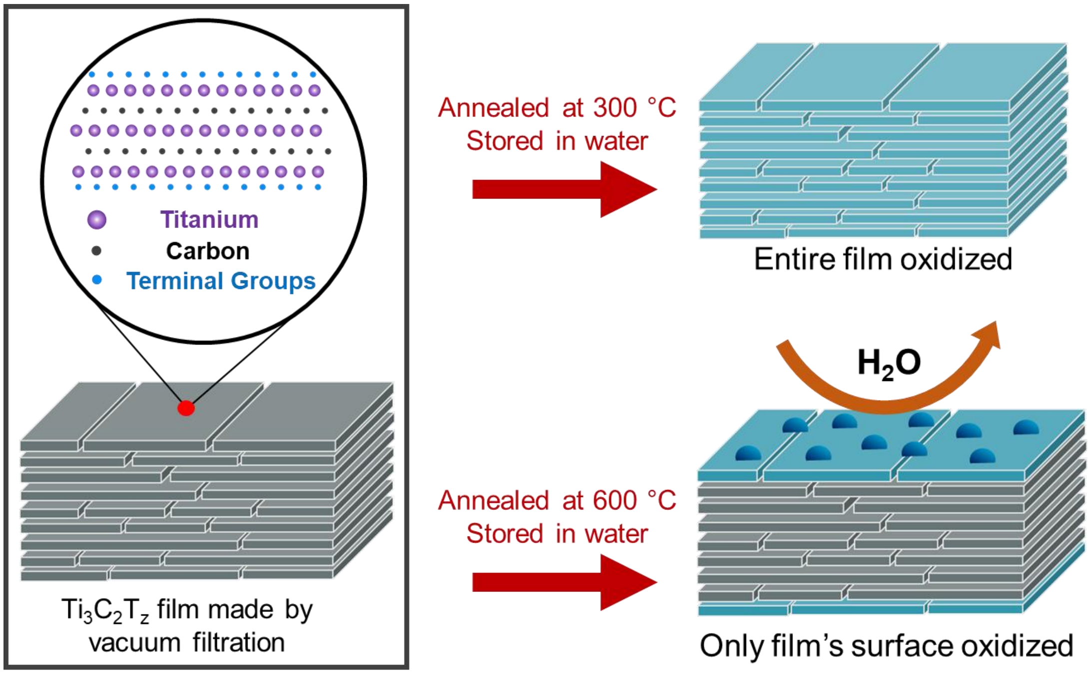

Figure 5-1 Schematic of $Ti_3C_2T_z$ film preparation: films were made by vacuum filtering $Ti_3C_2T_z$ MXene nanosheets and then annealing at high temperature under argon. Annealed MXene films were stored in distilled water for 10 months. The films annealed at 300 °C were completely oxidized and degraded. The films annealed at 600 °C only show oxidation on the surface; the oxidized layer acts as a barrier for water penetration and protects the inner layers of the film. Reprinted with permission from reference[74], Copyright 2020 American Chemical Society.

5.3. Materials and methods

5.3.1. Materials

Synthesis of $Ti_3C_2T_z$ MXene nanosheet

The synthesis of $Ti_3C_2T_z$ MXene followed an *in-situ* fluoride acid etching method. [8, 38, 44] First, 3.0 g of lithium fluoride (LiF) (with the purity of 98+%, Alfa Aesar) were mixed and dissolved in 30 ml 6 M HCl solution (ACS reagent, Millipore-Sigma) with a magnetic stir bar in a 100 ml polypropylene beaker. The mixture of HCl and LiF was then heated and kept at 40 °C. 3.0 g of as-prepared Ti_3AlC_2 MAX powder (sieved to obtain a particle size less than 45 µm) was slowly added into the solution over 15 minutes to prevent overheating. The mixture was agitated for 40 hours, and then centrifuged. The supernatant containing the HF and water-soluble ions was decanted. MXene clay produced after etching was washed by DI water for multiple times and the water effluent was removed after centrifugation until pH of the water effluent reached a minimum value around 6 to 7. $Ti_3C_2T_z$ clay was then intercalated with dimethyl sulfoxide (DMSO) (>99.5%, Sigma-Aldrich) for 26 hours with continuous agitation [123]. DMSO was removed by solvent exchange with deionized water. The expanded MXene clay was bath sonicated for 1 hour for delamination. The delaminated dispersion was centrifuged at 3500 rpm for 1 hour to crash out and separate the unexfoliated MXenes. The supernatant was collected as the $Ti_3C_2T_z$ nanosheet dispersion. The dispersion of $Ti_3C_2T_z$ nanosheet has a concentration of 6.0 mg/mL.

Preparation of $Ti_3C_2T_z$ freestanding films

The freestanding $Ti_3C_2T_z$ films were made by vacuum filtration of MXene dispersion with polysulfone membranes with a pore size of 0.2 µm. The filtered films were then vacuum dried after filtration at 30 °C for 12 hours. Freestanding MXene films were peeled off from the membrane filter with a tweezer and cut into halves.

Film annealing and storage

MXene films were placed in the tubular furnace purged with desiccated extra high purity argon gas for 72 hours to remove air and traceable water in the system. The films were then heated up at 5 °C/min and annealed at set temperatures for 30 mins. The system then was allowed to be rapidly cooled to room temperature. The annealed films were transferred into vials filled with distilled water and stored for 10 months in a dark environment.

5.3.2. Materials characterization

X-ray Diffraction (XRD)

XRD patterns of Ti_3AlC_2 powder and $Ti_3C_2T_z$ films were obtained using a Bruker D8 powder X-ray diffractometer fitted with LynxEye detector, in a Bragg Brentano geometry with CuKα ($\lambda = 1.5418$ Å) radiation source. The samples were scanned at a step size of 0.02° and a scan rate of 1.5 s per step. A zero-background sample holder was used in all the measurements.

X-ray Photoelectron Spectroscopy (XPS)

The chemical electronic states of Ti, C, O, and F on the surfaces of $Ti_3C_2T_z$ films were determined with an Omicron X-ray photoelectron spectrometer employing a Mg X-ray source. The emitted photoelectrons from the films were collected by a 180° hemispherical electron energy analyzer. A takeoff angle of 40° between sample surface and the path to the collector was set in all measurements. High-resolution Ti 2p, C 1s, O 1s, F 1s spectra were obtained at a pass energy (constant analyzer energy, CAE) of 30.0 eV with a step size of 0.05 eV. A dual beam charge neutralizer was used to eliminate the shift of binding energy in the recorded spectra. Component peak fitting and quantification of the spectra were carried out using CasaXPS curve fitting software (version No. 2.3.16). Argon sputtering the sample surface was carried out with ultra-pure Argon gas with a beam current density of 15 mA/cm^2.

Surface and cross-section morphology and elemental analysis

The surface and cross-section morphologies of $Ti_3C_2T_z$ films were imaged by an FEI Quanta 600 field emission scanning electron microscope (FE-SEM, JEOL JSM-7500F, JEOL Ltd., Japan). The acceleration voltage used for morphological study was 2.0 kV. Energy-dispersive X-ray spectroscopy (EDS) coupled with SEM was used to detect the elemental compositions of film cross-sections. An acceleration voltage of 20.0 kV was used for EDS. The surface morphology of individual $Ti_3C_2T_z$ nanosheets deposited on mica disc was studied with an atomic force microscopy (AFM, Bruker Dimension Icon). The tapping mode was used. Before measurements, dilute MXene dispersion (< 0.01 mg/ml) was drop-casted on a clean surface of mica disc and dried in vacuum oven for 24 hours.

Interfacial properties and wettability

The surface wettability of MXene film was investigated by checking the static water contact angle using the sessile drop configuration. The contact angle was analyzed by ImageJ software (developed by National Institutes of Health, United States) via low-bond axisymmetric drop shape analysis (LBADSA). [127]

Film electrical conductivity measurements

Electrical conductivities of $Ti_3C_2T_z$ films were measured using four-point resistivity probe powered by Keithley 2000, 6221 and two 6514. MXene films were dried under vacuum for at least 12 hours prior to conductivity measurements. The thickness of films used for conductivity calculation was measured by SEM. The AC conductivity in the cross-section direction of the MXene films were measured using a capacitive structure consisting of two conducting plates connected to a network analyzer with an N-type connector and a coaxial cable.

Radio frequency (RF)-induced heating on MXene films

A fringing-field applicator was used for RF heating of MXene films. The applicator was fabricated on a Teflon substrate using two copper strips (9 cm long, 6 mm wide) with a 2 mm spacing. Polyimide tape was used to coat the applicator. A signal generator (Rigol Inc., DSG815) connected to a 500 W power amplifier (Prana R&D, GN500D) were used to generator RF power which was transmitted to the fringing-field applicator via a 50 Ohm coaxial cable. The cable was terminated with an N-type connector and alligator clips were soldered to center pin and ground reference for smooth connection with the applicator. Temperature as a function of time was collected using a Forward-

Looking Infrared camera (FLIR systems Inc., A655sc). RF power and frequency used in this study were 32W (45 dBm) and 106 MHz. The frequency where the highest heating occurred was chosen for the study. MXene films with a dimension of 2 x 2 cm were used in the RF heating. These RF experimental methods were adapted from our group's prior studies in this area. [128, 129]

5.4. Results and discussions

$Ti_3C_2T_z$ nanosheets (**Figure 5-2a**) were first derived from Ti_3AlC_2 following prior methods; we use the *in situ* HF method with a solution of LiF and HCl as etchant, followed by intercalation and delamination (sonication) steps. [8, 44, 81, 98] MXene films used in this work were prepared by vacuum filtration of nanosheet dispersions through a polyethersulfone filter; these films were dried under vacuum and peeled off from the polymeric filter (**Figure 5-2b**). The free-standing films were heated and annealed at either 300 °C or 600 °C in a tube furnace under argon flow. Before heating, the quartz tube was purged with desiccated high-purity argon for 36 hours to remove trapped air and water molecules. After annealing, films were transferred into DI water and stored for 10 months.

X-ray diffraction, XRD, indicates the structural transformation from Ti_3AlC_2 MAX phase to $Ti_3C_2T_z$ nanosheets by the shift of the (002) XRD peak from $2\theta = 9.8°$ to $2\theta = 6.0°$ (**Figure 5-2c**). After annealing at 600 °C, the (002) peak shifted slightly back from $2\theta = 6.0°$ to $2\theta = 8.7°$ (**Figure 5-3)**, suggesting a decreased interlayer spacing which may be caused by the loss of bonded water and terminal groups. [9] Anayee *et al.* and

Persson *et al.* discovered that annealing MXenes up to 600 °C results in the release of intercalated and bonded H_2O, H_2, OH, CO_2, CH_4, and HF. [122, 130] The absence of these attached or desorbed species caused the nanosheet stacking to become more compact.

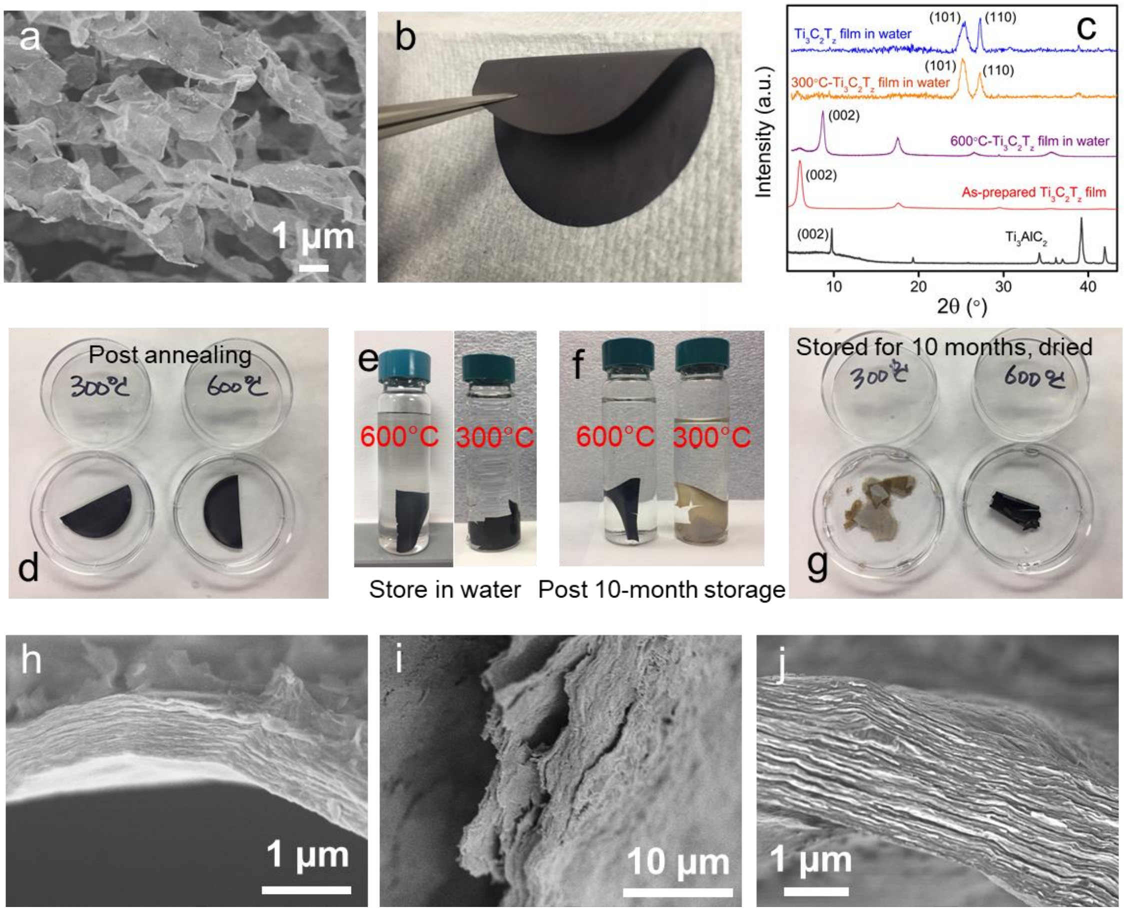

Figure 5-2 (a) Morphology of freeze-dried $Ti_3C_2T_z$ nanosheets by scanning electron microscopy (SEM), and (b) free-standing $Ti_3C_2T_z$ film made by vacuum filtration; (c) X-ray diffraction (XRD) spectra of Ti_3AlC_2 MAX phase particles, as-prepared film made by nanosheets prior to annealing, and MXene films subject to 10-month storage in water. Images of (d) films after annealing at 300 °C and 600 °C, (e) annealed films in water after 24 hours, (f) films stored in water after 10 months, and (g) annealed, stored films after being dried. Cross-section images for (h) as-prepared MXene film, (i) film annealed at 300 °C and then stored in water for 10 months, (j) film annealed at 600 °C and then stored in water for 10 months. Reprinted with permission from reference[74], Copyright 2020 American Chemical Society.

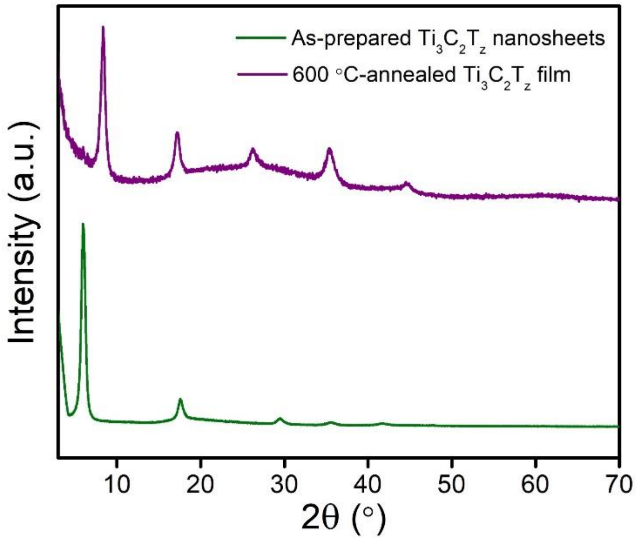

Figure 5-3 X-ray diffraction (XRD) spectra of as-prepared $Ti_3C_2T_z$ film and 600 °C-annealed film. Reprinted with permission from reference[74], Copyright 2020 American Chemical Society.

After the 10-month storage in water, MXene film previously annealed at 600 °C retains the pronounced (002) peak, however, the (002) peaks completely vanish for unannealed and 300 °C annealed films. Instead, (101) and (110) peaks appear indicating the formation of anatase TiO_2 and rutile TiO_2 respectively suggesting the complete oxidation and degradation of unannealed and 300 °C-annealed films. [131, 132] We observed that $Ti_3C_2T_z$ films become less flexible and more brittle after annealing and storage, likely due to the reduced number of functional groups. Functional groups can act as a "mortar" between nanosheet "bricks", similar to terminal group behavior for graphene oxide (GO).[133, 134] This may potentially limit the films' performance in particular applications.

$Ti_3C_2T_z$ films annealed at elevated temperatures did not show significant changes in appearance compared to as-prepared films (**Fig. 5-2d** and **5-2e**). However, after 10-month storage in DI water, films annealed at 300 °C turn cloudy white, while the samples annealed at 600 °C did not show any noticeable difference in appearance, as it is shown in **Figure 5-2f** and **5-2g**. The color change of the films suggests that the MXene film annealed at 300 °C fully degraded in water after the 10-month storage. MXenes typically degrade and lose properties in water within a month. [46, 64, 65, 69] However, MXene films annealed at 600 °C remained grey-black, with no visible changes in color before and after storage. This is remarkable because MXene films can be stable for over 10 months in water without any changes in synthesis recipes and introducing any antioxidation additives.

The cross-sectional SEM image of a film annealed at 600°C and then stored for 10-month in water appears similar to the as-prepared film displaying a layered structure (**Figure 5-2h, 5-2j** and **Figure 5-4**). However, the film annealed at 300 °C changed from a layered structure of stacked nanosheets to an amorphous structure after long-term storage in water (**Figure 5-2i**).

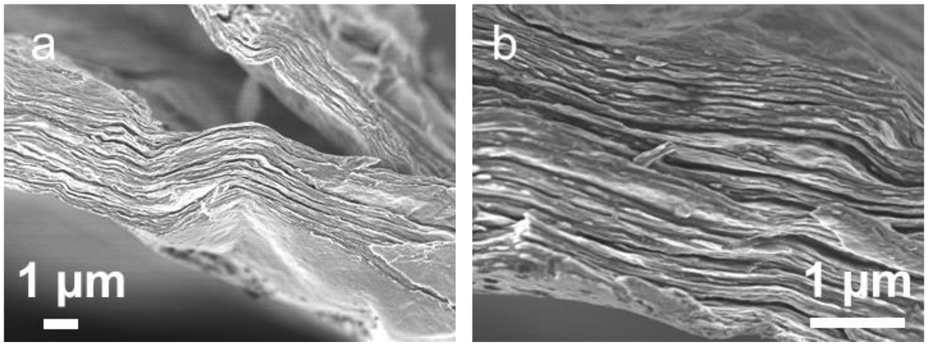

Figure 5-4 SEM Morphology of cross-section areas of MXene films after being annealed at 600 °C and being stored for 10 months in water at various magnifications. Reprinted with permission from reference[74], Copyright 2020 American Chemical Society.

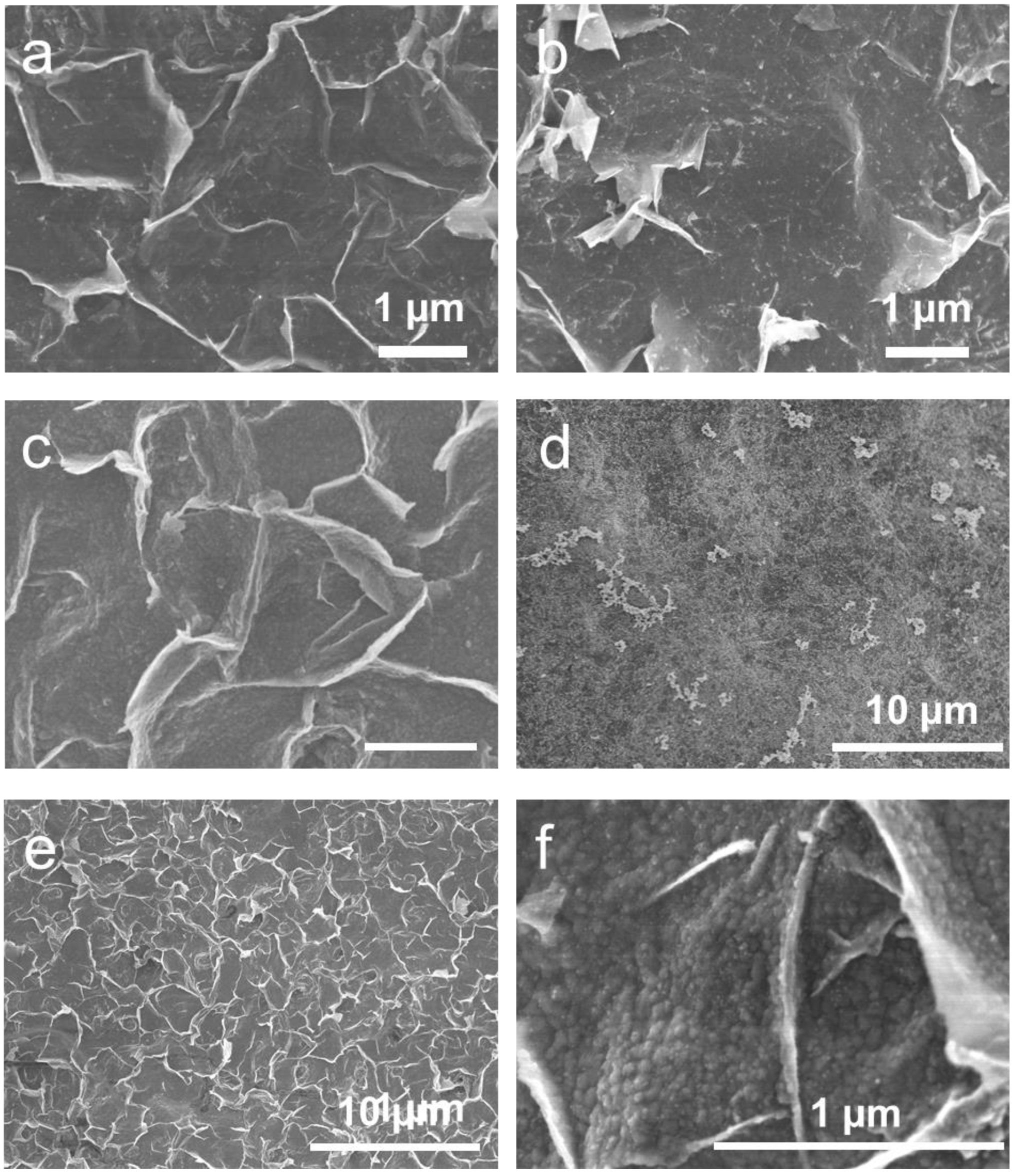

Figure 5-5 Surface morphology of (a) as-prepared film, (b) 300 °C annealed film, (c) 600 °C annealed film before storage in water. Images of (d) 300 °C annealed film and (e) 600 °C annealed film after 10-month storage in H_2O; (f) magnified morphology of 600 °C annealed film after storage; The films have been dried prior to SEM imaging. Reprinted with permission from reference[74], Copyright 2020 American Chemical Society.

The surface morphology of $Ti_3C_2T_z$ film after being annealed at 300 °C and stored in water for 10 months exhibited an amorphous nature with large aggregates present

(**Figure 5-5**). In contrast, stacked nanosheets were observed on surface of the film annealed at 600 °C and stored at same conditions. We next compare the surface of 600 °C-annealed film before and after 10-month storage; **Figure 5-5f** show that the surface of the stacked nanosheets is covered with 30-60 nm hills, which were not visible on the as-prepared (**Figure 5-5a**) and 300 °C-annealed films (**Figure 5-5b**).

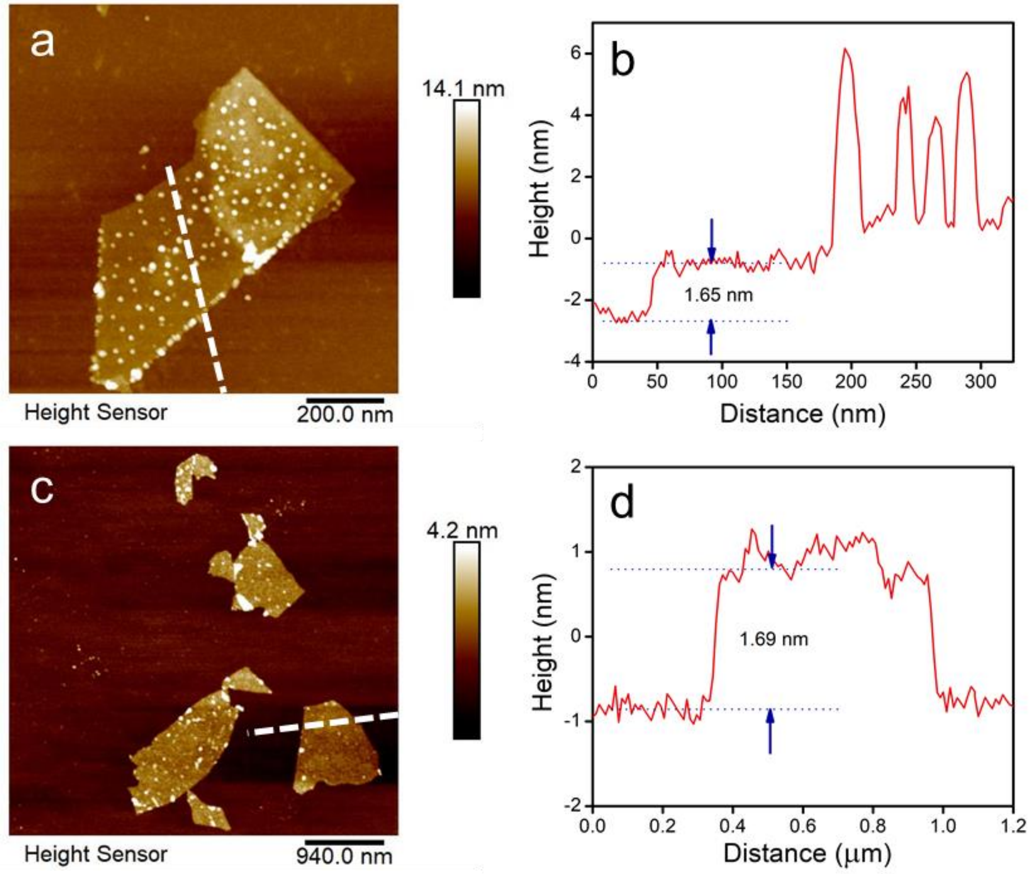

Figure 5-6 Morphology and height characteristics obtained by atomic force microscopy (AFM) for (a, b) $Ti_3C_2T_z$ nanosheets deposited on mica discs first by drop-casting dilute dispersions (0.01 mg/ml), then annealing at 550 °C under argon; (c, d) as-prepared $Ti_3C_2T_z$ nanosheets deposited on mica substrate by drop-casting without further annealing. Reprinted with permission from reference[74], Copyright 2020 American Chemical Society.

In addition, the effect of annealing on individual $Ti_3C_2T_z$ nanosheets was investigated. The nanosheets were first drop-casted and dried on a plasma-treated mica disc, and then annealed at 550 °C. Atomic force microscopy (AFM) suggested that small bumps 3 to 9 nm in height formed on annealed nanosheets (shown in **Figure 5-6**). In contrast, as-prepared nanosheets exhibited cleaner surfaces without bumps. This indicated that some TiO_2 particles may form on the nanosheets during high-temperature annealing even in an inert atmosphere.

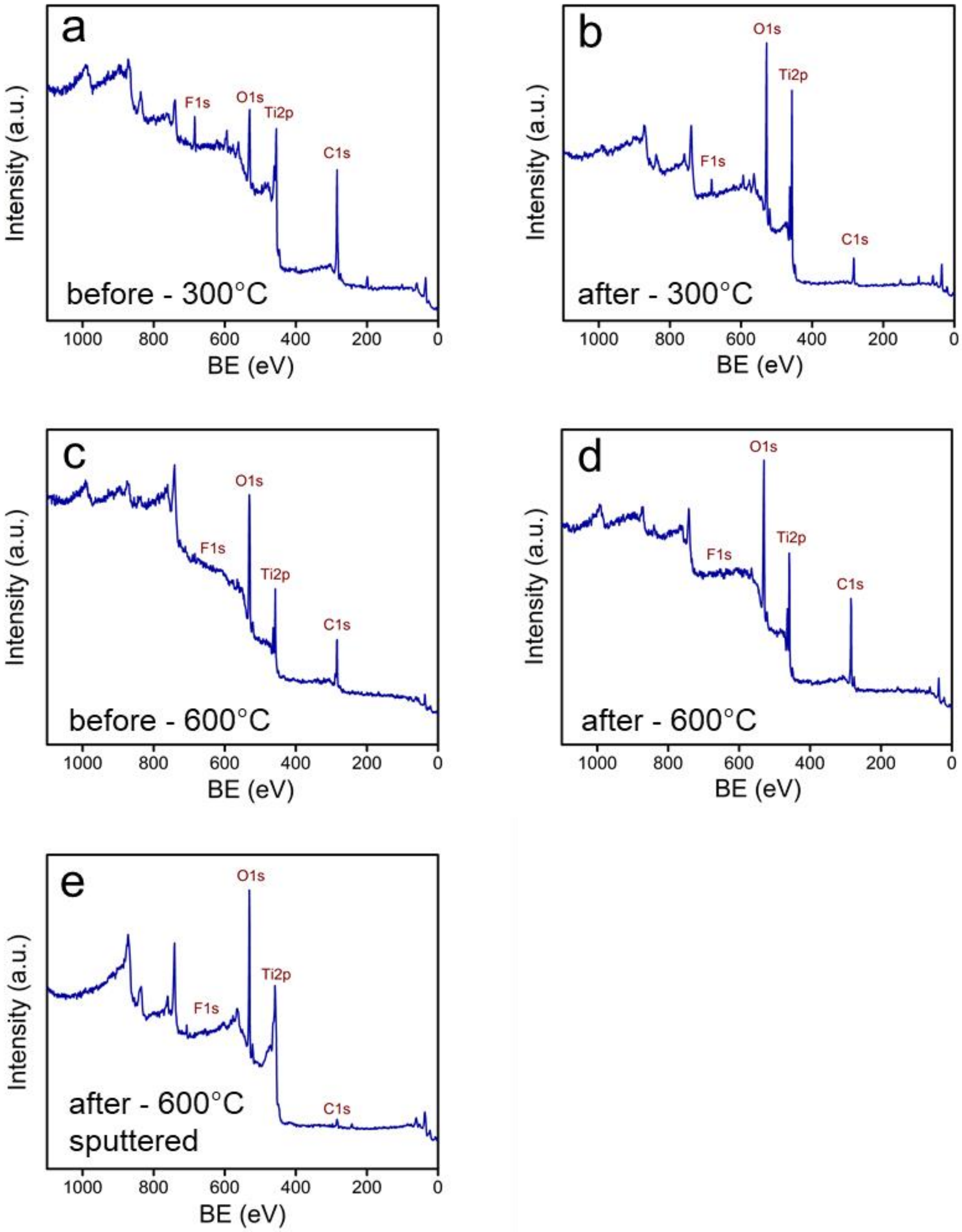

Figure 5-7 Survey spectra of XPS analysis covering from 0 eV to 1100 eV for (a) $Ti_3C_2T_z$ film after being annealed at 300 °C and (b) after subsequent storage; (c, d) film after being annealed at 600 °C and subsequent storage; (e) film tested in (d) after argon sputtering for 20 min. Reprinted with permission from reference[74], Copyright 2020 American Chemical Society.

Table 5-1 Composition changes from XPS summarized for elements Ti, C, O, F. Reprinted with permission from reference[74], Copyright 2020 American Chemical Society.

MXene films		**Elemental Compositions (at.%)**
Annealed at **300** °C	Ti	14.2
	C	61.4
	O	20.4
	F	4.1
Annealed at **300** °C Stored in water for 10 months	Ti	20.6
	C	24.2
	O	51.4
	F	3.9
Annealed at **600** °C	Ti	9.3
	C	45.3
	O	44.4
	F	1.1
Annealed at **600** °C Stored in water for 10 months	Ti	10.8
	C	51.7
	O	37.2
	F	0.4
Annealed at **600** °C Stored in water for 10 months [Argon Sputtered]	Ti	29.0
	C	12.6
	O	57.2
	F	1.3

X-ray photoelectron spectroscopy (XPS) was used to measure changes in the MXene film surface chemistry after annealing and 10-month storage in water. The survey spectra and surface elemental compositions obtained by XPS are displayed in **Figure 5-7** and **Table 5-1**. After being annealed at 300 °C, the high-resolution spectra of Ti 2p and C 1s did not vary much from the as-prepared films, except for a slight increase of Ti(IV) content (around 5 at.%), shown in **Figure 5-8a** and **5-8b**. The slight oxidation may be caused by the reaction between the de-bonded surface water and Ti-C. After 10 months storage in water, films annealed at 300 °C were completely oxidized, as it is indicated by the rise of Ti(IV) component percentage from 23.1 at.% to 88.1 at.% and the disappearance of C-Ti-T_z peak (shown in **Fig. 5-8e** and **Figure 5-9**). Combined with the evidence of the films color change, this data suggest that the film annealed at 300 °C were completely oxidized and degraded after the 10-month storage in water.

XPS suggests that the surface of MXene films was severely oxidized after being annealed at 600 °C by showing a Ti(IV) content of 56.0 at.% and decreased C-Ti-T_z content in **Fig. 5-8c** and **5-8d**. Titanium carbonates (-O-C=O-O-) were also observed after 600 °C annealing, suggested by a pronounced peak at around 290 eV. The Ti(IV) content increased even more to 87.0 at.% after the 10-month storage in water. In addition, films annealed at 600 °C showed relatively unchanged Ti, C, and O compositions before and after the long storage (indicated in **Table 5-1**). In combination with prior SEM observations, the results indicate that a surface layer of TiO_2 formed uniformly after the 600 °C annealing step. Since the system was purged with inert gas, the formation of TiO_2

and carbonates is more likely caused by the oxidation reaction from surface attached H_2O molecules and O-containing functional radicals.

However, the oxidation of 600 °C-annealed film surface as indicated by XPS is not obvious in the unchanged visible appearance of the film. Since XPS is limited to characterizing only the topmost surface of the films, the removal of the film top layer is needed to determine the interior film composition. Argon sputtering was used to remove outmost layer of the stored MXene film annealed at 600 °C. The interior composition of the film was much less oxidized, indicated by a significant drop of Ti(IV) content from 87.0 at.% to 33.0 at.% in Ti 2p XPS spectra before and after Ar-sputtering for 20 mins. In addition, pronounced C-Ti-T_z peaks (with binding energy of 281.6 eV and 282.4 eV) reappeared after sputtering, as it is shown in **Fig. 5-8h**. The chemical composition of Ti(IV) of sputtered sample may be even lower since Ar-sputtering etched the surface layer, at the same time could also mixed some surface TiO_2 components into the interior region, depending on the ion current and time applied in the sputtering. Sputtering at a reduced duration resulted in a relatively higher TiO_2 composition, while longer sputtering time leads to lower Ti(IV) content as it is shown in **Figure 5-10**. XPS results also suggest that a layer of TiO_2 formed on the film surface when the sample was annealed at 600 °C; however, the protected interior part of the film did not show severe oxidation even after 10-month of being in contact with water.

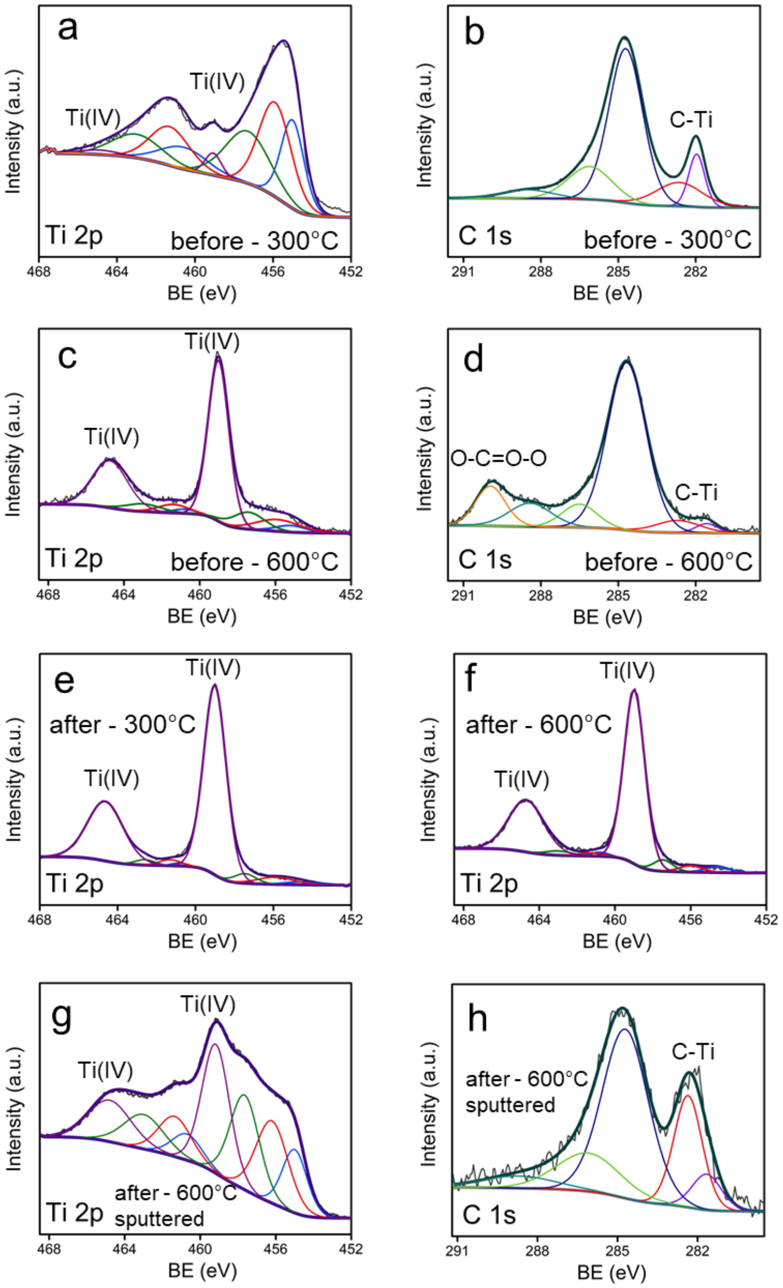

Figure 5-8 Ti 2p and C 1s spectra obtained by X-ray photoelectron spectroscopy (XPS) analysis for (a, b) $Ti_3C_2T_z$ film annealed at 300 °C, (c, d) $Ti_3C_2T_z$ film annealed at 600 °C, (e) 300 °C-annealed $Ti_3C_2T_z$ film after 10-month storage in water, (f) 600 °C-annealed $Ti_3C_2T_z$ film after 10-month storage in water, and (g, h) Ti 2p and C 1s spectra of the same film tested in (f) after being sputtered for 20 min by Ar^+ at a current of 15 mA. Reprinted with permission from reference[74], Copyright 2020 American Chemical Society.

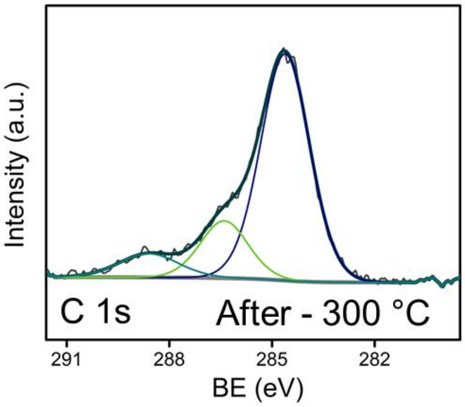

Figure 5-9 C 1s spectra obtained from XPS analysis for 300 °C annealed $Ti_3C_2T_z$ film after 10-month storage in H_2O. Reprinted with permission from reference[74], Copyright 2020 American Chemical Society.

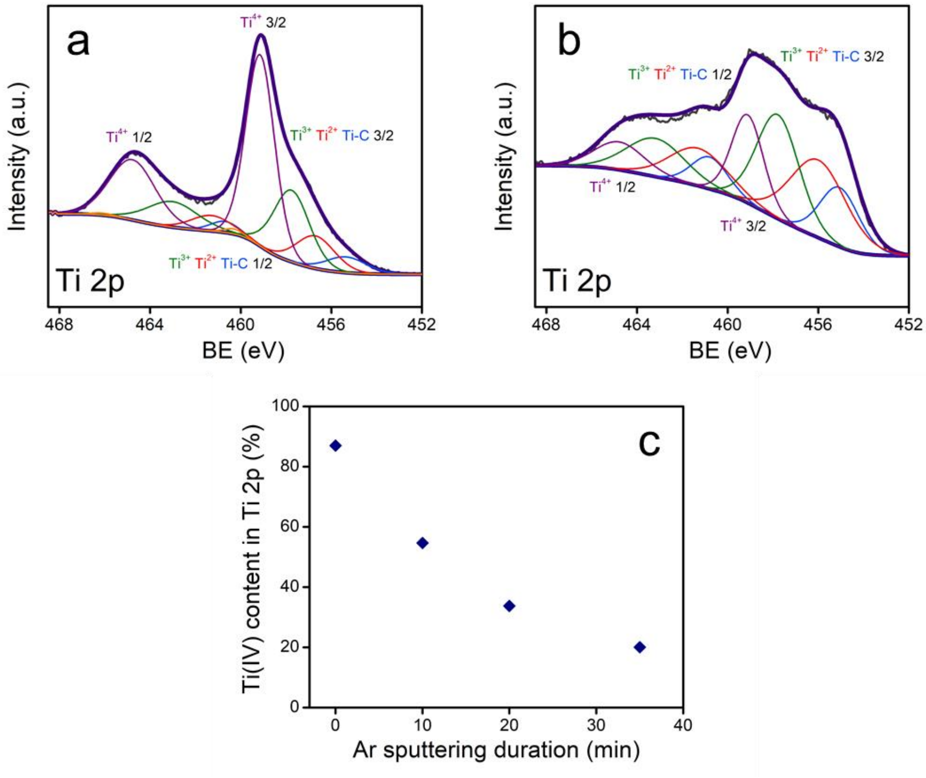

Figure 5-10 Ti 2p spectra obtained by X-ray photoelectron spectroscopy (XPS) analysis for 600 °C annealed $Ti_3C_2T_z$ film after 10-month storage in H_2O being sputtered by Ar^+ for (a) 10 min, (b) 35 min; (c) Ti(IV) content measured by deconvoluted XPS spectra changes sputtering time. Reprinted with permission from reference[74], Copyright 2020 American Chemical Society.

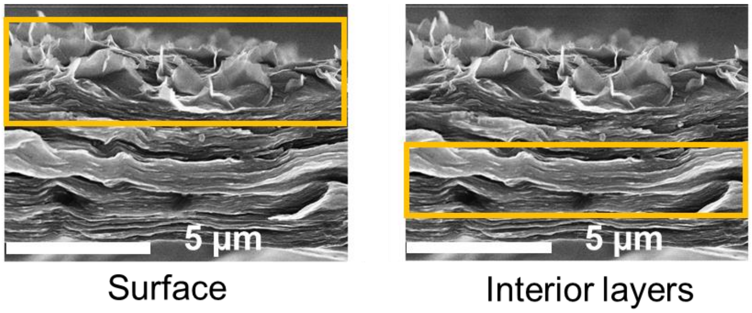

Element	Surface (wt.%)	Surface (at.%)	Interior (wt.%)	Interior (at. %)
C	12.1	20.6	14.1	27.5
O	45.4	57.8	25.6	37.5
F	5.3	5.7	6.9	8.6
Cl	0.9	0.5	1.8	1.2
Ti	36.2	15.3	51.6	25.2

Figure 5-11 Energy dispersive X-ray spectroscopy (EDS) analysis on the cross section of $Ti_3C_2T_z$ film annealed at 600 °C and stored for 10 months in water. Reprinted with permission from reference[74], Copyright 2020 American Chemical Society.

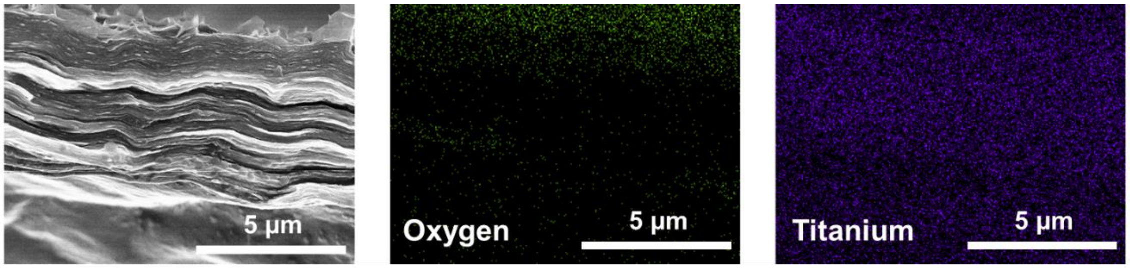

Figure 5-12 Elemental mapping for 600 °C-annealed film after 10 month-storage in water; film was dried prior to EDS mapping. Reprinted with permission from reference[74], Copyright 2020 American Chemical Society.

To better characterize the difference in the degree of oxidation between the $Ti_3C_2T_z$ film's surface and interior structure of the film, elemental analysis was conducted by energy dispersive X-ray spectroscopy (EDS), shown in **Figure 5-11**. The elemental mappings of oxygen and titanium are displayed in **Figure 5-12**. The extent of oxidation was determined by oxygen content in the defined regions of the film cross-section. The oxygen content in the region close to the surface of the film was calculated to be 45.4 wt. %, much higher than 25.6 wt. % in the interior of the film. In addition, the titanium percentage of the interior region was 51.6 wt. %, which was higher than the surface layers at 36.2 wt. %. The elemental contents of fluorine and chlorine are also found to be higher in the interior region than close to the film surface. Our findings with EDS confirm that the MXene film was more oxidized on the surface, while $Ti_3C_2T_z$ was mostly retained in the film interior.

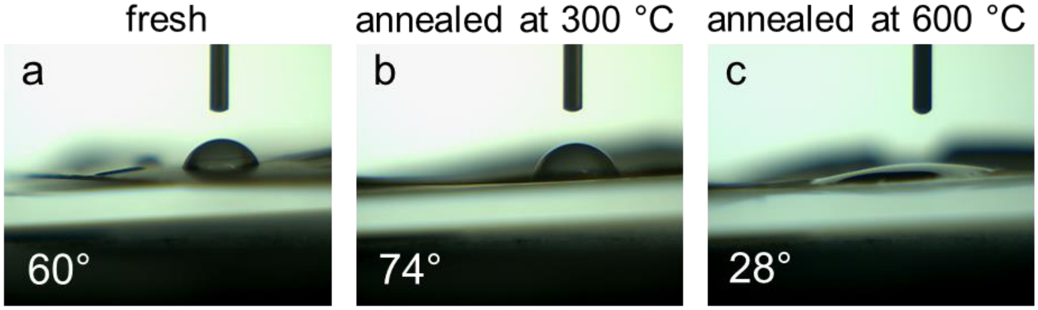

Figure 5-13 Surface wetting and contact angles of (a) fresh $Ti_3C_2T_z$ film without anneal and storage; (b) $Ti_3C_2T_z$ film annealed at 300 °C before storage, and (c) $Ti_3C_2T_z$ film annealed at 600 °C before storage. Reprinted with permission from reference[74], Copyright 2020 American Chemical Society.

The oxidation layer formed on the film's surface was also confirmed by the surface wetting behaviors. **Figure 5-13** shows that after being annealed at 300 °C, the contact angle of water on the film increased from 59.6° to 73.5°, indicating increased surface hydrophobicity. This may be caused by the loss of surface terminal groups and bonded water during annealing. However, the film annealed at 600 °C exhibits a much smaller contact angle of 27.6°. This suggests that the film surface turns hydrophilic with the formation of a TiO_2 layer at the elevated temperature.

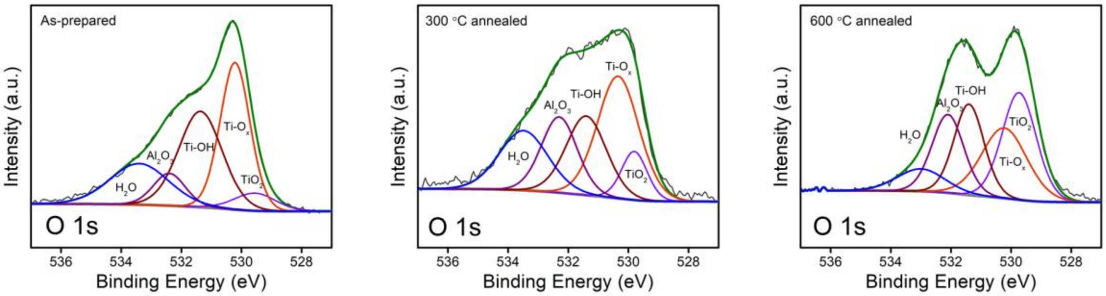

Figure 5-14 Analysis of O 1s spectra obtained by XPS for as-prepared $Ti_3C_2T_z$ films and films annealed at 300 °C and 600 °C, respectively. Reprinted with permission from reference[74], Copyright 2020 American Chemical Society.

Table 5-2 Composition contents obtained by O 1s XPS spectra for as-prepared $Ti_3C_2T_z$ films and films annealed at 300 °C, 600 °C, respectively. Reprinted with permission from reference[74], Copyright 2020 American Chemical Society.

Components in O 1s	As-prepared %	300 °C Annealed %	600 °C Annealed %
TiO_2	5.7	8.2	27.9
$Ti-O_x$	34.5	33.5	24.2
Ti-OH	32.7	21.1	20.7
Al_2O_3	8.1	18.0	19.0
H_2O	19.0	19.1	8.1

Based on XPS and EDS results, we propose that the dense TiO_2 surface layer covering the film's surface may act as barriers preventing water ingress and oxidation in the interior. However, there are difficulties to justify the surface property changes by experiments and needs to be justified in the future works. In addition, XRD suggests that annealing MXene films at elevated temperatures may cause the stacked nanosheets to form a more compact packing, which could be another obstacle for water permeation and oxidation. This is consistent with prior reports.[86, 108] Another possibility for the enhanced stability of 600 °C annealed film is reduction of the number of oxygen-containing groups in the films. This is indicated by the decreased content of Ti-O_x, Ti-OH, and bonded H_2O in of O1s XPS spectra shown in **Figure 5-14** and **Table 5-2**.

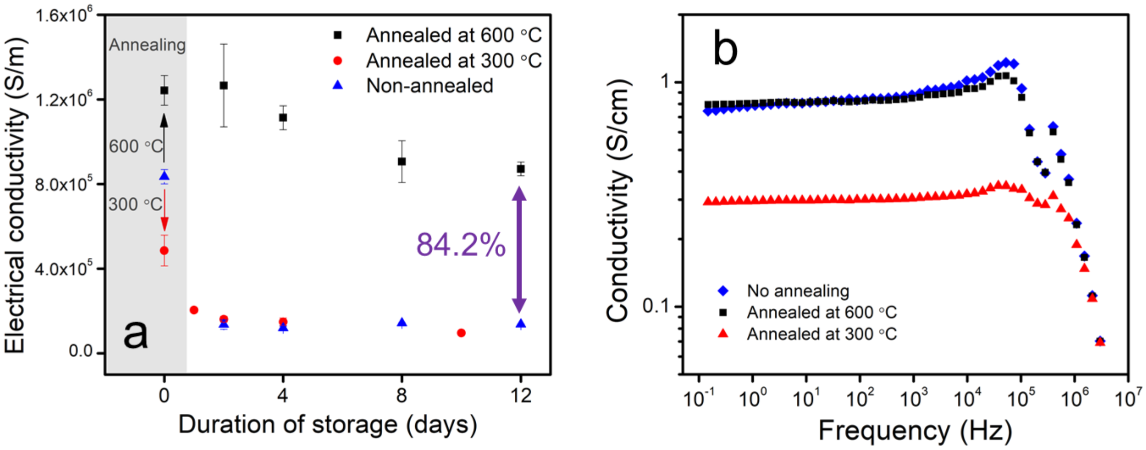

Figure 5-15 (a) Electronic conductivities of $Ti_3C_2T_z$ film before and after being annealed at 300 °C, 600 °C and then stored for consecutive days in humidity-controlled chamber at 80% RH; (b) frequency dependence of the AC conductivities measured by dielectric spectroscopy. Reprinted with permission from reference[74], Copyright 2020 American Chemical Society.

We next investigated how thermal annealing and storage changes the electrical properties of $Ti_3C_2T_z$ films (**Figure 5-15**). The electrical conductivity was found decreased after 300 °C-annealing but increased after 600 °C-annealing. First, the increased film conductivity after °C-annealing may be caused by the reduced amount of oxygen-containing functional groups attached to the MXene surface. Berdiyorov *et al.* and Jiang *et al.* reported that a considerable reduction of the electronic transmission can be caused by the terminated oxygen-containing groups.[135, 136] Attached functional groups may have electron-withdrawing ability which prevents the electronic transmission within nanosheets, [137] so removal of these oxygen-containing groups via high-temperature annealing (at 600 °C) will accelerate the electronic transmission. In addition, suggested by reduced d-spacing of MXene flakes after annealing, more compact MXene films may cause faster electronic transmission due to more nanosheets overlaps and contacts. The stability of MXene film conductivity is also investigated. When stored in a chamber with controlled humidity at 80% RH (high humidity is used to shorten the experimental duration), the film annealed at 600 °C exhibited more stable conductivities than both the as-prepared and 300 °C-annealed samples shown in **Figure 5-15a**.

We also investigated the frequency-dependent AC conductivity in the annealed films' cross section direction by dielectric spectroscopy, from 0.1 Hz to 10 MHz. The results (**Figure 5-15b)** show that the $Ti_3C_2T_z$ film annealed at 300 °C exhibited the lowest conductivity. However, the as-prepared and 600 °C-annealed $Ti_3C_2T_z$ films exhibited higher conductivity and show similar electronic properties. This suggests that the TiO_2 layer induced in annealing is thin and does not affect the electrical properties of the MXene film. In addition, despite the existence of the thin oxidized film, the conductivity of 600 °C annealed film was retained due to the more compact surface structure and reduced amount of surface functionalities.

Radio-frequency (RF)-induced heating can also be used to quantify the interactions between the MXene films and electromagnetic waves; this heating response is correlated with the structure and AC bulk conductivities of the samples. [22] **Figure 5-16** shows the dynamic thermal response of these structures; again, the 600 °C-annealed films (before storage in water) showed a response similar to the as-prepared structure, whereas the plateau temperature for the 300 °C-annealed films is far lower, indicating a loss of conductivity.

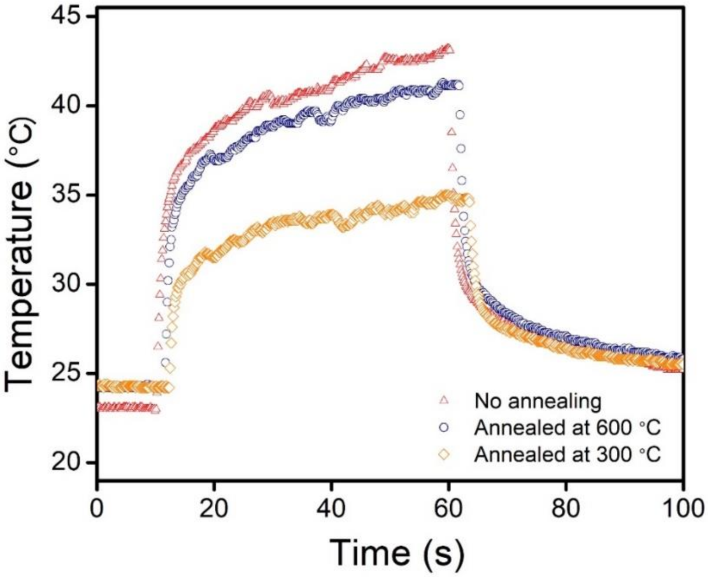

Figure 5-16 RF heating of the $Ti_3C_2T_z$ films before storage in water. Maximum temperature as a function of time for as-prepared (no annealing) $Ti_3C_2T_z$ film and films annealed at 300 °C and 600 °C. Films were heated using RF power of 32 W and frequency of 106 MHz. Reprinted with permission from reference[74], Copyright 2020 American Chemical Society.

5.5. Conclusion

Our study demonstrates that annealing $Ti_3C_2T_z$ films at elevated temperatures such as 600 °C helps to prevent film degradation, even for films stored in water for over a 10-month period. This method significantly extends the oxidation-resistance of $Ti_3C_2T_z$ MXene films, which may be potentially used as electrodes in batteries and supercapacitors, membranes, and catalytic surfaces, and may broaden the durable application of MXene devices in aqueous environments.

6. CONCLUSIONS

Low oxidation stability shortens the shelf life of MXene nanosheets, such as $Ti_3C_2T_x$ and Ti_2CT_x, and brings challenges in the implementation of these nanosheets in MXene-based devices. We devise unprecedented approaches to improve the oxidation stability of MXene nanosheets and films. It was found that introduction of antioxidants, such as sodium L-ascorbate, citric acid, tartaric acid, and oxalic acid, can prevent the transformation of titanium carbide MXenes into titanium dioxide, leading to the significant improvement of the oxidation and colloidal stability of $Ti_3C_2T_x$ and Ti_2CT_x nanosheets in aqueous dispersions. In addition, we proved that a simple pre-treatment step by antioxidants could make MXene nanosheets oxidation-resistant in the dry form as powders or films. We also analyze the relationship between an antioxidant's chemical structure and its effectiveness in protecting $Ti_3C_2T_x$ and Ti_2CT_x in a systematic study. This work indicates that the chelation effect induced by antioxidants with polydentate ligands helps to prevent or eliminate MXene oxidation. Our results represent an improvement in understanding the stabilization of MXene nanosheets in aqueous dispersion. In addition, we developed a method by thermally annealing free-standing $Ti_3C_2T_x$ MXene films under inert gas, which was found to induce surface and structural modifications. This method leads to remarkable increases in the chemical stability of the films and extended storage life in water. Effects of dispersion pH, nanosheet concentration, salt addition, and aggregation on the oxidation stability of MXene nanosheets were investigated in this work. We discovered that MXene oxidation can be accelerated by the introduction of hydroxide ions from a base. Our study emphasizes that MXene processing and utilization in basic environments, such as in TMAOH, TBAOH and NaOH, may lead to sub-optimal performance due to oxidation.

Moving forward, this study on MXene stabilization techniques is being extended to other types of MXenes, especially on the less-stable M_2X type of MXenes including Nb_2C and V_2C. Addition of antioxidants during MXene selective acid etching and exfoliation steps can also be explored to understand whether this will promote the nanosheet yield and oxidation stability. In addition, we will focus on investigating how the MXene stability will be affected by the species and amount of the functional groups on the basal plane of nanosheets. The molten salt etching technique is known to enable new surface terminations on derived MXenes where there are not much oxygen-containing groups. We aim to understand whether this new terminations will have an impact on the oxidation stability of MXene nanosheets.

REFERENCES

1. Gogotsi Y, Anasori B. The Rise of MXenes. ACS Nano. 2019;13(8):8491-8494.

2. Naguib M, Mashtalir O, Carle J, Presser V, Lu J, Hultman L, Gogotsi Y, Barsoum MW. Two-Dimensional Transition Metal Carbides. ACS Nano. 2012;6(2):1322-1331.

3. Anasori B, Lukatskaya MR, Gogotsi Y. 2D metal carbides and nitrides (MXenes) for energy storage. Nature Reviews Materials. 2017;2:16098.

4. Anasori B, Xie Y, Beidaghi M, Lu J, Hosler BC, Hultman L, Kent PRC, Gogotsi Y, Barsoum MW. Two-Dimensional, Ordered, Double Transition Metals Carbides (MXenes). ACS Nano. 2015;9(10):9507-9516.

5. Naguib M, Mochalin VN, Barsoum MW, Gogotsi Y. 25th Anniversary Article: MXenes: A New Family of Two-Dimensional Materials. Advanced Materials. 2014;26(7):992-1005.

6. Dillon AD, Ghidiu MJ, Krick AL, Griggs J, May SJ, Gogotsi Y, Barsoum MW, Fafarman AT. Highly Conductive Optical Quality Solution-Processed Films of 2D Titanium Carbide. Advanced Functional Materials. 2016;26(23):4162-4168.

7. Schultz T, Frey NC, Hantanasirisakul K, Park S, May SJ, Shenoy VB, Gogotsi Y, Koch N. Surface Termination Dependent Work Function and Electronic Properties of Ti3C2Tx MXene. Chemistry of Materials. 2019;31(17):6590-6597.

8. Alhabeb M, Maleski K, Anasori B, Lelyukh P, Clark L, Sin S, Gogotsi Y. Guidelines for Synthesis and Processing of Two-Dimensional Titanium Carbide (Ti3C2Tx MXene). Chemistry of Materials. 2017;29(18):7633-7644.

9. Hart JL, Hantanasirisakul K, Lang AC, Anasori B, Pinto D, Pivak Y, van Omme JT, May SJ, Gogotsi Y, Taheri ML. Control of MXenes' electronic properties through termination and intercalation. Nature Communications. 2019;10(1):522.

10. Sun W, Shah SA, Chen Y, Tan Z, Gao H, Habib T, Radovic M, Green MJ. Electrochemical etching of Ti2AlC to Ti2CTx (MXene) in low-concentration hydrochloric acid solution. Journal of Materials Chemistry A. 2017;5(41):21663-21668.

11. Xie Y, Naguib M, Mochalin VN, Barsoum MW, Gogotsi Y, Yu X, Nam K-W, Yang X-Q, Kolesnikov AI, Kent PRC. Role of Surface Structure on Li-Ion Energy Storage Capacity of Two-Dimensional Transition-Metal Carbides. Journal of the American Chemical Society. 2014;136(17):6385-6394.

12. Lipatov A, Alhabeb M, Lu H, Zhao S, Loes MJ, Vorobeva NS, Dall'Agnese Y, Gao Y, Gruverman A, Gogotsi Y, Sinitskii A. Electrical and Elastic Properties of Individual Single-Layer Nb4C3Tx MXene Flakes. Advanced Electronic Materials. 2020;6(4):1901382.

13. Yun J, Echols I, Flouda P, Chen Y, Wang S, Zhao X, Holta D, Radovic M, Green MJ, Naraghi M, Lutkenhaus JL. Layer-by-Layer Assembly of Reduced Graphene Oxide and MXene Nanosheets for Wire-Shaped Flexible Supercapacitors. ACS Applied Materials & Interfaces. 2021;13(12):14068-14076.

14. Sarang KT, Zhao X, Holta D, Radovic M, Green MJ, Oh E-S, Lutkenhaus JL. Minimizing two-dimensional Ti3C2Tx MXene nanosheet loading in carbon-free silicon anodes. Nanoscale. 2020;12(40):20699-20709.

15. Yun J, Echols I, Flouda P, Wang S, Easley A, Zhao X, Tan Z, Prehn E, Zi G, Radovic M, Green MJ, Lutkenhaus JL. Layer-by-Layer Assembly of Polyaniline Nanofibers and MXene Thin-Film Electrodes for Electrochemical Energy Storage. ACS Applied Materials & Interfaces. 2019;11(51):47929-47938.

16. An H, Habib T, Shah S, Gao H, Patel A, Echols I, Zhao X, Radovic M, Green MJ, Lutkenhaus JL. Water Sorption in MXene/Polyelectrolyte Multilayers for Ultrafast Humidity Sensing. ACS Applied Nano Materials. 2019;2(2):948-955.

17. Echols I, An H, Zhao X, Prehn EM, Tan Z, Radovic M, Green M, Lutkenhaus J. pH-Response of Polycation/Ti3C2Tx MXene Layer-by-Layer Assemblies for Use as Resistive Sensors. Molecular Systems Design & Engineering. 2019.

18. Shahzad F, Alhabeb M, Hatter CB, Anasori B, Man Hong S, Koo CM, Gogotsi Y. Electromagnetic interference shielding with 2D transition metal carbides (MXenes). Science. 2016;353(6304):1137-1140.

19. Ma Z, Kang S, Ma J, Shao L, Zhang Y, Liu C, Wei A, Xiang X, Wei L, Gu J. Ultraflexible and Mechanically Strong Double-Layered Aramid Nanofiber–Ti3C2Tx MXene/Silver Nanowire Nanocomposite Papers for High-Performance Electromagnetic Interference Shielding. ACS Nano. 2020;14(7):8368-8382.

20. An H, Habib T, Shah S, Gao H, Radovic M, Green MJ, Lutkenhaus JL. Surface-agnostic highly stretchable and bendable conductive MXene multilayers. Science Advances. 2018;4(3):eaaq0118.

21. Zeng M, Zhang Y. Colloidal nanoparticle inks for printing functional devices: emerging trends and future prospects. Journal of Materials Chemistry A. 2019;7(41):23301-23336.

22. Habib T, Patil N, Zhao X, Prehn E, Anas M, Lutkenhaus JL, Radovic M, Green MJ. Heating of Ti3C2Tx MXene/polymer composites in response to Radio Frequency fields. Scientific Reports. 2019;9(1):16489.

23. Cao H, Escamilla M, Arole KD, Holta D, Lutkenhaus JL, Radovic M, Green MJ, Pentzer EB. Flocculation of MXenes and Their Use as 2D Particle Surfactants for Capsule Formation. Langmuir. 2021;37(8):2649-2657.

24. Chaudhuri K, Alhabeb M, Wang Z, Shalaev VM, Gogotsi Y, Boltasseva A. Highly Broadband Absorber Using Plasmonic Titanium Carbide (MXene). ACS Photonics. 2018;5(3):1115-1122.

25. Xie X, Chen C, Zhang N, Tang Z-R, Jiang J, Xu Y-J. Microstructure and surface control of MXene films for water purification. Nature Sustainability. 2019;2(9):856-862.

26. Ren CE, Hatzell KB, Alhabeb M, Ling Z, Mahmoud KA, Gogotsi Y. Charge- and Size-Selective Ion Sieving Through Ti3C2Tx MXene Membranes. The Journal of Physical Chemistry Letters. 2015;6(20):4026-4031.

27. Peng X, Peng L, Wu C, Xie Y. Two dimensional nanomaterials for flexible supercapacitors. Chemical Society Reviews. 2014;43(10):3303-3323.

28. An H, Habib T, Shah S, Gao H, Radovic M, Green MJ, Lutkenhaus JL. Surface-agnostic highly stretchable and bendable conductive MXene multilayers. Science Advances. 2018;4(3).

29. Han M, Yin X, Wu H, Hou Z, Song C, Li X, Zhang L, Cheng L. Ti3C2 MXenes with Modified Surface for High-Performance Electromagnetic Absorption and Shielding in the X-Band. ACS Applied Materials & Interfaces. 2016;8(32):21011-21019.

30. Er D, Li J, Naguib M, Gogotsi Y, Shenoy VB. Ti3C2 MXene as a High Capacity Electrode Material for Metal (Li, Na, K, Ca) Ion Batteries. ACS Applied Materials & Interfaces. 2014;6(14):11173-11179.

31. Yuan W, Cheng L, An Y, Wu H, Yao N, Fan X, Guo X. MXene Nanofibers as Highly Active Catalysts for Hydrogen Evolution Reaction. ACS Sustainable Chemistry & Engineering. 2018;6(7):8976-8982.

32. Seh ZW, Fredrickson KD, Anasori B, Kibsgaard J, Strickler AL, Lukatskaya MR, Gogotsi Y, Jaramillo TF, Vojvodic A. Two-Dimensional Molybdenum Carbide (MXene) as an Efficient Electrocatalyst for Hydrogen Evolution. ACS Energy Letters. 2016;1(3):589-594.

33. Peng J, Chen X, Ong W-J, Zhao X, Li N. Surface and Heterointerface Engineering of 2D MXenes and Their Nanocomposites: Insights into Electro- and Photocatalysis. Chem. 2019;5(1):18-50.

34. Wang Z, Wu H-H, Li Q, Besenbacher F, Li Y, Zeng XC, Dong M. Reversing Interfacial Catalysis of Ambipolar WSe2 Single Crystal. Advanced Science. 2020;7(3):1901382.

35. Shah SA, Habib T, Gao H, Gao P, Sun W, Green MJ, Radovic M. Template-free 3D titanium carbide (Ti3C2Tx) MXene particles crumpled by capillary forces. Chemical Communications. 2017;53(2):400-403.

36. Naguib M, Kurtoglu M, Presser V, Lu J, Niu J, Heon M, Hultman L, Gogotsi Y, Barsoum MW. Two-Dimensional Nanocrystals Produced by Exfoliation of Ti3AlC2. Advanced Materials. 2011;23(37):4248-4253.

37. Eklund P, Rosen J, Persson POÅ. Layered ternary Mn+1AXnphases and their 2D derivative MXene: an overview from a thin-film perspective. Journal of Physics D: Applied Physics. 2017;50(11):113001.

38. Ghidiu M, Lukatskaya MR, Zhao M-Q, Gogotsi Y, Barsoum MW. Conductive two-dimensional titanium carbide ‘clay’ with high volumetric capacitance. Nature. 2014;516:78.

39. Naguib M, Gogotsi Y. Synthesis of Two-Dimensional Materials by Selective Extraction. Accounts of Chemical Research. 2015;48(1):128-135.

40. Anasori B, Gogotsi Y. Introduction to 2D Transition Metal Carbides and Nitrides (MXenes). In: Anasori B, Gogotsi Y, editors. 2D Metal Carbides and Nitrides (MXenes): Structure, Properties and Applications. Cham: Springer International Publishing; 2019. p. 3-12.

41. Halim J, Lukatskaya MR, Cook KM, Lu J, Smith CR, Näslund L-Å, May SJ, Hultman L, Gogotsi Y, Eklund P, Barsoum MW. Transparent Conductive Two-Dimensional Titanium Carbide Epitaxial Thin Films. Chemistry of Materials. 2014;26(7):2374-2381.

42. Zhao X, Radovic M, Green MJ. Synthesizing MXene Nanosheets by Water-free Etching. Chem. 2020;6(3):544-546.

43. Natu V, Pai R, Sokol M, Carey M, Kalra V, Barsoum MW. 2D Ti3C2Tz MXene Synthesized by Water-free Etching of Ti3AlC2 in Polar Organic Solvents. Chem. 2020;6(3):616-630.

44. Maleski K, Alhabeb M. Top-Down MXene Synthesis (Selective Etching). In: Anasori B, Gogotsi Y, editors. 2D Metal Carbides and Nitrides (MXenes): Structure, Properties and Applications. Cham: Springer International Publishing; 2019. p. 69-87.

45. Mashtalir O, Cook KM, Mochalin VN, Crowe M, Barsoum MW, Gogotsi Y. Dye adsorption and decomposition on two-dimensional titanium carbide in aqueous media. Journal of Materials Chemistry A. 2014;2(35):14334-14338.

46. Habib T, Zhao X, Shah SA, Chen Y, Sun W, An H, Lutkenhaus JL, Radovic M, Green MJ. Oxidation stability of Ti3C2Tx MXene nanosheets in solvents and composite films. npj 2D Materials and Applications. 2019;3(1):8.

47. Halim J, Kota S, Lukatskaya MR, Naguib M, Zhao M-Q, Moon EJ, Pitock J, Nanda J, May SJ, Gogotsi Y, Barsoum MW. Synthesis and Characterization of 2D Molybdenum Carbide (MXene). Advanced Functional Materials. 2016;26(18):3118-3127.

48. Sang X, Naguib M, Alhabeb M, Unocic RR. Effect of Synthesis Methods on the Structure and Defects of Two-Dimensional MXenes. In: Anasori B, Gogotsi Y, editors. 2D Metal Carbides and Nitrides (MXenes): Structure, Properties and Applications. Cham: Springer International Publishing; 2019. p. 111-123.

49. Sang X, Xie Y, Lin M-W, Alhabeb M, Van Aken KL, Gogotsi Y, Kent PRC, Xiao K, Unocic RR. Atomic Defects in Monolayer Titanium Carbide (Ti3C2Tx) MXene. ACS Nano. 2016;10(10):9193-9200.

50. Mashtalir O, Naguib M, Dyatkin B, Gogotsi Y, Barsoum MW. Kinetics of aluminum extraction from Ti3AlC2 in hydrofluoric acid. Materials Chemistry and Physics. 2013;139(1):147-152.

51. Naguib M, Unocic RR, Armstrong BL, Nanda J. Large-scale delamination of multi-layers transition metal carbides and carbonitrides “MXenes”. Dalton Transactions. 2015;44(20):9353-9358.

52. Lipatov A, Alhabeb M, Lukatskaya MR, Boson A, Gogotsi Y, Sinitskii A. Effect of Synthesis on Quality, Electronic Properties and Environmental Stability of Individual Monolayer Ti3C2 MXene Flakes. Advanced Electronic Materials. 2016;2(12):1600255.

53. Hope MA, Forse AC, Griffith KJ, Lukatskaya MR, Ghidiu M, Gogotsi Y, Grey CP. NMR reveals the surface functionalisation of Ti3C2 MXene. Physical Chemistry Chemical Physics. 2016;18(7):5099-5102.

54. VahidMohammadi A, Kayali E, Orangi J, Beidaghi M. Techniques for MXene Delamination into Single-Layer Flakes. In: Anasori B, Gogotsi Y, editors. 2D Metal Carbides and Nitrides (MXenes): Structure, Properties and Applications. Cham: Springer International Publishing; 2019. p. 177-195.

55. Urbankowski P, Anasori B, Makaryan T, Er D, Kota S, Walsh PL, Zhao M, Shenoy VB, Barsoum MW, Gogotsi Y. Synthesis of two-dimensional titanium nitride Ti 4 N 3 (MXene). Nanoscale. 2016;8(22):11385-11391.

56. Li M, Lu J, Luo K, Li Y, Chang K, Chen K, Zhou J, Rosen J, Hultman L, Eklund P. Element replacement approach by reaction with Lewis acidic molten salts to synthesize nanolaminated MAX phases and MXenes. Journal of the American Chemical Society. 2019;141(11):4730-4737.

57. Li Y, Shao H, Lin Z, Lu J, Liu L, Duployer B, Persson PO, Eklund P, Hultman L, Li M. A general Lewis acidic etching route for preparing MXenes with enhanced electrochemical performance in non-aqueous electrolyte. Nature Materials. 2020:1-6.

58. Kamysbayev V, Filatov AS, Hu H, Rui X, Lagunas F, Wang D, Klie RF, Talapin DV. Covalent surface modifications and superconductivity of two-dimensional metal carbide MXenes. Science. 2020;369(6506):979-983.

59. Hong Ng VM, Huang H, Zhou K, Lee PS, Que W, Xu JZ, Kong LB. Recent progress in layered transition metal carbides and/or nitrides (MXenes) and their composites: synthesis and applications. Journal of Materials Chemistry A. 2017;5(7):3039-3068.

60. Natu V, Sokol M, Verger L, Barsoum MW. Effect of Edge Charges on Stability and Aggregation of Ti3C2Tz MXene Colloidal Suspensions. The Journal of Physical Chemistry C. 2018;122(48):27745-27753.

61. Zhao X, Vashisth A, Blivin JW, Tan Z, Holta DE, Kotasthane V, Shah SA, Habib T, Liu S, Lutkenhaus JL, Radovic M, Green MJ. pH, Nanosheet Concentration, and Antioxidant Affect the Oxidation of Ti3C2Tx and Ti2CTx MXene Dispersions. Advanced Materials Interfaces. 2020;7(20):2000845.

62. Ying Y, Liu Y, Wang X, Mao Y, Cao W, Hu P, Peng X. Two-Dimensional Titanium Carbide for Efficiently Reductive Removal of Highly Toxic Chromium(VI) from Water. ACS Applied Materials & Interfaces. 2015;7(3):1795-1803.

63. Ghassemi H, Harlow W, Mashtalir O, Beidaghi M, Lukatskaya MR, Gogotsi Y, Taheri ML. In situ environmental transmission electron microscopy study of oxidation of two-dimensional Ti3C2 and formation of carbon-supported TiO2. Journal of Materials Chemistry A. 2014;2(35):14339-14343.

64. Zhang CJ, Pinilla S, McEvoy N, Cullen CP, Anasori B, Long E, Park S-H, Seral-Ascaso A, Shmeliov A, Krishnan D, Morant C, Liu X, Duesberg GS, Gogotsi Y, Nicolosi V. Oxidation Stability of Colloidal Two-Dimensional Titanium Carbides (MXenes). Chemistry of Materials. 2017;29(11):4848-4856.

65. Huang S, Mochalin VN. Hydrolysis of 2D Transition-Metal Carbides (MXenes) in Colloidal Solutions. Inorganic Chemistry. 2019;58(3):1958-1966.

66. Maleski K, Mochalin VN, Gogotsi Y. Dispersions of Two-Dimensional Titanium Carbide MXene in Organic Solvents. Chemistry of Materials. 2017;29(4):1632-1640.

67. Chertopalov S, Mochalin VN. Environment-Sensitive Photoresponse of Spontaneously Partially Oxidized Ti3C2 MXene Thin Films. ACS Nano. 2018;12(6):6109-6116.

68. Li J, Qin R, Yan L, Chi Z, Yu Z, Li N, Hu M, Chen H, Shan G. Plasmonic Light Illumination Creates a Channel To Achieve Fast Degradation of Ti3C2Tx Nanosheets. Inorganic Chemistry. 2019;58(11):7285-7294.

69. Chae Y, Kim SJ, Cho S-Y, Choi J, Maleski K, Lee B-J, Jung H-T, Gogotsi Y, Lee Y, Ahn CW. An investigation into the factors governing the oxidation of two-dimensional Ti3C2 MXene. Nanoscale. 2019;11(17):8387-8393.

70. Xia F, Lao J, Yu R, Sang X, Luo J, Li Y, Wu J. Ambient oxidation of Ti3C2 MXene initialized by atomic defects. Nanoscale. 2019;11(48):23330-23337.

71. Huang S, Mochalin VN. Understanding Chemistry of Two-Dimensional Transition Metal Carbides and Carbonitrides (MXenes) with Gas Analysis. ACS Nano. 2020;14(8):10251-10257.

72. Halim J, Cook KM, Naguib M, Eklund P, Gogotsi Y, Rosen J, Barsoum MW. X-ray photoelectron spectroscopy of select multi-layered transition metal carbides (MXenes). Applied Surface Science. 2016;362:406-417.

73. Natu V, Benchakar M, Canaff C, Habrioux A, Célérier S, Barsoum MW. A critical analysis of the X-ray photoelectron spectra of Ti3C2Tz MXenes. Matter. 2021;4(4):1224-1251.

74. Zhao X, Holta DE, Tan Z, Oh J-H, Echols IJ, Anas M, Cao H, Lutkenhaus JL, Radovic M, Green MJ. Annealed Ti3C2Tz MXene Films for Oxidation-Resistant Functional Coatings. ACS Applied Nano Materials. 2020.

75. Zhao X, Vashisth A, Prehn E, Sun W, Shah SA, Habib T, Chen Y, Tan Z, Lutkenhaus JL, Radovic M, Green MJ. Antioxidants Unlock Shelf-Stable Ti3C2Tx (MXene) Nanosheet Dispersions. Matter. 2019;1(2):513-526.

76. Hanlon D, Backes C, Doherty E, Cucinotta CS, Berner NC, Boland C, Lee K, Harvey A, Lynch P, Gholamvand Z, Zhang S, Wang K, Moynihan G, Pokle A, Ramasse QM, McEvoy N, Blau WJ, Wang J, Abellan G, Hauke F, Hirsch A, Sanvito S, O'Regan DD, Duesberg GS, Nicolosi V, Coleman JN. Liquid exfoliation of solvent-stabilized few-layer black phosphorus for applications beyond electronics. Nature Communications. 2015;6(1):8563.

77. Zhang J, Kong N, Hegh D, Usman KAS, Guan G, Qin S, Jurewicz I, Yang W, Razal JM. Freezing Titanium Carbide Aqueous Dispersions for Ultra-long-term Storage. ACS Applied Materials & Interfaces. 2020;12(30):34032-34040.

78. Wu X, Wang Z, Yu M, Xiu L, Qiu J. Stabilizing the MXenes by Carbon Nanoplating for Developing Hierarchical Nanohybrids with Efficient Lithium Storage and Hydrogen Evolution Capability. Advanced Materials. 2017;29(24):1607017.

79. Ji J, Zhao L, Shen Y, Liu S, Zhang Y. Covalent stabilization and functionalization of MXene via silylation reactions with improved surface properties. FlatChem. 2019;17:100128.

80. Lee Y, Kim SJ, Kim Y-J, Lim Y, Chae Y, Lee B-J, Kim Y-T, Han H, Gogotsi Y, Ahn CW. Oxidation-resistant titanium carbide MXene films. Journal of Materials Chemistry A. 2020;8(2):573-581.

81. Shuck CE, Han M, Maleski K, Hantanasirisakul K, Kim SJ, Choi J, Reil WEB, Gogotsi Y. Effect of Ti3AlC2 MAX Phase on Structure and Properties of Resultant Ti3C2Tx MXene. ACS Applied Nano Materials. 2019;2(6):3368-3376.

82. Mathis TS, Maleski K, Goad A, Sarycheva A, Anayee M, Foucher AC, Hantanasirisakul K, Shuck CE, Stach EA, Gogotsi Y. Modified MAX Phase Synthesis for Environmentally Stable and Highly Conductive Ti3C2 MXene. ACS Nano. 2021;15(4):6420-6429.

83. Lotfi R, Naguib M, Yilmaz DE, Nanda J, van Duin ACT. A comparative study on the oxidation of two-dimensional Ti3C2 MXene structures in different environments. Journal of Materials Chemistry A. 2018;6(26):12733-12743.

84. Liang X, Rangom Y, Kwok CY, Pang Q, Nazar LF. Interwoven MXene Nanosheet/Carbon-Nanotube Composites as Li–S Cathode Hosts. Advanced Materials. 2017;29(3):1603040.

85. Biesinger MC, Lau LWM, Gerson AR, Smart RSC. Resolving surface chemical states in XPS analysis of first row transition metals, oxides and hydroxides: Sc, Ti, V, Cu and Zn. Applied Surface Science. 2010;257(3):887-898.

86. Osti NC, Naguib M, Ostadhossein A, Xie Y, Kent PRC, Dyatkin B, Rother G, Heller WT, van Duin ACT, Gogotsi Y, Mamontov E. Effect of Metal Ion Intercalation on the Structure of MXene and Water Dynamics on its Internal Surfaces. Acs Appl Mater Inter. 2016;8(14):8859-8863.

87. Plimpton S. Fast Parallel Algorithms for Short-Range Molecular-Dynamics. J Comput Phys. 1995;117(1):1-19.

88. Humphrey W, Dalke A, Schulten K. VMD: Visual molecular dynamics. J Mol Graph Model. 1996;14(1):33-38.

89. Li Z, Wang L, Sun D, Zhang Y, Liu B, Hu Q, Zhou A. Synthesis and thermal stability of two-dimensional carbide MXene Ti3C2. Materials Science and Engineering: B. 2015;191:33-40.

90. Liu R, Li W. High-Thermal-Stability and High-Thermal-Conductivity Ti3C2Tx MXene/Poly(vinyl alcohol) (PVA) Composites. ACS Omega. 2018;3(3):2609-2617.

91. Ahmed B, Anjum DH, Hedhili MN, Gogotsi Y, Alshareef HN. H2O2 assisted room temperature oxidation of Ti2C MXene for Li-ion battery anodes. Nanoscale. 2016;8(14):7580-7587.

92. Deysher G, Sin S, Gogotsi Y, Anasori B. Oxidized 2D titanium carbide MXene: Flash oxidized powders. Materials Today. 2018;21(10):1064-1065.

93. Khan K, Tareen AK, Aslam M, Wang R, Zhang Y, Mahmood A, Ouyang Z, Zhang H, Guo Z. Recent developments in emerging two-dimensional materials and their applications. Journal of Materials Chemistry C. 2020;8(2):387-440.

94. VahidMohammadi A, Mojtabavi M, Caffrey NM, Wanunu M, Beidaghi M. Assembling 2D MXenes into Highly Stable Pseudocapacitive Electrodes with High Power and Energy Densities. Advanced Materials. 2019;31(8):1806931.

95. Natu V, Hart JL, Sokol M, Chiang H, Taheri ML, Barsoum MW. Edge Capping of 2D-MXene Sheets with Polyanionic Salts To Mitigate Oxidation in Aqueous Colloidal Suspensions. Angewandte Chemie. 2019;131(36):12785-12790.

96. van Duin ACT, Dasgupta S, Lorant F, Goddard WA. ReaxFF: A Reactive Force Field for Hydrocarbons. The Journal of Physical Chemistry A. 2001;105(41):9396-9409.

97. Maleski K, Ren CE, Zhao M-Q, Anasori B, Gogotsi Y. Size-Dependent Physical and Electrochemical Properties of Two-Dimensional MXene Flakes. ACS Applied Materials & Interfaces. 2018;10(29):24491-24498.

98. Mashtalir O, Naguib M, Mochalin VN, Dall'Agnese Y, Heon M, Barsoum MW, Gogotsi Y. Intercalation and delamination of layered carbides and carbonitrides. Nature Communications. 2013;4(1):1716.

99. van Duin ACT, Dasgupta S, Lorant F, Goddard WA. ReaxFF: A reactive force field for hydrocarbons. J Phys Chem A. 2001;105(41):9396-9409.

100. Fan Z, Wang Y, Xie Z, Wang D, Yuan Y, Kang H, Su B, Cheng Z, Liu Y. Modified MXene/Holey Graphene Films for Advanced Supercapacitor Electrodes with Superior Energy Storage. Advanced Science. 2018;5(10):1800750.

101. Papagianni M. Advances in citric acid fermentation by Aspergillus niger: Biochemical aspects, membrane transport and modeling. Biotechnology Advances. 2007;25(3):244-263.

102. Echols IJ, Holta DE, Kotasthane VS, Tan Z, Radovic M, Lutkenhaus JL, Green MJ. Oxidative Stability of Nbn+1CnTz MXenes. The Journal of Physical Chemistry C. 2021.

103. VahidMohammadi A, Liang W, Mojtabavi M, Wanunu M, Beidaghi M. 2D Titanium and Vanadium Carbide MXene Heterostructures for Electrochemical Energy Storage. Energy Storage Materials. 2021.

104. Shan Q, Mu X, Alhabeb M, Shuck CE, Pang D, Zhao X, Chu X-F, Wei Y, Du F, Chen G, Gogotsi Y, Gao Y, Dall'Agnese Y. Two-dimensional vanadium carbide (V2C) MXene as electrode for supercapacitors with aqueous electrolytes. Electrochemistry Communications. 2018;96:103-107.

105. Lukatskaya MR, Mashtalir O, Ren CE, Dall’Agnese Y, Rozier P, Taberna PL, Naguib M, Simon P, Barsoum MW, Gogotsi Y. Cation Intercalation and High Volumetric Capacitance of Two-Dimensional Titanium Carbide. Science. 2013;341(6153):1502-1505.

106. Zhang C, Anasori B, Seral-Ascaso A, Park S-H, McEvoy N, Shmeliov A, Duesberg GS, Coleman JN, Gogotsi Y, Nicolosi V. Transparent, Flexible, and Conductive 2D Titanium Carbide (MXene) Films with High Volumetric Capacitance. Advanced Materials. 2017;29(36):1702678.

107. Djire A, Bos A, Liu J, Zhang H, Miller EM, Neale NR. Pseudocapacitive Storage in Nanolayered Ti2NTx MXene Using Mg-Ion Electrolyte. ACS Applied Nano Materials. 2019;2(5):2785-2795.

108. Sarycheva A, Polemi A, Liu Y, Dandekar K, Anasori B, Gogotsi Y. 2D titanium carbide (MXene) for wireless communication. Science Advances. 2018;4(9):eaau0920.

109. Cui Z, Gao C, Fan Z, Wang J, Cheng Z, Xie Z, Liu Y, Wang Y. Lightweight MXene/Cellulose Nanofiber Composite Film for Electromagnetic Interference Shielding. Journal of Electronic Materials. 2021;50(4):2101-2110.

110. Han M, Shuck CE, Rakhmanov R, Parchment D, Anasori B, Koo CM, Friedman G, Gogotsi Y. Beyond Ti3C2Tx: MXenes for Electromagnetic Interference Shielding. ACS Nano. 2020;14(4):5008-5016.

111. Hantanasirisakul K, Zhao M-Q, Urbankowski P, Halim J, Anasori B, Kota S, Ren CE, Barsoum MW, Gogotsi Y. Fabrication of Ti3C2Tx MXene Transparent Thin Films with Tunable Optoelectronic Properties. Advanced Electronic Materials. 2016;2(6):1600050.

112. Hantanasirisakul K, Alhabeb M, Lipatov A, Maleski K, Anasori B, Salles P, Ieosakulrat C, Pakawatpanurut P, Sinitskii A, May SJ, Gogotsi Y. Effects of Synthesis and Processing on Optoelectronic Properties of Titanium Carbonitride MXene. Chemistry of Materials. 2019;31(8):2941-2951.

113. Kim SJ, Koh H-J, Ren CE, Kwon O, Maleski K, Cho S-Y, Anasori B, Kim C-K, Choi Y-K, Kim J, Gogotsi Y, Jung H-T. Metallic Ti3C2Tx MXene Gas Sensors with Ultrahigh Signal-to-Noise Ratio. ACS Nano. 2018;12(2):986-993.

114. Gao G, O'Mullane AP, Du A. 2D MXenes: A New Family of Promising Catalysts for the Hydrogen Evolution Reaction. ACS Catalysis. 2017;7(1):494-500.

115. Rasool K, Helal M, Ali A, Ren CE, Gogotsi Y, Mahmoud KA. Antibacterial Activity of Ti3C2Tx MXene. ACS Nano. 2016;10(3):3674-3684.

116. Rasool K, Mahmoud KA, Johnson DJ, Helal M, Berdiyorov GR, Gogotsi Y. Efficient Antibacterial Membrane based on Two-Dimensional Ti3C2Tx (MXene) Nanosheets. Scientific Reports. 2017;7(1):1598.

117. Yang L, Dall'Agnese C, Dall'Agnese Y, Chen G, Gao Y, Sanehira Y, Jena AK, Wang X-F, Gogotsi Y, Miyasaka T. Surface-Modified Metallic Ti3C2Tx MXene as

Electron Transport Layer for Planar Heterojunction Perovskite Solar Cells. Advanced Functional Materials. 2019;29(46):1905694.

118. Sun Y, Zhou D, Shahidi F. Antioxidant properties of tyrosol and hydroxytyrosol saturated fatty acid esters. Food Chemistry. 2018;245:1262-1268.

119. Di Benedetto R, Varì R, Scazzocchio B, Filesi C, Santangelo C, Giovannini C, Matarrese P, D'Archivio M, Masella R. Tyrosol, the major extra virgin olive oil compound, restored intracellular antioxidant defences in spite of its weak antioxidative effectiveness. Nutrition, Metabolism and Cardiovascular Diseases. 2007;17(7):535-545.

120. Vlachogianni IC, Fragopoulou E, Kostakis IK, Antonopoulou S. In vitro assessment of antioxidant activity of tyrosol, resveratrol and their acetylated derivatives. Food Chemistry. 2015;177:165-173.

121. Rosales M, Garcia A, Fuenzalida VM, Espinoza-González R, Song G, Wang B, Yu J, Gracia F, Rosenkranz A. Unprecedented arsenic photo-oxidation behavior of few- and multi-layer Ti3C2Tx nano-sheets. Applied Materials Today. 2020;20:100769.

122. Anayee M, Kurra N, Alhabeb M, Seredych M, Hedhili MN, Emwas A-H, Alshareef HN, Anasori B, Gogotsi Y. Role of acid mixtures etching on the surface chemistry and sodium ion storage in Ti3C2Tx MXene. Chemical Communications. 2020;56(45):6090-6093.

123. Mashtalir O, Naguib M, Mochalin VN, Dall’Agnese Y, Heon M, Barsoum MW, Gogotsi Y. Intercalation and delamination of layered carbides and carbonitrides. Nature Communications. 2013;4:1716.

124. Ding L, Wei Y, Li L, Zhang T, Wang H, Xue J, Ding L-X, Wang S, Caro J, Gogotsi Y. MXene molecular sieving membranes for highly efficient gas separation. Nature Communications. 2018;9(1):155.

125. Weng G-M, Mariano M, Lipton J, Taylor AD. MXene Films, Coatings, and Bulk Processing. In: Anasori B, Gogotsi Y, editors. 2D Metal Carbides and Nitrides (MXenes): Structure, Properties and Applications. Cham: Springer International Publishing; 2019. p. 197-219.

126. Carey M, Hinton Z, Natu V, Pai R, Sokol M, Alvarez NJ, Kalra V, Barsoum MW. Dispersion and Stabilization of Alkylated 2D MXene in Nonpolar Solvents and Their Pseudocapacitive Behavior. Cell Reports Physical Science. 2020;1(4):100042.

127. Liu S, Zheng J, Hao L, Yegin Y, Bae M, Ulugun B, Taylor TM, Scholar EA, Cisneros-Zevallos L, Oh JK, Akbulut M. Dual-Functional, Superhydrophobic Coatings with Bacterial Anticontact and Antimicrobial Characteristics. ACS Applied Materials & Interfaces. 2020;12(19):21311-21321.

128. Patil N, Zhao X, Mishra NK, Saed MA, Radovic M, Green MJ. Rapid Heating of Silicon Carbide Fibers under Radio Frequency Fields and Application in Curing Preceramic Polymer Composites. ACS Applied Materials & Interfaces. 2019;11(49):46132-46139.

129. Anas M, Zhao Y, Saed MA, Ziegler KJ, Green MJ. Radio frequency heating of metallic and semiconducting single-walled carbon nanotubes. Nanoscale. 2019;11(19):9617-9625.

130. Persson I, Näslund L-Å, Halim J, Barsoum MW, Darakchieva V, Palisaitis J, Rosen J, Persson POÅ. On the organization and thermal behavior of functional groups on Ti 3 C 2 MXene surfaces in vacuum. 2D Materials. 2017;5(1):015002.

131. Huang H, Song Y, Li N, Chen D, Xu Q, Li H, He J, Lu J. One-step in-situ preparation of N-doped TiO2@C derived from Ti3C2 MXene for enhanced visible-light driven photodegradation. Applied Catalysis B: Environmental. 2019;251:154-161.

132. Gao Y, Chen H, Zhou A, Li Z, Liu F, Hu Q, Wang L. Novel Hierarchical TiO2/C Nanocomposite with Enhanced Photocatalytic Performance. Nano. 2015;10(05):1550064.

133. Wang Y, Li T, Ma P, Zhang S, Zhang H, Du M, Xie Y, Chen M, Dong W, Ming W. Artificial Nacre from Supramolecular Assembly of Graphene Oxide. ACS Nano. 2018;12(6):6228-6235.

134. Li D, Müller MB, Gilje S, Kaner RB, Wallace GG. Processable aqueous dispersions of graphene nanosheets. Nature Nanotechnology. 2008;3(2):101-105.

135. Jiang X, Kuklin AV, Baev A, Ge Y, Ågren H, Zhang H, Prasad PN. Two-dimensional MXenes: From morphological to optical, electric, and magnetic properties and applications. Physics Reports. 2020;848:1-58.

136. Berdiyorov GR. Effect of surface functionalization on the electronic transport properties of Ti 3 C 2 MXene. EPL (Europhysics Letters). 2015;111(6):67002.

137. Lioi DB, Neher G, Heckler JE, Back T, Mehmood F, Nepal D, Pachter R, Vaia R, Kennedy WJ. Electron-Withdrawing Effect of Native Terminal Groups on the Lattice Structure of Ti3C2Tx MXenes Studied by Resonance Raman Scattering: Implications for Embedding MXenes in Electronic Composites. ACS Applied Nano Materials. 2019;2(10):6087-6091.